Interner Bericht

DLR-IB-SY-BS-2025-144

Characterizing Lamination Parameters Realizable Domain for Practical Composite Layups

Masterarbeit

Mithra Iyangar Ramesh

Deutsches Zentrum für Luft- und Raumfahrt

Institut für Systemleichtbau





Dokumenteigenschaften

Titel	Characterizing Lamination Parameters Realizable Domain for Practical Composite Layups
Betreff	Masterarbeit
Institut	Systemleichtbau
Erstellt von	Mithra Iyangar Ramesh, B. Sc.
Beteiligte	Rakshith Manikandan, M. Sc.; Andela Babaja, M. Sc.; Eduardo Rodrigues Della Noce, M. Sc.
Geprüft von	Prof. Dr. Markus Zimmermann
Freigabe von	Prof. DrIng. Christian Hühne
Zugänglichkeit	☑ Stufe 1: Allgemein zugänglich (in elib ohne Zugangsbeschränkung)
	☐ Stufe 2: DLR intern zugänglich (in elib mit Beschränkung "nur DLR-intern zugänglich")
Datum	07.05.2025
Version	1.0
Datei Info	IB_2025_144_MA_Ramesh.pdf



Characterizing Lamination Parameters Realizable Domain for Practical Composite Layups

Master's Thesis Nr. 229

Scientific Thesis for Acquiring the Master of Science Degree at the School of Engineering and Design of the Technical University of Munich.

Thesis Advisor Laboratory for Product Development and Lightweight Design

Prof. Dr. Markus Zimmermann

Supervisor Laboratory for Product Development and Lightweight Design

Anđela Babaja, M.Sc.

Eduardo Rodrigues Della Noce, M.Sc. (Second corrector) Rakshith Manikandan, M.Sc. (External Supervisor, DLR)

Submitted by Mithra Iyangar Ramesh, B.Sc.

Pappelallee 3A, 38110, Braunschweig

Matriculation number:

mithra.ramesh@tum.de

Submitted on Garching, 07.05.2025

Declaration

I assure that I have written this work autonomously and with the aid of no other than the sources and additives indicated.



Project Definition (1/2)

Initial Situation

The optimization of composite laminates often begins in a mathematically feasible design space defined with respect to lamination parameters, which represent the mechanical behavior (stiffness matrix) of a laminate independent of its stacking sequence. However, this notion introduces a critical gap between the mathematically feasible lamination parameter vectors and those that correspond to stacking sequences that are physically realizable and compliant with design guidelines such as symmetry, balance, 10% rule, disorientation, damage tolerance, and contiguity.

Evaluation of optimal stiffness and designing a stacking sequence matching it are the two levels of bi-level optimization process. If the selected lamination parameter lies outside the realizable region, this retrieval fails and results in a mismatch, compromising structural performance.

This thesis addresses the need to systematically define and validate the realizable domain, a subset of the lamination parameter space that corresponds to stacking sequences satisfying practical design guidelines.

Goals

The goal of this thesis is to analytically characterize the realizable domains of lamination parameters under selected design guidelines and validate these domains through numerical experiments and bi-level optimization. This involves:

- Deriving analytical bounds in lamination parameter space for individual and combined design guidelines (disorientation, contiguity, and damage tolerance).
- Validating the derived domains against laminate datasets for varying ply counts.
- Integrating these domains into a bi-level optimization framework to study their effect on design consistency and structural performance.
- Quantifying the reduction in mismatch between optimization levels when realizable domains are enforced.

Project Definition (2/2)

Contents of this Thesis

- Theoretical Formulation of Realizable Domains
 - Introduction of the realizable domain concept with respect to lamination parameters.
 - Analytical characterization of individual design guidelines in lamination parameter space.
 - Derivation of combined realizable domain equations for multiple guidelines.
- Numerical Validation of Derived Domains
 - Brute-force laminate dataset generation using discrete angle steps for varying ply counts.
 - Visualization of realizable vs. mathematically feasible regions through scatter plots.
 - Quantification of misclassified laminates across various design guidelines.
- Implementation in Bi-Level Optimization
 - Setup of a bi-level optimization scheme for single-panel laminate design.
 - Comparison of performance with and without realizable domain constraints.
 - Analysis of safety factor mismatch due to design guidelines.
- Interpretation and Evaluation of Results
 - Inference from the trends across ply counts and guideline combinations.
 - Discussion on the robustness and limitations of the characterized domains.
 - Identification of potential improvements for practical deployment.

Project Note

Master's Thesis Nr. 229

Supervisor Anđela Babaja, M.Sc., Rakshith Manikandan, M.Sc. Partners in industry/research Deutsches Zentrum für Luft- und Raumfahrt (DLR)

Time period 01.10.2024 - 07.05.2025

The dissertation project of Rakshith Manikandan, M.Sc. set the context for the work presented. My supervisors Anđela Babaja, M.Sc. and Rakshith Manikandan, M.Sc. mentored me during the compilation of the work and gave continuous input. We exchanged and coordinated approaches and results biweekly.

An accurate elaboration, a comprehensible and complete documentation of all steps and applied methods, and a good collaboration with industrial partners are of particular importance.

Publication

I consent to the laboratory and its staff members using content from my thesis for publications, project reports, lectures, seminars, dissertations and postdoctoral lecture qualifications.

The full thesis as PDF and Word/IAT_EX file, as well as all used calculation models and data, will be made available to the supervisor for storage on the central drive of the lab.

The chair checks the students' theses and dissertations with the Turnitin software in accordance with the GDPR. I agree to the terms and conditions of Turnitin and agree that the chair and its employees may use the software to detect and identify plagiarism in the submitted work. In the event of any reservation, I undertake to submit a version of the thesis without restrictive information (e.g. name, matriculation number, acknowledgements) that complies with the relevant data protection clauses.

Garching, 07.05.2025	r
	T.I
50	M Rakshith
	Wat share
Anđela Babaja, M.Sc.	Rakshith Manikandan, M.Sc.

Contents

Ac	ronyı	ms		ix
1	Intro	duction	າ	1
2	State	e of the	art	3
	2.1	Lamin	ated composites	3
		2.1.1	Classical Laminate Theory	6
		2.1.2	Laminate design guidelines	7
	2.2	Optimi	ization	12
	2.3	Lamin	ate optimization using lamination parameters	14
	2.4	Design	guidelines as optimization constraints	20
	2.5	Resear	ch gap	23
3	Res	earch Q	uestions	24
4	Meth	nodolog	ıy	25
	4.1	_	Analysis of lamination parameters	
	4.2		etical Formulation of realizable domains	
		4.2.1	Disorientation	
		4.2.2	Damage Tolerance	35
		4.2.3	Contiguity	
		4.2.4	Balance	43
		4.2.5	Disorientation – Damage Tolerance – Balance	46
	4.3	Lamin	ate optimization using lamination parameters	52
		4.3.1	Benchmark case setup	52
		4.3.2	First-Level stiffness optimization	53
		4.3.3	Second-level stacking sequence design	53
5				
	5.1		tion of Realizable Domains	
		5.1.1	Disorientation	
		5.1.2	Damage Tolerance	
		5.1.3	Contiguity	
		5.1.4	Balance	
	_	5.1.5	Disorientation – Damage Tolerance – Balance	
	5.2	Bench	mark optimization problem	70

6	Con	clusions	76
	6.1	Summary of the Thesis	76
	6.2	Inferences from the Results	76
	6.3	Future work	77
Bik	oliogr	aphy	79
Ар	pend	ix	85
Ар	pend	ix A Computational approach for laminate dataset generation and filtering.	86
Ар	pend	ix B Contiguity design guideline enforced on conventional laminates	93
Аp	pend	ix C Different interpretation of damage tolerance design guideline	96

Acronyms

ADG Attribute Dependency Graph

CLT Classical Laminate Theory

FEA Finite Element Analysis

IPOPT Interior Point Optimizer

LP Lamination Parameter

Qol Quantity of Interest

SF Safety Factor

SS Stacking Sequence

1 Introduction

Composite materials are paramount in modern aerospace engineering due to their superior specific mechanical properties [Daniel and Ishai 1994; Kaw 2005]. In comparison to using metals in traditional structural configurations, they offer higher stiffness-to-weight and strength-to-weight ratios, resulting in substantial weight savings, improved fuel economy, greater payloads, and greater ranges of operation [Barbero 2010; Herakovich 1998]. As a result of these advantages, composite materials have been widely adopted in aircraft structures, rotorcrafts, satellites, and launch vehicles [Mallick 2007; Soutis 2005].

A unique advantage of composites is their directional stiffness, which allows engineers to tailor structural performance by adjusting the fiber orientation in each ply. Unlike isotropic materials whose mechanical properties are the same in every direction, composites require deliberate decisions concerning fiber angles and SS for obtaining performance specifications. Fibre orientation of plies in a laminate is specified by a SS, which defines the angle and position of each ply along the laminate's thickness. However, this flexibility introduces intricacy to the design process. The number of plies, their directions, and several performance requirements (such as strength, stiffness, stability, and design guidelines) should be treated in a unified manner [Gürdal et al. 1999].

Laminate stiffness is typically modelled via CLT. It employs **A**, **B**, and **D** matrices to describe extension, coupling, and bending responses, which are calculated by adding individual ply contributions. CLT is computationally expensive if applied directly in optimization since it leads to a growing number of design variables with an increase in plies.

To overcome this, Lamination Parameters (LPs) were introduced in Tsai and N. J. Pagano 1968. LPs are a compact continuous laminate stiffness approximations and are one set of alternate design variables. The same stiffness matrices are characterized in terms of a fixed number of LPs (at most 12 for an arbitrary laminate), which otherwise requires specifying the fibre orientation of each ply.

However, for a set of LPs to be feasible, a corresponding real SS must exist. A set of all LP vectors for which at least one real SS exists is called a mathematically feasible domain. In physical design, engineers follow specific design guidelines, which are defined based on industry experience. Without being aware of these guidelines, optimization can produce theoretically optimal but practically infeasible solutions.

Bi-level optimization process while using LPs as design variables is as follows:

- In the **first level**, optimal LPs are determined by treating them as continuous design variables.
- In the **second level**, a corresponding SS is retrieved to match these LPs as closely as possible.

Mismatch between the LPs and their derived SS introduces an epistemic uncertainty, resulting from undefined design guidelines in the first level and the discrete nature of plies. The main hypothesis of the present work is that by defining the realizable domain, this uncertainty is reduced.

To validate the outcomes, the optimization is performed on a single panel test case. The panel has a fixed aspect ratio, subjected to multiple load cases [Bloomfield et al. 2008].

The structure of this thesis is as follows:

- Chapter 2: State of the art introduces the fundamentals of composites, design guidelines, and different parameterization techniques like CLT and LPs. Moreover, this chapter identifies the research gap addressed in this work.
- Chapter 3: Research Questions enumerates the formulated research questions that guide the findings of this work.
- Chapter 4: Methodology presents the theoretical framework describing the realizable domain in LP space with respect to each design guideline. In addition to this, it states the computation method used to validate and incorporate the described domains into the bi-level optimization tool.
- Chapter 5: Results provides quantitative and graphical validation of the described spaces, as well as the performance evaluation in the bi-level optimization using an in-house tool. Outcomes are compared under different load cases.
- Chapter 6: Conclusion summarizes the findings and provides suggestions for future work.

2 State of the art

This chapter introduces the fundamental concepts necessary to understand the findings of the current work. The basic principles of composites, macromechanical behaviour, industry guidelines, optimization, and laminate optimization using LPs are clarified. Bailie et al. 1997 outlines the design guidelines, based on laminate definitions, that form the basis for the SS design of most composite structures in the aerospace industry.

However, not all guidelines are accounted for when using LPs as design variables in the optimization stage. These guidelines are presented in the context of optimization, meaning they are defined with respect to the chosen design variables to facilitate their analytical characterization.

This chapter focuses on the design guidelines characterized in the literature, namely symmetry, balance, and the 10% rule. Additional design guidelines, disorientation, damage tolerance, and contiguity are likewise introduced in the current chapter and are characterized in Chapter 4. At the end of the chapter, the consequent research gap is summarized.

2.1 Laminated composites

Composite materials can be described as a mixture of two or more different types of materials with micro- or macroscopic dimensions and clearly identifiable boundaries [Chawla 1988]. Fibre-reinforced laminated composites are commonly used in the industry and are the focus of this work.

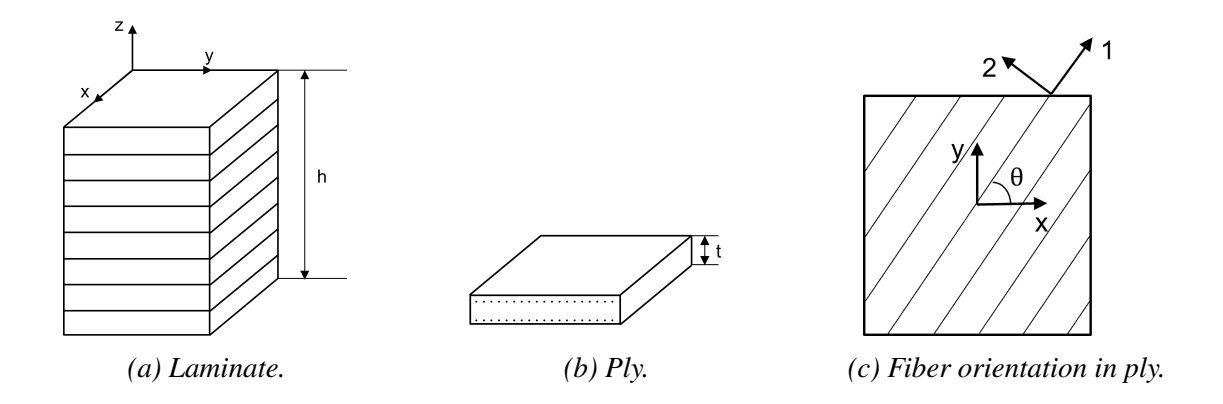


Figure 2.1: Constituents of a laminate.

Figure 2.1 shows a laminate of height h, comprised of plies stacked together. Each ply with a certain thickness t constitutes fibres bound within a matrix. The orientation of these fibres is measured with respect to the global coordinates of the laminate and can vary in the range of $[-90^{\circ}, 90^{\circ}]$. The material axis of a composite ply refers to the local coordinate system aligned with the fibre direction (axis-1) and the transverse direction (axis-2), while the axis-3 points through the thickness of the ply, aligning with the global z-coordinate (see Figure 2.1c). SS of a laminate defines the stacking order of plies with certain fibre orientation θ . The laminate SS is represented in Figure 2.2. Laminates with plies stacked symmetrically about the mid-plane are known as symmetric laminates (Figure 2.2b). Figure 2.2b and 2.2c illustrate equivalent alternatives to present the same laminate. Notation with subscript s is commonly used for symmetric laminates (see Figure 2.2c).

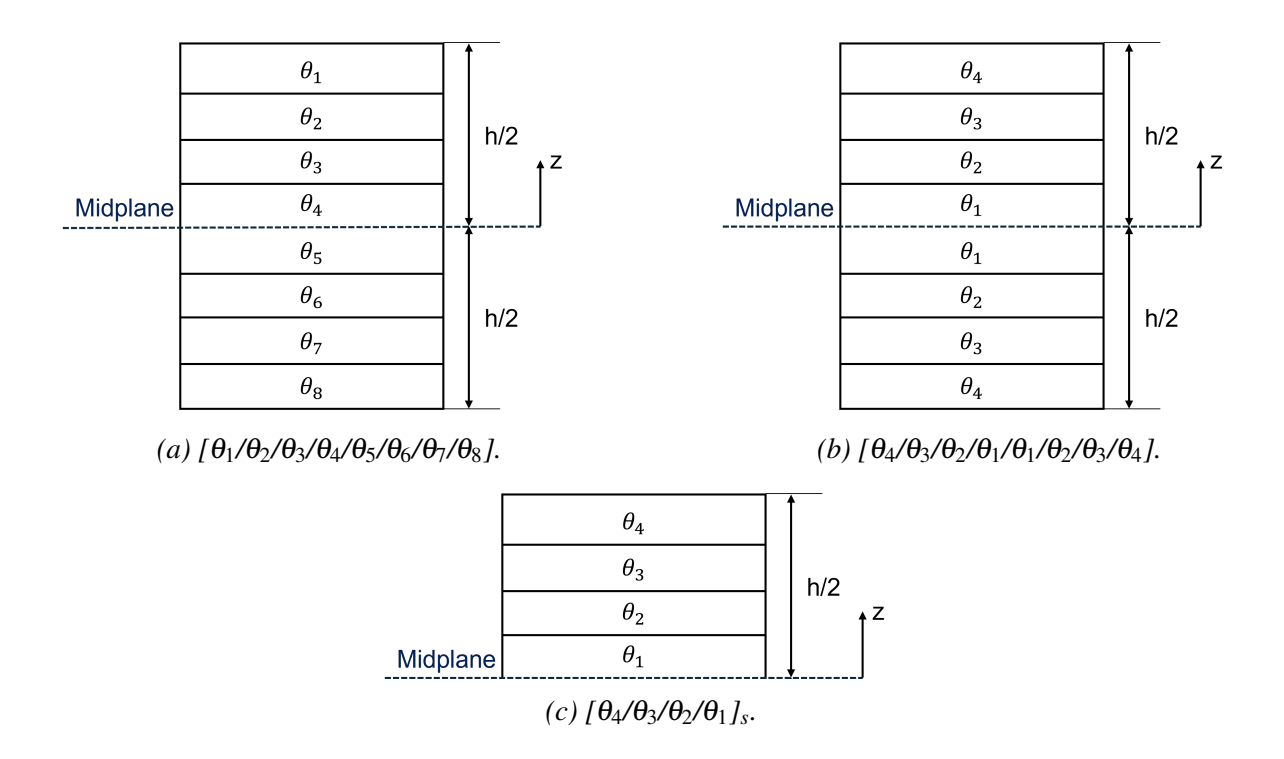


Figure 2.2: Laminate SS notation.

Combinations of two different materials are utilized to benefit from both of their individual properties. Fibres govern axial stiffness, and the matrix governs shear and transverse properties. However, this generates a complex inhomogeneous stress distribution in the material. Unlike their isotropic counterparts (metallic alloys), composites exhibit anisotropic/orthotropic properties derived from the combined effect of stiff load-bearing fibres and a ductile matrix.

At the ply level, fibre and matrix properties are studied under micro-mechanics. Micro-mechanics is not further discussed, as it is out of the scope of this thesis. For further details on micromechanics, Aboudi 1991 can be referred.

A homogenization approach is applied to simplify the analysis associated with the inhomogeneous stress distribution. Here, the fibre and matrix properties are averaged to define an equivalent homogeneous material. This enables the use of traditional mechanics formulations, such as stiffness matrices, without explicitly modelling individual fibres and matrices and their interaction. Hooke's law provides stress-strain relationships along the material axis. The homogenized properties are used in the stress-strain relationships. Mathematically, Hooke's law is represented as:

$$\sigma = \mathbf{Q}\varepsilon \tag{2.1}$$

$$\begin{bmatrix} \sigma_{1} \\ \sigma_{2} \\ \sigma_{3} \\ \tau_{23} \\ \tau_{31} \\ \tau_{12} \end{bmatrix} = \begin{bmatrix} Q_{11} & Q_{12} & Q_{13} & Q_{14} & Q_{15} & Q_{16} \\ Q_{21} & Q_{22} & Q_{23} & Q_{24} & Q_{25} & Q_{26} \\ Q_{31} & Q_{32} & Q_{33} & Q_{34} & Q_{35} & Q_{36} \\ Q_{41} & Q_{42} & Q_{43} & Q_{44} & Q_{45} & Q_{46} \\ Q_{51} & Q_{52} & Q_{53} & Q_{54} & Q_{55} & Q_{46} \\ Q_{61} & Q_{62} & Q_{63} & Q_{64} & Q_{65} & Q_{66} \end{bmatrix} \begin{bmatrix} \varepsilon_{1} \\ \varepsilon_{2} \\ \varepsilon_{3} \\ \gamma_{23} \\ \gamma_{31} \\ \gamma_{12} \end{bmatrix}$$

$$(2.2)$$

In Equation 2.1, σ and ε represent the stress and strain tensors, respectively. **Q** matrix defines the stiffness of the ply in the material axis. Since the ratio of ply thickness to its in-plane dimensions is extremely small, the out-of-plane stresses (σ_3 , τ_{13} , and τ_{23}) are considered negligible compared to the in-plane stresses [Nettles 1994]. Hence, the plane stress assumptions are applied and the Equation 2.2 reduces to:

$$\begin{bmatrix} \sigma_1 \\ \sigma_2 \\ \tau_{12} \end{bmatrix} = \begin{bmatrix} Q_{11} & Q_{12} & 0 \\ Q_{21} & Q_{22} & 0 \\ 0 & 0 & Q_{66} \end{bmatrix} \begin{bmatrix} \varepsilon_1 \\ \varepsilon_2 \\ \gamma_{12} \end{bmatrix}$$
(2.3)

Elements of the stiffness matrix \mathbf{Q} are defined based on material properties (Young's modulus (E), Poisson's ratio (v), and Shear modulus (G)). For a homogenized ply, these properties are defined by moduli E_1 , E_2 , G_{12} , and Poisson's ratio v_{12} (or v_{21}) in the material axis (Figure 2.1c). Equation 2.3 can be expressed as:

$$\begin{bmatrix} \sigma_1 \\ \sigma_2 \\ \tau_{12} \end{bmatrix} = \begin{bmatrix} \frac{E_1}{1 - v_{12}v_{21}} & \frac{v_{21}E_1}{1 - v_{12}v_{21}} & 0 \\ \frac{v_{12}E_2}{1 - v_{12}v_{21}} & \frac{E_2}{1 - v_{12}v_{21}} & 0 \\ 0 & 0 & G_{12} \end{bmatrix} \begin{bmatrix} \varepsilon_1 \\ \varepsilon_2 \\ \gamma_{12} \end{bmatrix}$$
(2.4)

where:

$$\frac{v_{12}}{E_1} = \frac{v_{21}}{E_2} \tag{2.5}$$

Since each ply in a laminate is generally oriented at a different angle θ , the stiffness contribution of each ply must be expressed in a common coordinate system for analysis. Transforming the stiffness matrix from material coordinates to laminate global coordinates allows for a consistent representation of the stiffness across all plies. Using fibre orientation information, Hooke's law is expressed in global coordinates by using the transformation matrix T:

$$[\mathbf{T}] = \begin{bmatrix} \cos^{2}\theta & \sin^{2}\theta & -2\sin\theta\cos\theta \\ \sin^{2}\theta & \cos^{2}\theta & 2\sin\theta\cos\theta \\ \sin\theta\cos\theta & -\sin\theta\cos\theta & \cos^{2}\theta - \sin^{2}\theta \end{bmatrix}$$
$$[\mathbf{R}] = \begin{bmatrix} 1 & 0 & 0 \\ 0 & 1 & 0 \\ 0 & 0 & 2 \end{bmatrix}$$
$$\begin{bmatrix} \sigma_{x} \\ \sigma_{y} \\ \tau_{xy} \end{bmatrix} = [\mathbf{T}]^{-1}[\mathbf{Q}][\mathbf{R}][\mathbf{T}][\mathbf{R}]^{-1} \begin{bmatrix} \varepsilon_{x} \\ \varepsilon_{y} \\ \gamma_{xy} \end{bmatrix}$$
$$\begin{bmatrix} \sigma_{x} \\ \sigma_{y} \\ \tau_{xy} \end{bmatrix} = \begin{bmatrix} \overline{Q_{11}} & \overline{Q_{12}} & \overline{Q_{13}} \\ \overline{Q_{21}} & \overline{Q_{22}} & \overline{Q_{23}} \\ \overline{Q_{31}} & \overline{Q_{32}} & \overline{Q_{33}} \end{bmatrix} \begin{bmatrix} \varepsilon_{x} \\ \varepsilon_{y} \\ \gamma_{xy} \end{bmatrix}$$
(2.6)

Achenbach 1975 can be reffered for the detailed derivation of Equation 2.6.

2.1.1 Classical Laminate Theory

Having understood the stress-strain relation at the ply level, CLT is used for studying the combined effect of all stacked plies in a laminate, accounting for both in-plane forces and bending moments. In a laminate subjected to external loads, forces, and moments are not applied directly to the individual plies but to the laminate. Hence, the resultant in-plane forces **N** and bending moments **M** are obtained by integrating the stress components through the laminate thickness as per Equation 2.7 and 2.8.

$$\mathbf{N} = \begin{bmatrix} N_x \\ N_y \\ N_{xy} \end{bmatrix} = \int_{-\frac{h}{2}}^{\frac{h}{2}} \begin{bmatrix} \sigma_x \\ \sigma_y \\ \tau_{xy} \end{bmatrix} dz$$
 (2.7)

$$\mathbf{M} = \begin{bmatrix} M_x \\ M_y \\ M_{xy} \end{bmatrix} = \int_{-\frac{h}{2}}^{\frac{h}{2}} \begin{bmatrix} \sigma_x \\ \sigma_y \\ \tau_{xy} \end{bmatrix} z dz$$
 (2.8)

According to Love 1888, the total strain at any point ε in thin elastic shells is a linear variation of midplane strain ε_0 and the curvature of the shell κ . Mathematically, it is expressed as:

$$\varepsilon = \varepsilon^0 + z\kappa \tag{2.9}$$

By substituting Equations 2.9 and 2.6 into the integrals given in Equations 2.7 and 2.8, a set of coupled linear equations is obtained, expressing laminate forces and moments as functions of midplane strains and curvatures. This leads to the compact matrix form of CLT shown in Equation 2.10, where the **A**,**B**,**D** matrices represent the extensional, coupling, and bending stiffness of the laminate, respectively.

$$\begin{bmatrix} \mathbf{N} \\ \mathbf{M} \end{bmatrix} = \begin{bmatrix} \mathbf{A} & \mathbf{B} \\ \mathbf{B} & \mathbf{D} \end{bmatrix} \begin{bmatrix} \boldsymbol{\varepsilon}^{\mathbf{0}} \\ \boldsymbol{\kappa} \end{bmatrix}$$

$$\begin{bmatrix} N_{x} \\ N_{y} \\ N_{xy} \\ M_{x} \\ M_{y} \\ M_{xy} \end{bmatrix} = \begin{bmatrix} A_{11} & A_{12} & A_{16} & B_{11} & B_{12} & B_{16} \\ A_{12} & A_{22} & A_{26} & B_{12} & B_{22} & B_{26} \\ A_{16} & A_{26} & A_{66} & B_{16} & B_{26} & B_{66} \\ B_{11} & B_{12} & B_{16} & D_{11} & D_{12} & D_{16} \\ B_{12} & B_{22} & B_{26} & D_{12} & D_{22} & D_{26} \\ B_{16} & B_{26} & B_{66} & D_{16} & D_{26} & D_{66} \end{bmatrix} \begin{bmatrix} \varepsilon_{x}^{0} \\ \varepsilon_{y}^{0} \\ \gamma_{xy}^{0} \\ \kappa_{x} \\ \kappa_{y} \\ \kappa_{xy} \end{bmatrix}$$

$$(2.10)$$

Equations 2.10 and 2.9 are used for computing the midplane strains and curvatures under applied loads. These can be extended to determine strain and stress distributions within individual plies, which are the basis for further analyses such as ply-level failure assessment or buckling checks [Jones 1999]. With experience in designing laminates for manufacturing aircraft structures, certain guidelines have been commonly adopted in the industry to avoid practical and manufacturing complications.

2.1.2 Laminate design guidelines

Experience-based knowledge stemmed from designing composite aircraft for many years, resulted in the development of the so-called design guidelines for the laminate SS [Bailie et al. 1997]. Through the thickness design guidelines described in the literature are listed below:

- Symmetry
- Balance
- 10 % Rule
- Disorientation
- Damage Tolerance

Contiguity

Design guidelines related to constant thickness structures are discussed in the current work. For completeness, it is important to note that laminates can have variable stiffness by changing thickness or the constituent fibre orientation across the structure. Related design guidelines pertaining to ply-drop/blending, bonding, assemblies, and repair of composite structures are not focused on in this study and can be found in US Dept of Defense 1999.

Symmetric laminates

Figure 2.2b shows a laminate with fibre orientations distributed symmetrically about the midplane. This type of laminate is called a symmetric laminate. Such a design results in uncoupling a laminate's bending and membrane response. This uncoupling simplifies the evaluation of the ply-level strain and stress distribution. It also prevents the warping effect during manufacturing [Niu 1992]. For completeness, it is worth noting that symmetry is a sufficient but not a necessary condition for uncoupling the bending and membrane responses [Verchery 2011].

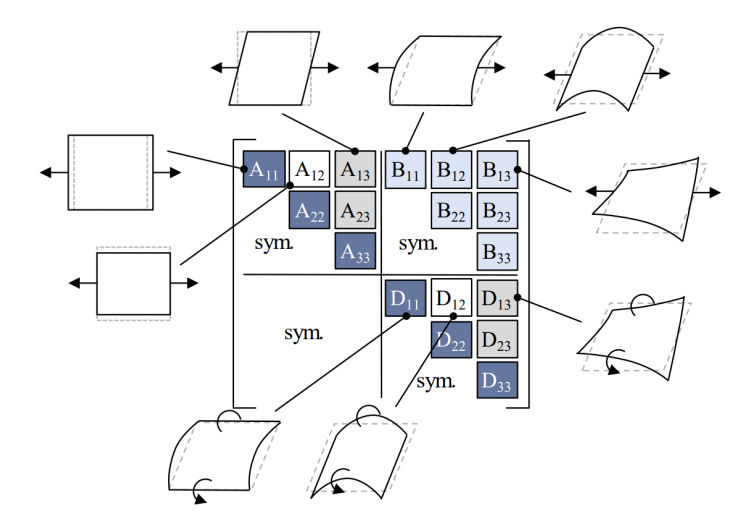


Figure 2.3: Effects of [ABD] coefficients on deformation [Franz et al. 2019].

Mathematically, the uncoupling is expressed as:

$$[\mathbf{B}] = 0 \tag{2.11}$$

Balanced laminates

In this type of laminate, plies oriented at $+\theta$ (excluding 0° and 90°) are always paired with corresponding $-\theta$ plies, ensuring a balanced fiber arrangement (see Figure 2.4).

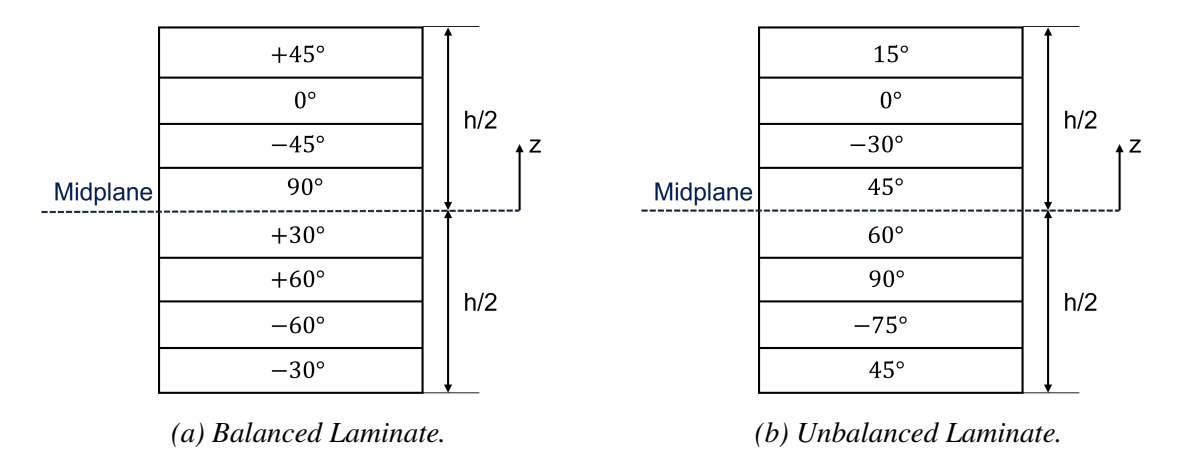


Figure 2.4: Example for a balanced and unbalanced laminate.

The guideline is enforced to decouple the laminates' in-plane normal and shear properties. As a result of implementing this guideline, the mechanical properties and behavior of the laminate become more intuitive. It also reduces the cost of tests, such as determining open-hole strength [Bailie et al. 1997].

Uncoupling the normal and shear properties of the in-plane is called in-plane orthotropy. This can be satisfied by nullifying the coupling terms in Equation 2.10:

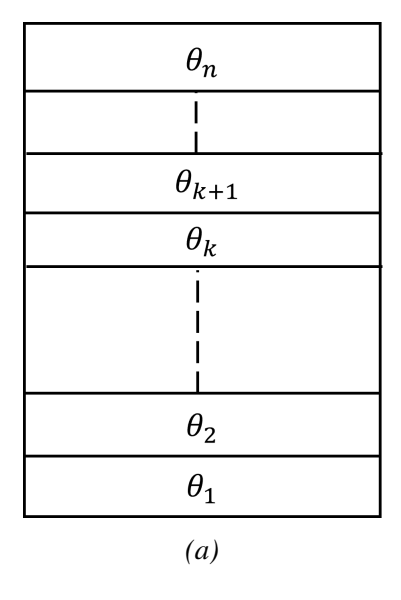
$$A_{16}, A_{26} = 0 (2.12)$$

10% rule

Although laminates are designed for known primary loads, failure might occur due to uncertain secondary loads. To mitigate this problem, the 10% rule is enforced to maintain minimum stiffness across 4 principal directions, or uniaxial load states. The 10% rule requires at least ten percent of the fibres to be oriented in 0° , $+45^\circ$, -45° and 90° angles. Since the rule is enforced on the ply counts, it is not straightforward to generalize it for laminates with arbitrary ply angles. Hence, Abdalla et al. 2009 proposes a generalized 10% rule, which ensures a minimum amount of in-plane stiffness in each principal direction of the laminate. Constraints on stiffness make it more intuitive to understand the guideline as a robustness criterion for the laminate.

Disorientation

The guideline restricts the absolute maximum difference between the fibre orientation of two consecutive plies to 45°. This mitigates the delamination due to the high stiffness and coefficient of thermal expansion difference between consecutive plies [Niu 1992]. Figure 2.5b shows an arbitrary laminate obeying the disorientation design guideline.



45°
30°
60°
15°
-30°
-60°
90°
75°
(b)

Figure 2.5: Disorientation design guideline. (a) The constraint is defined as $|\Delta\theta| \le 45^{\circ}$ (see Equation 2.13). (b) Example of a laminate SS that satisfies the disorientation requirement.

$$|\theta_k - \theta_{k+1}| \le 45^\circ \tag{2.13}$$

Damage tolerance

To ensure the safety of primary load-carrying plies and increase the impact resistance, e.g., against tool drop while manufacturing or assembly, damage tolerance design guideline is enforced. It requires $\pm 45^{\circ}$ plies to be placed on the outer laminate surface. Three common interpretations of the damage tolerance design guideline are:

• The outermost plies are assigned 45° or -45° individually, while the remaining fibre orientations of the plies are selected based on the remaining design guidelines enforced.

- The outermost two plies are oriented at 45° and -45° . This way, the remaining plies can be treated as a sublaminate while enforcing other design guidelines independent of damage tolerance.
- Separating the outermost $\pm 45^{\circ}$ plies with 0° or 90° ply to account for disorientation design guideline.

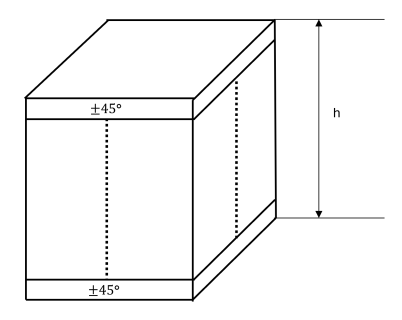


Figure 2.6: Top and bottom plies of an arbitrary laminate fixed at $\pm 45^{\circ}$.

Contiguity

Contiguous plies are defined as consecutive plies with identical fibre orientation. Figure 2.7 illustrates a laminate segment with n contiguous plies. Contiguity design guideline constrains the total thickness of contiguous plies t_p .

The CLT predicts the plane stress in laminates under membrane loading. However, when adjacent plies are oriented in different fibre directions, a mismatch in their Poisson's ratios leads to the development of interlaminar stresses. These interlaminar stresses are not captured by CLT but play a significant role in the onset of delamination, particularly near the free edges of the laminate. According to Love's hypothesis for thin shells [Love 1888], the membrane stress at the free edge must vanish. Consequently, the normal stress component σ_y is balanced by an interlaminar shear stress τ_{zy} . However, the forces resulting from σ_y and τ_{zy} are not collinear [Pipes and N. Pagano 1970], generating a local moment. An additional interlaminar normal stress σ_z is induced to maintain equilibrium.

The magnitude of this interlaminar stress σ_z is directly proportional to the thickness of the contiguous region t_P . Therefore, the contiguity design guideline is imposed to mitigate excessive interlaminar stress and reduce the risk of delamination. In practice, the guideline constrains the total thickness of contiguous plies to 0.6 mm. However, based on the standard ply thickness used in most laminates, this translates to a maximum of 4 or 5 plies.

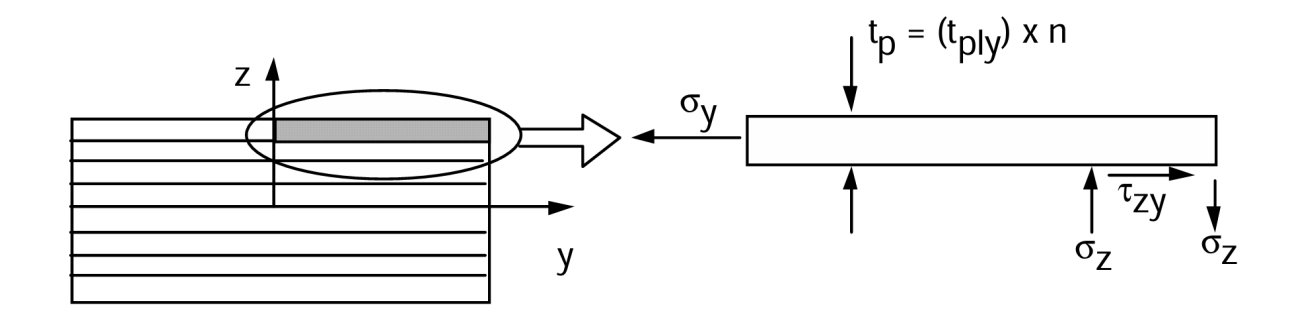


Figure 2.7: Free body diagram of outer ply illustrating the interlaminar stress [Pipes and N. Pagano 1970].

Fibres are the primary load-bearing elements in composite laminates, and the stiffness is maximized along the direction of fibre orientation. Engineers can tailor the stiffness distribution to achieve desired mechanical properties by strategically varying fibre angles across plies. Optimizing fibre orientation is a key aspect of composite design, as it involves balancing trade-offs among stiffness, weight, and performance. Optimizing laminated composites amidst all this is challenging.

2.2 Optimization

In optimization problems, attributes are typically categorized as design variables, parameters, or Quantities of Interest (QoIs). Requirements posed on QoIs serve as a mean to evaluate performance requirements or objectives, which help determine whether an optimized solution is acceptable or not. The values of QoIs are directly influenced by the chosen design variables and parameters. They are usually bounded considering, for example, manufacturing or geometrical constraints. These bounds span the design space. One of the main challenges of the optimization process is to explore the available design space and find the best possible set of design variables that are feasible. Optimization is an inverse process of verification, where the design variables are optimized based on the system requirements [Zimmermann 2022a]. Mathematically, an optimization problem is expressed as:

$$\begin{aligned} \min_{\mathbf{x}} \quad \mathbf{f}(\mathbf{x}) \\ \text{subject to:} \quad \mathbf{g}(\mathbf{x}) \leq 0 \\ \quad \mathbf{h}(\mathbf{x}) = 0 \\ \quad \mathbf{x_l} \leq \mathbf{x} \leq \mathbf{x_u} \end{aligned}$$

The objective function of an optimization is defined by the function $\mathbf{f}(\mathbf{x})$, where \mathbf{x} represents the vector of design variables. The goal of an optimization process is to minimize the value of the objective function. The search for an optimal solution is carried out within a n-dimensional design space (n being the number of design variables), constrained by the lower and upper bounds $\mathbf{x_l}$ and $\mathbf{x_u}$, respectively. Additionally, the optimization problem is mostly constrained by a set of inequality constraints $\mathbf{g}(\mathbf{x})$ and equality constraints $\mathbf{h}(\mathbf{x})$, which are satisfied for a feasible design.

Some optimization methods include gradient-based methods, population-based methods, or datadriven approaches. A detailed discussion is beyond the scope of this work; readers interested in an overview of optimization methods are referred to [Papalambros and Wilde 2017].

The objective function contains either a single optimum or multiple optima. Determining properties, such as convexity, supports the decision making process regarding choosing the appropriate optimization algorithm for the specific problem. A function is convex if a straight line connecting any two points on the function lies entirely above the function itself [Ekeland and Turnbull 1983].

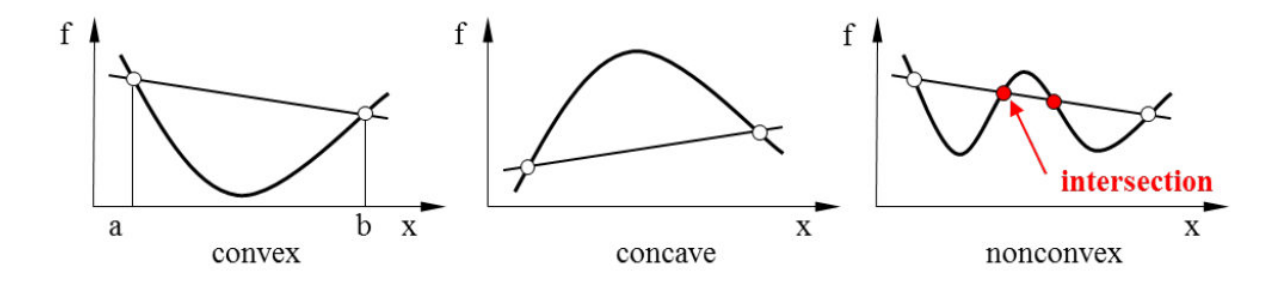


Figure 2.8: Visual representation of convex, concave, and non-convex functions [Bletzinger 2021].

As illustrated in Figure 2.8, convex problems are characterized as functions having one local/global minimum. This does not imply that there is just one minimum but that the entire collection of minima lies within a convex region [Boyd and Vandenberghe 2004]. However, nonconvex problems may possess multiple local minima. Convexity thus facilitates the optimization task by removing the ambiguity in the local and global solution.

Gradient-based methods, dependent on the gradient information with respect to design variables for iteratively optimizing the design, are utilized for solving convex optimization problems. The methods include the steepest descent, conjugate gradient, and feasible direction methods, among others. These methods are particularly effective in convex spaces for which no constraints

are applied because any descent direction improves the objective value, and the absence of non-global local minima ensures convergence to the global optimum [Belegundu 1985].

If gradient information is available, and the design space is restricted by (in)equality constraints, Sequential linear or quadratic programming is suitable. When dealing with non-convex problems, where there are multiple local optima, one can utilize methods such as Sequential Convex Programming to solve the original problem by an approximation via a sequence of convex subproblems, leveraging the solvability of convexity while addressing larger non-convex problems [Bruyneel 2008; Zimmermann 2022b]. However, for the problems where multiple local minima are present, and if the gradient of 1^{st} and 2^{nd} order is not available, population-based methods, such as Evolutionary algorithms, are more appropriate [Zimmermann 2022c]. The following section introduces how laminates are optimized using CLT and LP.

2.3 Laminate optimization using lamination parameters

Laminates must be designed to satisfy the requirements on its QoIs. As discussed in Chapter 2.1, tailoring elastic properties in different directions with ease is one advantage compared to metals. To formulate the optimization problem, appropriate design variables influencing the QoIs (e.g., displacement) are to be selected.

The structural properties of a laminate can be tailored by modifying the SS, which in turn influences the coefficients of the stiffness matrices [ABD] defined in Equation 2.10. Recalling the equations describing the [ABD] matrices, the coefficients are mathematically represented as:

$$A_{ij} = \sum_{k=1}^{n} [Q_{ij}(\theta_k)](h_k - h_{k-1}) \iff A_{ij} = \sum_{k=1}^{n} [Q_{ij}(\theta_k)]t_k$$

$$B_{ij} = \frac{1}{2} \sum_{k=1}^{n} [\overline{Q_{ij}}(\theta_k)](h_k^2 - h_{k-1}^2) \iff B_{ij} = \sum_{k=1}^{n} [Q_{ij}(\theta_k)]t_k z_k$$
(2.14)

$$D_{ij} = \frac{1}{3} \sum_{k=1}^{n} [\overline{Q_{ij}}(\theta_k)](h_k^3 - h_{k-1}^3) \quad \iff \quad D_{ij} = \sum_{k=1}^{n} [\overline{Q_{ij}}(\theta_k)] \left(t_k z_k^2 + \frac{t_k^3}{12}\right)$$
$$i, j = 1, 2, 6$$

The fibre orientation θ and the number of plies n are used as design variables to optimize the stiffness matrix. This choice of design variables - corresponding to the physical parameters

directly used in manufacturing - facilitates the evaluation of local stresses and strains using Equation 2.6. This optimization setup is also beneficial when considering multiple materials. However, the number of design variables in this parameterization depends on the number of plies in a laminate. For n number of plies, there are n design variables. The dimension of the optimization problem rises with the number of plies.

For this reason, a continuous parameterization independent of SS is introduced [Tsai and N. J. Pagano 1968]. Each term in the [ABD] matrix is represented as a linear combination of LPs, with the corresponding lamina invariants Γ_0 to Γ_4 serving as constant coefficient matrices. LPs define the [ABD] matrices in a compact form. To express the stiffness coefficients of the laminate compactly, the A, B, and D matrices in CLT are written in terms of LPs and lamina invariants as follows:

$$\mathbf{A} = h\mathbf{\Gamma}_0 + \mathbf{\Gamma}_1 V_1^{\mathbf{A}} + \mathbf{\Gamma}_2 V_2^{\mathbf{A}} + \mathbf{\Gamma}_3 V_3^{\mathbf{A}} + \mathbf{\Gamma}_4 V_4^{\mathbf{A}}$$
 (2.15)

$$\mathbf{B} = \mathbf{\Gamma}_1 V_1^{\mathbf{B}} + \mathbf{\Gamma}_2 V_2^{\mathbf{B}} + \mathbf{\Gamma}_3 V_3^{\mathbf{B}} + \mathbf{\Gamma}_4 V_4^{\mathbf{B}}$$
 (2.16)

$$\mathbf{D} = \frac{h^3}{12} \mathbf{\Gamma}_0 + \mathbf{\Gamma}_1 V_1^{\mathbf{D}} + \mathbf{\Gamma}_2 V_2^{\mathbf{D}} + \mathbf{\Gamma}_3 V_3^{\mathbf{D}} + \mathbf{\Gamma}_4 V_4^{\mathbf{D}}$$
(2.17)

Here, $V^{\mathbf{A}}$, $V^{\mathbf{B}}$, and $V^{\mathbf{D}}$ represent the in-plane, coupling, and bending LPs, respectively. These are defined as integrals over the ply orientations as follows:

$$V_{[1,2,3,4]}^{\mathbf{A}} = \int_{-h/2}^{h/2} \left[\cos 2\theta(z), \cos 4\theta(z), \sin 2\theta(z), \sin 4\theta(z) \right] dz$$
 (2.18)

$$V_{[1,2,3,4]}^{\mathbf{B}} = \int_{-h/2}^{h/2} z \left[\cos 2\theta(z), \cos 4\theta(z), \sin 2\theta(z), \sin 4\theta(z) \right] dz$$
 (2.19)

$$V_{[1,2,3,4]}^{\mathbf{D}} = \int_{-h/2}^{h/2} z^2 \left[\cos 2\theta(z), \cos 4\theta(z), \sin 2\theta(z), \sin 4\theta(z) \right] dz$$
 (2.20)

LPs are defined by separating the lamina invariants from the CLT formulation. The matrices Γ_0 to Γ_4 contain material stiffness information and are functions of the lamina invariants U_1 through U_5 :

$$\mathbf{\Gamma}_{0} = \begin{bmatrix} U_{1} & U_{4} & 0 \\ & U_{1} & 0 \\ sym & U_{5} \end{bmatrix} \quad \mathbf{\Gamma}_{1} = \begin{bmatrix} U_{2} & 0 & 0 \\ & -U_{2} & 0 \\ sym & 0 \end{bmatrix}
\mathbf{\Gamma}_{2} = \begin{bmatrix} U_{3} & -U_{3} & 0 \\ & U_{3} & 0 \\ sym & -U_{3} \end{bmatrix} \quad \mathbf{\Gamma}_{3} = \begin{bmatrix} 0 & 0 & \frac{U_{2}}{2} \\ & 0 & \frac{U_{2}}{2} \\ sym & 0 \end{bmatrix} \quad \mathbf{\Gamma}_{4} = \begin{bmatrix} 0 & 0 & U_{3} \\ & 0 & -U_{3} \\ sym & 0 \end{bmatrix}$$
(2.21)

The lamina invariants are given by:

$$U_1 = \frac{1}{8} (3Q_{11} + 3Q_{22} + 2Q_{12} + 4Q_{66})$$

$$U_2 = \frac{1}{2} (Q_{11} - Q_{22})$$

$$U_3 = \frac{1}{8} (Q_{11} + Q_{22} - 2Q_{12} - 4Q_{66})$$

$$U_4 = \frac{1}{8} (Q_{11} + Q_{22} + 6Q_{12} - 4Q_{66})$$

$$U_5 = \frac{1}{8} (Q_{11} + Q_{22} - 2Q_{12} + 4Q_{66})$$

In Equations 2.15, 2.16, and 2.17, h denotes the total thickness of the laminate, z denotes the distance of each ply from the mid-plane. These equations compactly represent the full set of 12 LPs. As described in Equations 2.18 to 2.20, LPs are independent of the total number of plies in a laminate. Regardless of the laminate size, a maximum of twelve LPs and laminate thickness are sufficient to characterize its stiffness, making them a more compact and scalable alternative to CLT. For instance, the compact form of the second coupling parameter is given by:

$$V_2^{\mathbf{B}} = \int_{-h/2}^{h/2} z \cos 4\theta(z) \, dz \tag{2.22}$$

LPs are expressed as integrals of trigonometric functions of the fibre angle $\theta(z)$, as shown in Equations 2.18 to 2.20. Hence, the design space of LPs is [-1,1], collectively forming a 12-dimensional hypercube. Each point represents a vector of LPs. However, not all vectors within this hypercube correspond to real laminates, since all LPs in a single vector are derived from the same SS. These interdependencies define the "mathematically feasible domain" of LPs, which is a subset of the 12-dimensional hypercube. Each point in this subset represents a combination of LPs that can be obtained from at least one real SS.

A vector of LPs is said to be feasible if there exists a physical laminate whose SS produces that exact set of parameters. Conversely, an infeasible vector does not correspond to any real laminate and leads to an inconsistent or complex stiffness matrix. Miki 1983 presents the feasible region of two in-plane LPs which was later extended to bending LPs in Miki and Sugiyama 1993. Mathematically, it is represented as:

$$V_2^{\mathbf{A},\mathbf{D}} \ge 2(V_1^{\mathbf{A},\mathbf{D}})^2 - 1$$
 (2.23)

The derivation stemmed from the trignometric relation between $\cos 4\theta$ and $\cos 2\theta$ ($\cos 4\theta = 2\cos^2\theta - 1$). The inequality trigonometric relation is represented as an inequality when the laminate has more than one fibre orientation angle. The feasible domain shown in Equation 2.23

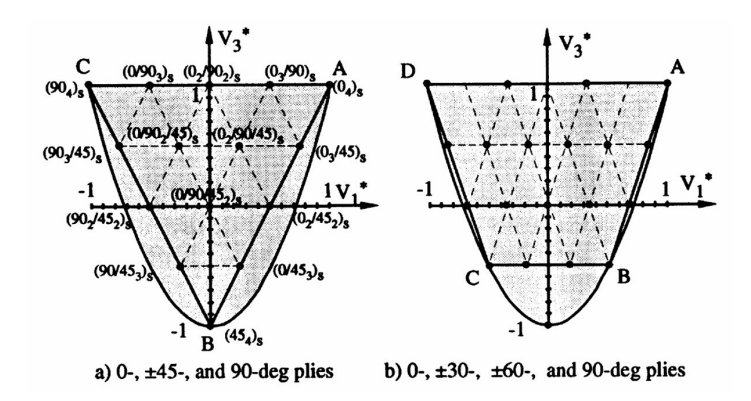


Figure 2.9: Feasible in-plane LP values for a 4-ply SS, considering two different sets of allowed fibre angles [Haftka and Gürdal 1992].

can be visualized in the $V_1^{\mathbf{A}} - V_2^{\mathbf{A}}$ space, generally known as Miki's diagram (see Figure 2.9).

Equation 2.23 was derived for LPs, when $V_{3,4}^{\mathbf{A}}$ is zero. However, for a fixed value of $V_1^{\mathbf{A}}$ and $V_2^{\mathbf{A}}$ the relation between the four in-plane LPs is derived in Fukunaga and Sekine 1992 as:

$$2(1+V_2^{\mathbf{A}})(V_3^{\mathbf{A}})^2 - 4V_1^{\mathbf{A}}V_3^{\mathbf{A}}V_4^{\mathbf{A}} + (V_4^{\mathbf{A}})^2 \le (V_2^{\mathbf{A}} - 2(V_1^{\mathbf{A}})^2 + 1)(1-V_2^{\mathbf{A}})$$
(2.24)

Although certain equations are derived considering in-plane and bending LPs, a unified relation between all 12 parameters is still not derived. C. Diaconu et al. 2002 discussed the feasible region of any two LPs, with a numerical derivation of the complete feasible domain using a variational approach. The equations defining the feasible region of LPs are discussed in C. G. Diaconu et al. 2002 and C. Diaconu and Sekine 2004, and can be referred to for further interest.

The fixed number of design variables (LPs) simplifies the formulation of optimization problems for stiffness tailoring. However, optimization using LPs yields just an optimal stiffness matrix; it does not provide the corresponding physical SS required for manufacturing. Therefore, laminate optimization is done on two levels. This bi-level optimization process refers to: (1) optimizing the stiffness using LPs, and then (2) retrieving a manufacturable SS that closely matches the optimal parameters (see Figure 2.10).

In the first level of the procedure, stiffness is optimized with respect to LPs as design variables. Grenestedt and Gudmundson 1993 discuss the convex nature of LPs. With the feasible region of the LPs defined, gradient-based optimization algorithms are generally utilized to optimize problems with continuous design variables.

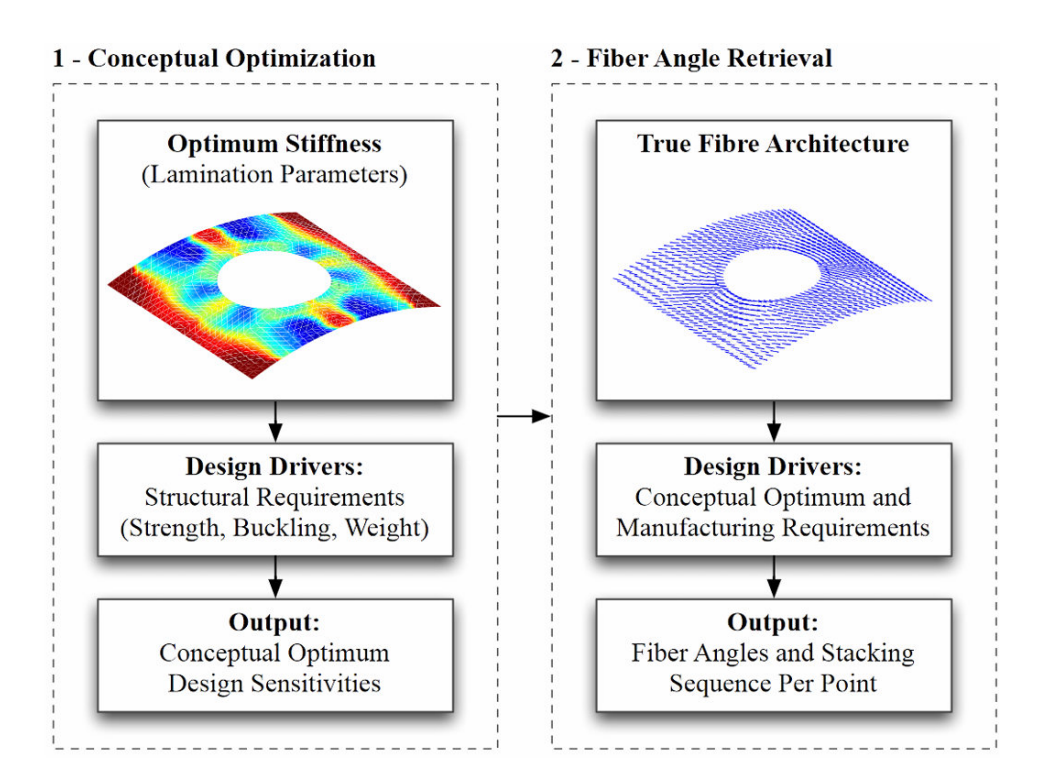


Figure 2.10: Bi-level optimization procedure of composite laminates [IJsselmuiden 2011].

The second level of the bi-level procedure addresses the inverse problem: retrieving a SS that corresponds to a target vector of LPs. Due to the periodic nature of trigonometric functions, the mapping from LP to SS is generally one-to-many because multiple SSs can produce the same set of LPs, preventing a direct inversion. To address this, various discrete optimization techniques are explored in the literature - such as Genetic Algorithms [Ghiasi et al. 2010, 2009; Irisarri et al. 2014] and Branch-and-bound strategies [Matsuzaki and Todoroki 2007] - to efficiently search for SS that best approximates a given LP vector.

An ADG is a graph that models how attributes (properties) of a system depend on one another. Each node represents an attribute that may vary during the design or use of a product, and each directed edge indicates a dependency [Zimmermann 2024]. Such an overview serves as a tool for the visualization of dependencies of the system (see Figure 2.11).

The graph can be interpreted in two directions:

• **Bottom-up:** This direction represents verification - checking whether a given set of design variables satisfies the laminate performance criteria.

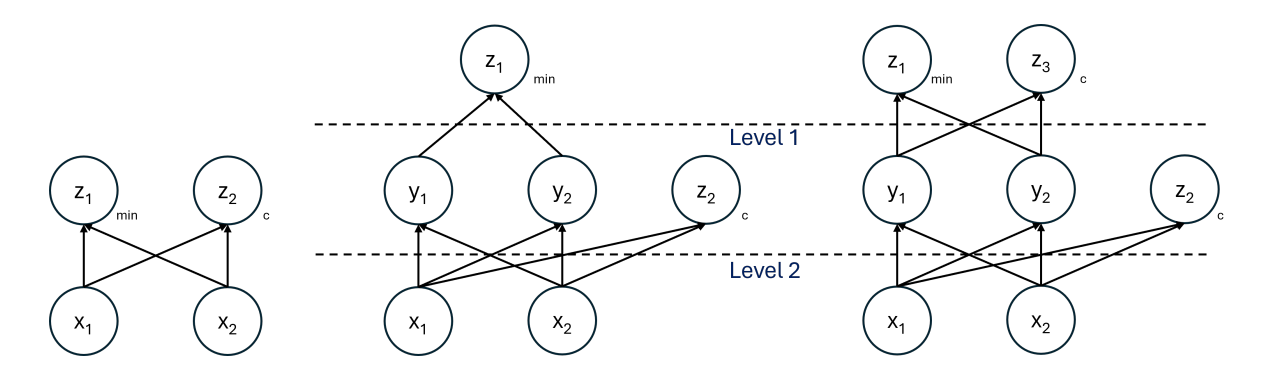


Figure 2.11: Visualization of bi-level ADG.

• **Top-down:** This direction outlines the optimization path - starting from high-level objectives and progressively determining the required design variables.

As the initial optimization problem is split into two levels, it becomes essential to correctly allocate constraints at every stage of the graph. However, not all constraints naturally align with intermediate variables. For example, a constraint defined at the SS level may not be directly definable with respect to LPs. When such constraints are omitted in early stages, the result is a mismatch between optimized variables and realizable designs, introducing epistemic uncertainty (uncertainty due to missing or incomplete information in the modelling process) (Figure 2.13). Figure 2.11 provides an overview of an ADG, in which the attributes at Level 1 serve as design variables for the optimization of the QoI at the top of the hierarchy. Simultaneously, the attributes at Level 2 act as design variables for optimizing the Level 1 attributes, which in this context serve as the QoIs for the lower level of optimization.

The design guidelines discussed in Chapter 2.1.2 are defined on SSs. They can be easily described as constraints in the optimization when considering fibre orientation and ply thickness as design variables. This is because of the presence of SS information during optimization. While considering LPs as design variables, the constraints are defined in the second optimization level where the information of SS is present. But, at the first level of the bi-level procedure, optimization is carried out based on the geometric bounds on the LPs and the described feasible region. The absence of the SS information poses a difficulty in enforcing the design guidelines in this step. This epistemic uncertainty creates a mismatch between the optimal set of LPs found and the retrieved SS. Addressing this mismatch is important, as it poses a structural and/or instability failure potential (see Figure 2.13).

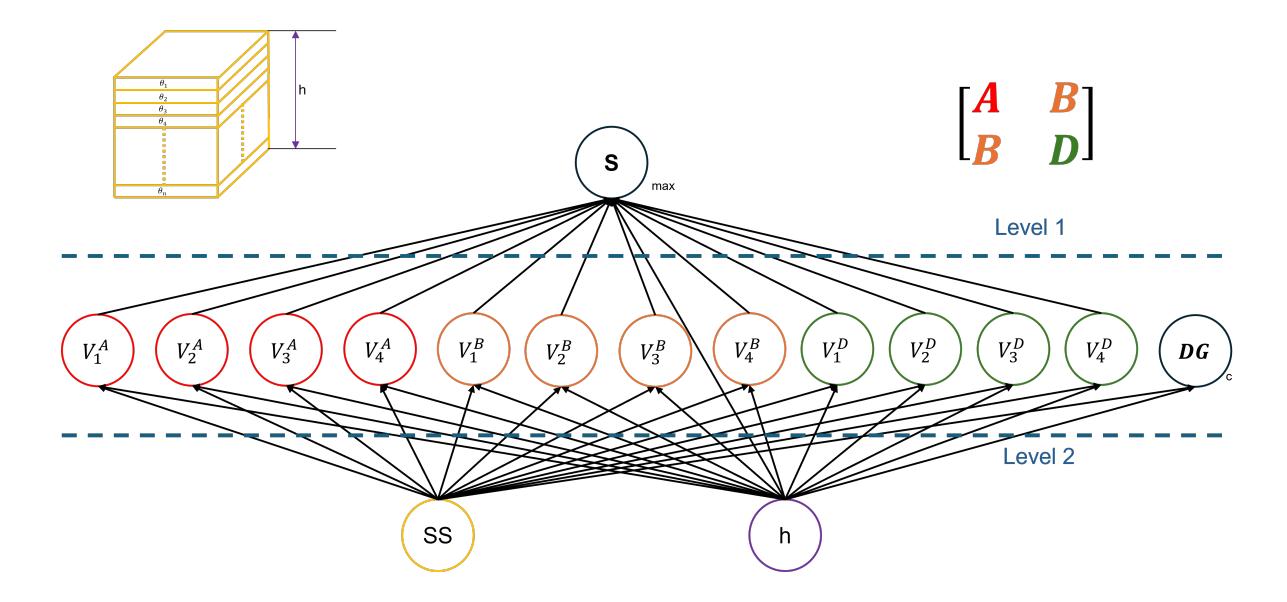


Figure 2.12: ADG for the laminate design.

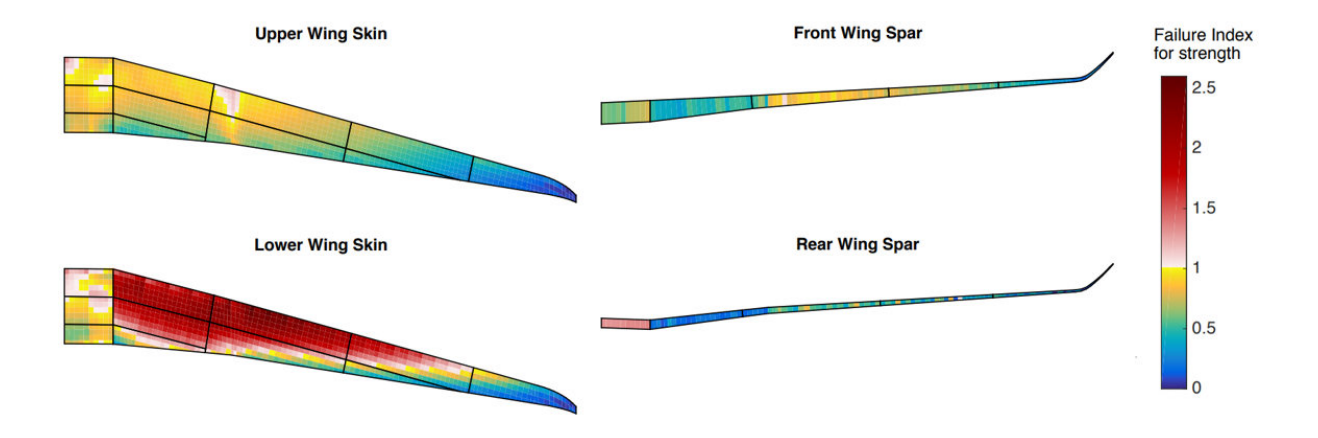


Figure 2.13: Unsatisfied strength constraint due to the mismatch error [Bordogna et al. 2016].

2.4 Design guidelines as optimization constraints

To mitigate the effects of mismatch error, numerous studies have been carried out to characterize the design guidelines in the LP space [Abdalla et al. 2009; Miki and Sugiyama 1993]. In this work, the term realizable domain refers to the set of LP vectors that correspond to real SSs which satisfy the imposed design guidelines.

The work carried out by Tsai and N. J. Pagano 1968 defines the LPs for symmetric and balanced laminates. As described in Chapter 2.1.2, symmetric laminates uncouple the in-plane and out-of-plane properties of the laminate. In the LP space, the four parameters $(V_{1,2,3,4}^{\mathbf{B}})$ used to calculate the corresponding \mathbf{B} matrix are equated to zero, characterizing the realizable domain for the symmetry design guideline.

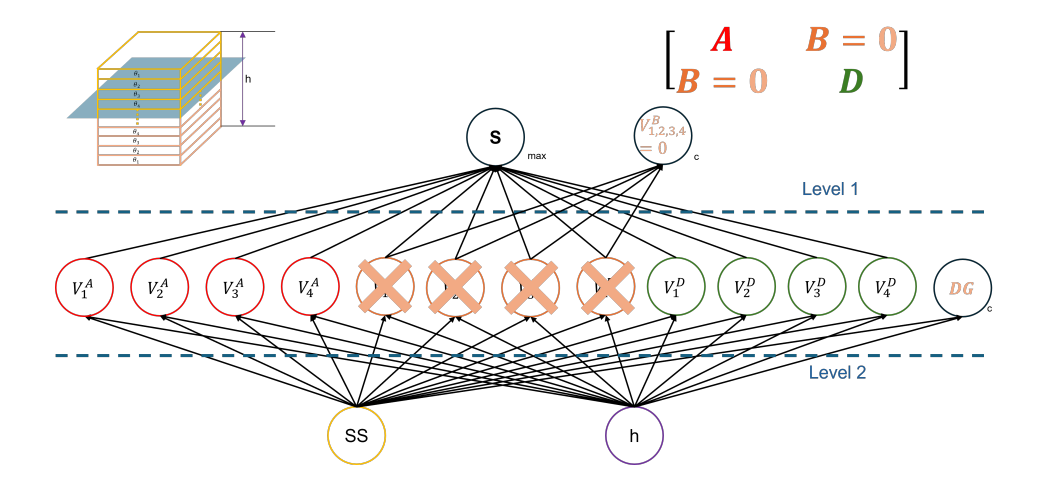


Figure 2.14: Adapted ADG for the laminate design when the symmetry design guideline characterized in LP space is enforced.

Similarly, the balance design guideline, enforced to maintain in-plane orthotropy, is defined by equating $V_{3,4}^{\mathbf{A}}$ defining the coupling terms in the \mathbf{A} matrix $(A_{16} \text{ and } A_{26})$ to 0.

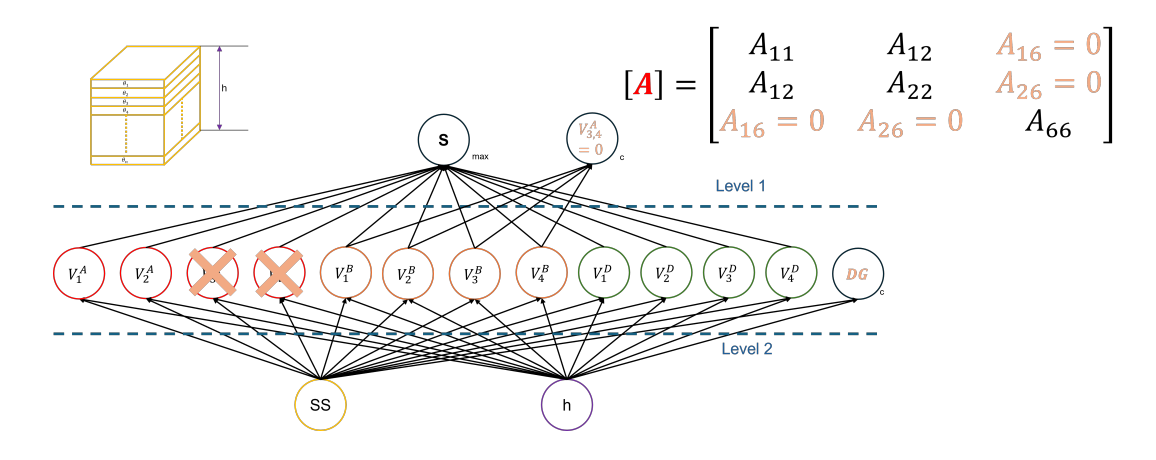


Figure 2.15: Adapted ADG for the laminate design when the balance design guideline characterized in LP space is enforced.

The two guidelines, symmetry and balance, are characterized as equality constraints. The 10% rule defines the constraint on the percentage of plies with certain fibre orientations. Abdalla et al. 2009 characterized the realizable domain as a shrinkage of the feasible domain by 40% (Figure 2.16). This is mathematically expressed as:

$$(1-4p)^{2} + (1-4p)V_{\mathbf{A}}^{2} - 2(V_{\mathbf{I}}^{\mathbf{A}})^{2} \ge 0$$
(2.25)

$$1 - 4p - V_2^{\mathbf{A}} \ge 0 \tag{2.26}$$

The rule visualized in Figure 2.17 is characterized for symmetric and balanced laminates in the literature [Abdalla et al. 2009]. The aforementioned percentage (in this case, 10%) in the characterized design guideline (Equation 2.25 and 2.26) is denoted by p.

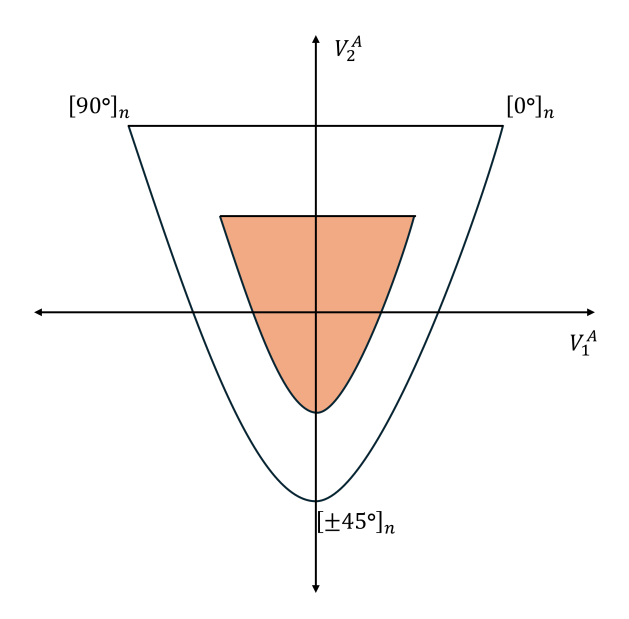


Figure 2.16: Shaded region illustrates the shrunk feasible domain due to the enforced 10% rule.

Table 2.1: Design guidelines characterized in the literature [Abdalla et al. 2009; Miki and Sugiyama 1993].

Design Guideline	Characterized Equation	Eq. Ref.
Symmetry	$V^{\mathbf{B}} = 0$	2.11
Balance	$V_1^{\mathbf{A}} = V_3^{\mathbf{A}} = 0$	2.12
10% Rule	$(1-4p)^2 + (1-4p)V_{\mathbf{A}}^2 - 2(V_1^{\mathbf{A}})^2 \ge 0$	
	where: $p = 0.1$	2.25

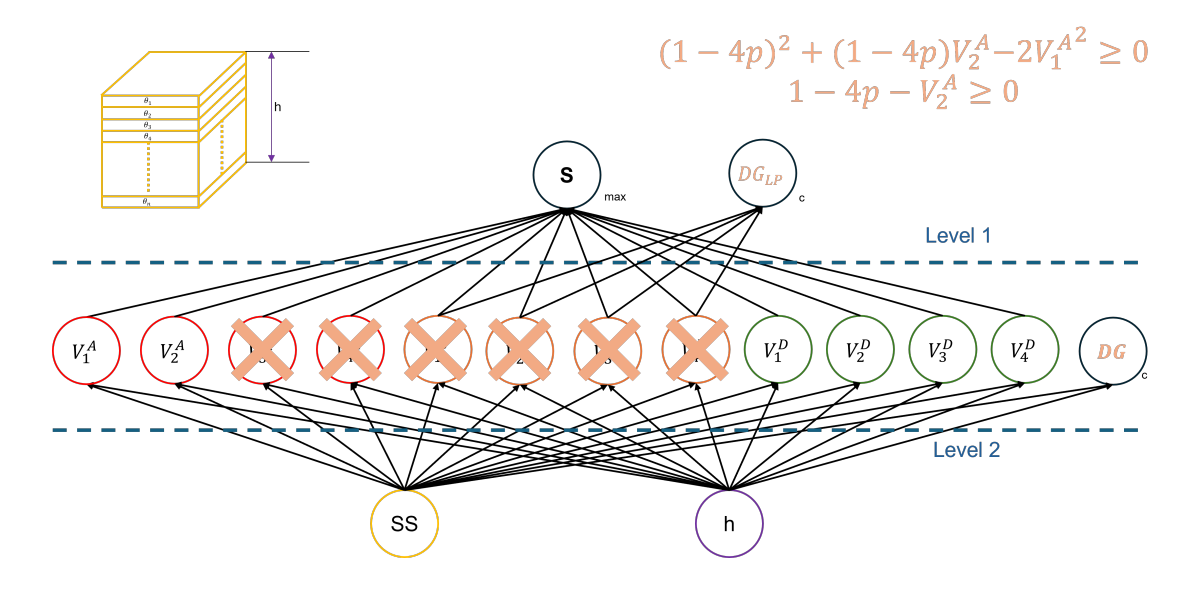


Figure 2.17: Adapted ADG for the laminate design when the 10% design guideline characterized in LP space is enforced.

2.5 Research gap

Design guidelines, namely symmetry, balance, and 10% rule, have been characterized as constraints for the optimization (see Table 2.1). However, some key guidelines, namely disorientation, damage tolerance, and contiguity, remain uncharacterized. Additionally, the explicit impact of existing guidelines on reducing mismatch between the optimal LPs and the designed SS has not yet been systematically quantified.

Three design guidelines, namely disorientation, damage tolerance, and contiguity, have not been mathematically characterized. Although symmetry, balance, and the 10% rule have been mathematically characterized in the literature, it doesn't explicitly explain how they reduce the epistemic uncertainty. This generates a gap in understanding the importance of defining the realizable domain. The characterized region of design guidelines with respect to LP is known as the realizable domain. Moreover, the question of epistemic uncertainty stemming from the lack of characterization of these design guidelines is to be explored.

Posed research questions addressing this gap are given in Chapter 3, followed by the derivation of the missing guidelines in Chapter 4.

3 Research Questions

This work is dedicated to addressing the research gaps identified in Chapter 2. In particular, mathematically defining disorientation, damage tolerance, contiguity, and quantitatively evaluating the reduction in mismatch between the two levels of bi-level optimization. Therefore, the research questions addressed by this thesis are:

- 1. How can the design guidelines be defined with respect to LPs without the SS information?
 - a) What are the implications on the size of the LP space given the derived design guidelines?
 - b) What is the accuracy of the classified realizable domain?
- 2. How do the characterized design guidelines influence the mismatch between the conceptual and the designed laminate stiffness?
 - a) How can the mismatch occurring due to the uncharacterized design guidelines be quantified?
 - b) Is the mismatch sensitive to the nature of applied loads?

4 Methodology

One of the fundamental issues in specifying design guidelines in the LP space stems from the absence of explicit SS information, which is discussed in Chapter 2. To deal with this limitation, vector analysis of LPs is employed, offering an intuitive approach to understanding and visualizing the impact of design guidelines in the LP space.

The framework has three main components: vector analysis, theoretical formulation, and computational verification. Vector analysis is performed by considering the 2D projections of LPs. The theoretical framework formulates the equations defining the realizable domain for disorientation, damage tolerance, contiguity, and balance guidelines individually, and studies their combined interaction. The computational process employs a brute-force search approach to verify the correctness and feasibility of the constraints.

4.1 Vector Analysis of lamination parameters

Irrespective of the SS, LPs individually always range between [-1, 1]. However, while each parameter is mathematically valid within this range, a vector representation of multiple LPs must satisfy interdependencies which define the mathematically feasible domain [Grenestedt and Gudmundson 1993; Miki and Sugiyama 1993].

Similarly, to gain deeper insight into the influence of individual ply contributions on the overall stiffness of a laminate, this study examines pairs of LPs. The contribution of each ply is understood by decomposing the LP equations into summation terms, each representing a vector. The components of the resultant vector, formed by summing these individual contributions, determine the final value of the respective LPs. The vector analysis approach clarifies how design guidelines influence the feasible domain in LP space. The laminates that follow the design guidelines are called practically feasible. The region defined by these guidelines in the LP space is called the realizable domain. The key aspects considered include:

- Pairwise Representation of LPs: By analyzing LPs in pairs, the interdependencies between different parameters become more apparent, aiding in the visualization of realizable solutions.
- **Geometric Interpretation:** The spatial distribution of feasible laminates is analyzed within the parameter space, allowing for a structured representation of realizability constraints.

A graphical representation of vector addition helps visualize how SSs influence the resulting LPs. The resultant vector can be broken down into components by summing the individual

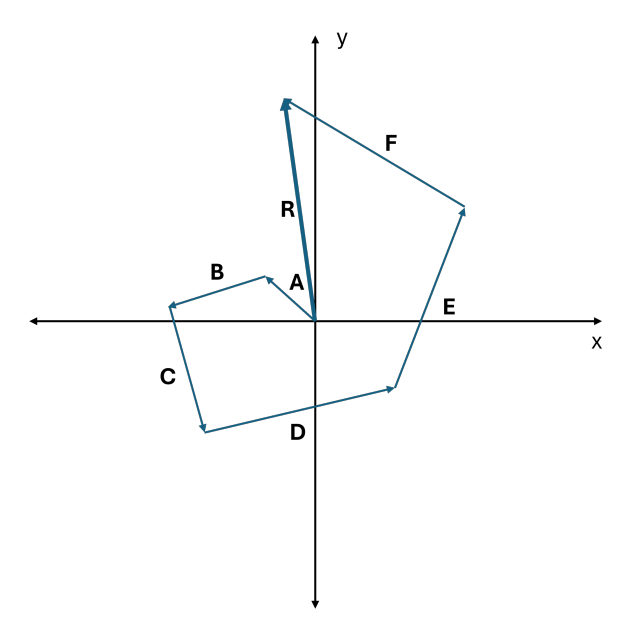


Figure 4.1: Visualization of vector summation.

effects of each vector in the system. Considering arbitrary vectors **A**, **B**, **C**, **D**, **E** and **F** as shown in Figure 4.1, the resultant vector is mathematically represented as:

$$\mathbf{R} = \mathbf{A} + \mathbf{B} + \mathbf{C} + \mathbf{D} + \mathbf{E} + \mathbf{F} \tag{4.1}$$

Each vector in Equation 4.1 is defined by its x and y components.

$$\mathbf{A} = M_A (\cos \theta_A \,\hat{i} + \sin \theta_A \,\hat{j})$$

$$\mathbf{B} = M_B (\cos \theta_B \,\hat{i} + \sin \theta_B \,\hat{j})$$

$$\mathbf{C} = M_C (\cos \theta_C \,\hat{i} + \sin \theta_C \,\hat{j})$$

$$\mathbf{D} = M_D (\cos \theta_D \,\hat{i} + \sin \theta_D \,\hat{j})$$

$$\mathbf{E} = M_E (\cos \theta_E \,\hat{i} + \sin \theta_E \,\hat{j})$$

$$\mathbf{F} = M_F (\cos \theta_F \,\hat{i} + \sin \theta_F \,\hat{j})$$
(4.2)

 $M_{\rm A}, M_{\rm B}, M_{\rm C}, M_{\rm D}, M_{\rm E}$ and $M_{\rm F}$ in Equation 4.2 represents the magnitudes of respective vectors. This formulation can be extended to an arbitrary number of vectors as:

$$\mathbf{R} = \sum_{k=1}^{n} M_k \cos \theta_k \,\hat{i} + \sum_{k=1}^{n} M_k \sin \theta_k \,\hat{j}$$
 (4.3)

In Equation 4.3, M_k represents the magnitude of each vector, and the components of the vectors are scaled by the trigonometric terms $\cos \theta_k$ and $\sin \theta_k$. This representation aligns with the physical behavior of LPs, reinforcing the idea behind representing plies as vectors.

4.2 Theoretical Formulation of realizable domains

For a structured analysis of LPs obeying different design guidelines, the LPs are represented in their summation form with respect to discrete number of layers. For a symmetric laminate of height h, ply thickness t, and total number of layers n, the eight LPs can be mathematically expressed as:

$$V_{1,2,3,4}^{\mathbf{A}} = \frac{2t}{h} \sum_{k=1}^{\frac{n}{2}} \left[\cos 2\theta_k, \cos 4\theta_k, \sin 2\theta_k, \sin 4\theta_k \right]$$

$$V_{1,2,3,4}^{\mathbf{D}} = \sum_{k=1}^{\frac{n}{2}} \left(\left(\frac{2z_k}{h} \right)^3 - \left(\frac{2z_{k-1}}{h} \right)^3 \right) \left[\cos 2\theta_k, \cos 4\theta_k, \sin 2\theta_k, \sin 4\theta_k \right]$$
(4.4)

Following this equation, constraints for four design guidelines - Disorientation, Damage tolerance, Contiguity, and Balance - are derived in terms of LPs.

4.2.1 Disorientation

The disorientation design guideline constraints the maximum angle jump between consecutive plies as per Chapter 2.1.2. Mathematically, it is represented as:

$$|\theta_k - \theta_{k-1}| \le 45^\circ$$

$$|\delta_k| \le 45^\circ \tag{4.5}$$

$$V_1^{\mathbf{D}} - V_3^{\mathbf{D}}$$

Since the constraint is enforced on the SS, LP pair $(V_1^{\mathbf{D}}, V_3^{\mathbf{D}})$ is used to visualize the effects of the design guideline in LP space. From Equation 4.4, $V_1^{\mathbf{D}}$ and $V_2^{\mathbf{D}}$ are written as:

$$V_1^{\mathbf{D}} = \sum_{k=1}^{\frac{n}{2}} w_k \cos 2\theta_k$$

$$V_3^{\mathbf{D}} = \sum_{k=1}^{\frac{n}{2}} w_k \sin 2\theta_k$$
(4.6)

Where,

$$w_k = \left(\frac{2z_k}{h}\right)^3 - \left(\frac{2z_{k-1}}{h}\right)^3$$

$$= \left(\frac{2kt}{nt}\right)^3 - \left(\frac{2(k-1)t}{nt}\right)^3$$

$$= \frac{8}{n^3}(k^3 - (k-1)^3)$$

$$w_k = \frac{8}{n^3} (3k^2 - 3k + 1) \tag{4.7}$$

While representing the summation terms as vectors, the following needs to be noted:

- Each summation term, representing its corresponding ply contribution, constitutes a vector.
- The orientation of each vector is measured by $2\theta_k$. Hence, the maximum angle difference between two consecutive plies, allowed by the disorientation guideline, is 90° ($|2\delta_k| \le 90^{\circ}$).

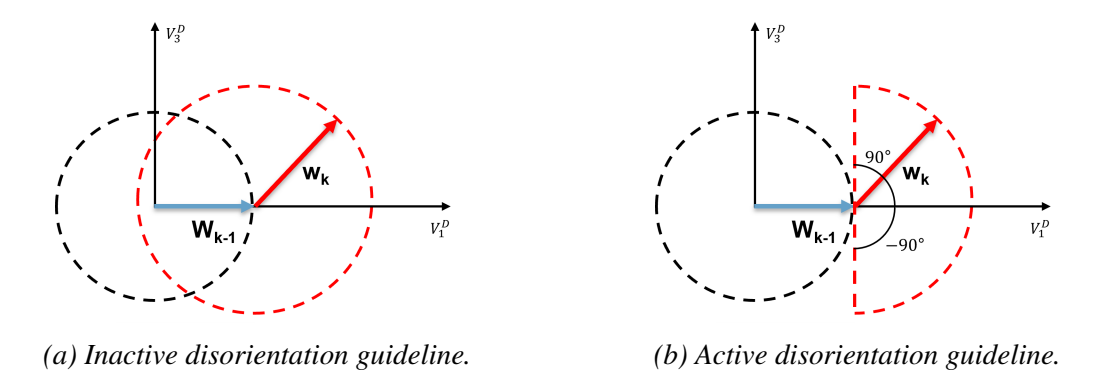


Figure 4.2: Influence of disorientation design guideline visualized by representing ply contributions as vectors in LP space.

Since the disorientation design guideline constrains the consecutive vectors, they can only rotate by a maximum of 90° relative to their previous vector. This restriction directly affects the realizability of certain LP combinations.

In an unconstrained system (Figure 4.2a), the vectors are free to rotate 360° , meaning that for any arbitrary ply angle θ_k , the set of possible resultant vectors forms a full circular region. However, under the disorientation constraint, the set of realizable resultant vectors is reduced to a semicircle (Figure 4.2b). This reduction affects the minimum attainable magnitude of the resultant vector.

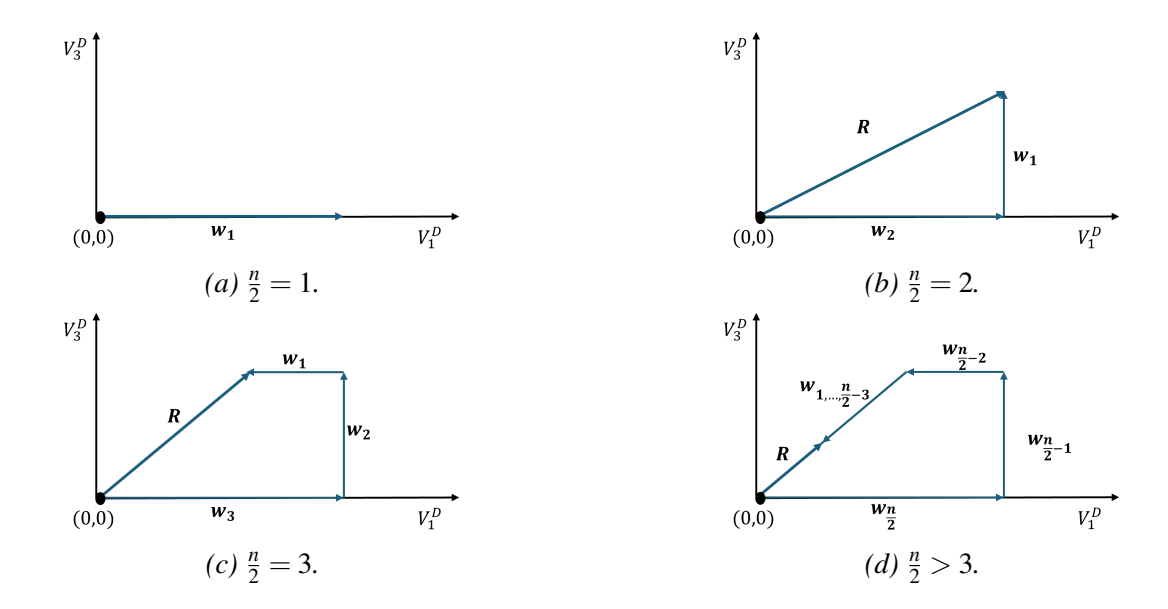


Figure 4.3: Sequential ply orientation selection to attain the minimum possible $(V_1^{\mathbf{D}}, V_3^{\mathbf{D}})$ pair.

The influence of fiber orientation on the resultant vector in lamination parameter space can be better understood by examining laminates with increasing numbers of plies. In a single-ply laminate, the contribution forms a vector with a fixed magnitude, and since there are no other plies to balance or cancel it, the resultant vector remains unchanged (see Figure 4.3a). When a second ply is added, even if it is oriented at the maximum allowable 90° relative to the first, the resultant vector does not decrease in magnitude. Instead, it changes direction, forming a right-angle path that increases the overall magnitude (see Figure 4.3b). With three plies, it becomes possible to partially cancel the effect of the previous vectors. This is most effective when each ply maintains the 90° disorientation limit, keeping all orientations within the allowed semicircle. However, even in this case, full cancellation is not possible because the added vectors only redirect the resultant rather than completely reverse it (see Figure 4.3c). In laminates with four or more plies, the additional vectors can be oriented more effectively to reduce the magnitude of the resultant vector (see Figure 4.3d). Each new vector offers more flexibility to redirect the overall direction of the resultant, allowing it to gradually move closer to the origin. The most effective reduction occurs when each new vector is chosen to counterbalance the influence of the previous ones.

A finite magnitude of the resultant vector would signify that the disorientation design guideline is active, and the entire mathematically feasible domain is not accessible. A crucial requirement in this process is that all vectors must follow the same rotation direction - clockwise or counterclockwise. If the vectors alternate in direction, the resultant vector will not be minimized but

instead oscillate away from the origin. This behavior occurs because alternating the rotation direction between consecutive plies prevents the sequential reduction of the contributions made by previous vectors. Instead of progressively canceling out earlier effects, the resultant vector oscillates, which maintains or even increases its magnitude rather than moving it closer to zero.

Thus, for a symmetric laminate of n plies, the minimum magnitude of the resultant vector is achieved when the maximum number of vectors are oriented in a single direction (either all clockwise or all counterclockwise). Up to three vectors are oriented at the maximum allowable angle difference of 90° relative to the previous vector. The remaining vectors are oriented towards the origin, progressively minimizing the magnitude of the resultant vector \mathbf{R}_d . Mathematically, this can be calculated as:

$$|\mathbf{R}_d| = OA - AB$$

$$= |\mathbf{w}_{\frac{\mathbf{n}}{2}} + \mathbf{w}_{\frac{\mathbf{n}}{2} - 1} + \mathbf{w}_{\frac{\mathbf{n}}{2} - 2}| - \sum_{k=1}^{\frac{n}{2} - 3} |\mathbf{w}_{\mathbf{k}}|$$

Equation 4.7 gives each vector's magnitude. Using said equation, the magnitude of the resultant vector shown in Figure 4.3d is calculated as:

$$|\mathbf{R}_d| = \frac{8}{n^3} \left(\sqrt{\frac{9n^4}{16} - \frac{27n^3}{4} + \frac{267n}{4} - 279n + 373} - \left(\frac{n}{2} - 3\right)^3 \right) \tag{4.8}$$

Since the LPs $V_1^{\mathbf{D}}$ and $V_3^{\mathbf{D}}$ are derived from the vector summation of individual ply contributions, their relationship inherently follows a circular equation due to the underlying trigonometric terms $(\cos 2\theta_k)$ and $(\sin 2\theta_k)$ present in their definitions (Equation 4.6). The derived expression for the magnitude of resultant vector $|\mathbf{R}_d|$ (Equation 4.8) represents the minimum attainable value under the disorientation constraint. Consequently, the realizable domain for the disorientation design guideline in the $V_1^{\mathbf{D}}$ - $V_3^{\mathbf{D}}$ space is characterized as:

$$(V_1^{\mathbf{D}})^2 + (V_3^{\mathbf{D}})^2 \ge |\mathbf{R}_d|^2 \tag{4.9}$$

This inequality ensures that the calculated LPs stay within the realizable domain. It confirms that at least one SS is available to accommodate the favourable $(V_1^{\mathbf{D}}, V_3^{\mathbf{D}})$ combination while respecting the disorientation guideline.

$$V_1^{\mathbf{A}} - V_3^{\mathbf{A}}$$

Representing $V_1^{\mathbf{A}}$ and $V_3^{\mathbf{A}}$ in the form of Equation 4.6, it is observed that the magnitude of the vectors is independent of the ply position (Equation 4.10).

$$V_3^{\mathbf{A}} = \sum_{k=1}^{\frac{n}{2}} w_k \sin 2\theta_k$$
$$V_1^{\mathbf{A}} = \sum_{k=1}^{\frac{n}{2}} w_k \cos 2\theta_k$$

Where,

$$w_k = \frac{2}{n} \tag{4.10}$$

Since the magnitude of every vector is a constant, for a symmetric laminate with more than 3 vectors, the disorientation guideline becomes inactive in the $V_1^{\mathbf{A}}$ - $V_3^{\mathbf{A}}$ space.

$$\underline{V_1^{\mathbf{D}} - V_2^{\mathbf{D}}}$$

$$V_{1}^{\mathbf{D}} = \sum_{k=1}^{\frac{n}{2}} w_{k} \cos 2\theta_{k}$$

$$V_{2}^{\mathbf{D}} = \sum_{k=1}^{\frac{n}{2}} w_{k} \cos 4\theta_{k}$$
(4.11)

Where,

$$w_k = \frac{8}{n^3} (3k^2 - 3k + 1)$$

The k^{th} summation term in Equation 4.11 is represented as $(V^{\mathbf{D}})_k$, and the relation between each summation term is parabolic in nature (see Equation 2.23). Which is represented as:

$$(V_2^{\mathbf{D}})_k = w_k \cos 4\theta_k$$

= $w_k (2(\cos 2\theta_k)^2 - 1)$

$$(V_2^{\mathbf{D}})_k = \frac{2}{w_k} (V_1^{\mathbf{D}})^2 - w_k \tag{4.12}$$

As per Equation 4.11, the LP $V_2^{\mathbf{D}}$ attains a value of one for laminates composed exclusively of 0° and 90° plies, due to $\cos(4\times0^{\circ})$ and $\cos(4\times90^{\circ})$. In contrast, the value of $V_1^{\mathbf{D}}$ is influenced by the through-thickness distribution and relative proportion of these ply orientations within the laminate. Hence, to account for the disorientation guideline 0° and 90° plies are clubbed together, and at least one $\pm 45^{\circ}$ ply is placed between them. The subsequent mathematical derivation accounts for this constraint.

For a symmetric laminate consisting of $\frac{n}{2}$ plies above the mid-plane, the first "a" number of plies are oriented at 90°, followed by a single ply at 45°, with the remaining plies oriented at 0°. This stacking arrangement is designed to achieve the maximum possible value of the LP $V_2^{\mathbf{D}}$ while ensuring compliance with the disorientation design guideline.

The value of a can be varied from $[2, \frac{n}{2} - 1]$ to obtain the exact fit of the curve. The following mathematical derivation demonstrates the procedure for determining the realizable maximum value of $V_2^{\mathbf{D}}$ when $V_1^{\mathbf{D}} = 0$.

$$V_1^{\mathbf{D}} = \sum_{k=1}^{a} w_k \cos 2 \times 90^\circ + w_{a+1} \cos 2 \times 45^\circ + \sum_{k=a+2}^{\frac{n}{2}} w_k \cos 2 \times 0^\circ$$
$$= (\frac{2a}{n})^3 \times (-1) + 0 + (1 - (\frac{2(a+1)}{n})^3) \times 1$$
$$= -(\frac{1}{n})^3 (2a^3 + 3a^2 + 3a + 1 - (\frac{n}{2})^3)$$

The value of a, when $V_1^{\mathbf{D}}$ is equal to 0, is calculated by solving the polynomial:

$$2a^3 + 3a^2 + 3a + 1 - (\frac{n}{2})^3 = 0 (4.13)$$

To simplify the analytical model, a linear fit was applied to the root of this cubic polynomial as a function of the total number of plies n, as shown in Figure 4.4.

The fit shows a high R^2 value of 1.000, indicating an excellent linear correlation. This enables an approximation for constructing the disorientation boundary across varying ply counts, thereby reducing computational cost in practical evaluations.

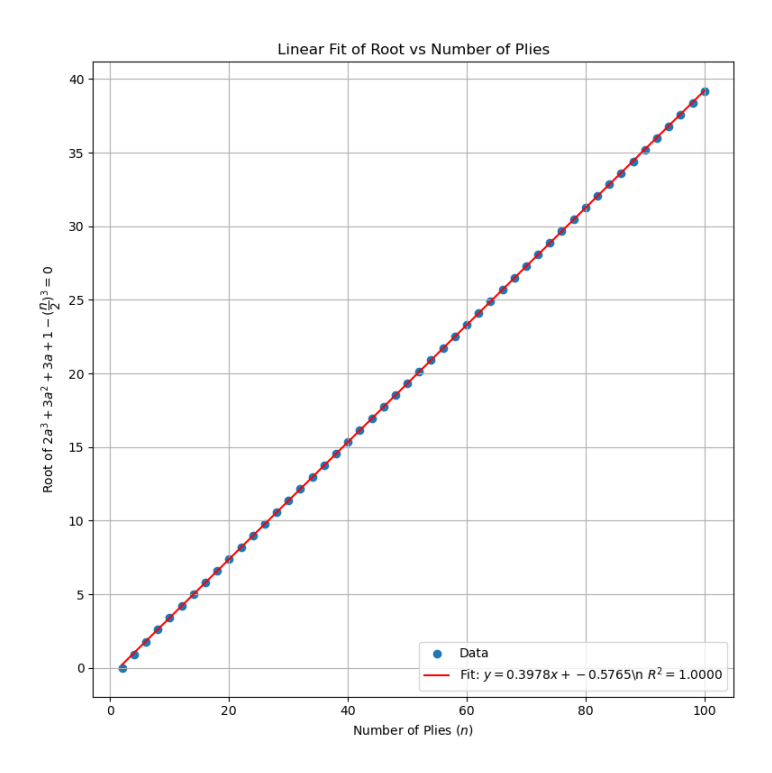


Figure 4.4: Linear regression of the root of the cubic equation $2a^3 + 3a^2 + 3a + 1 = \left(\frac{n}{2}\right)^3$ with respect to total number of plies n.

Similarly,

$$V_2^{\mathbf{D}} = \sum_{k=1}^{a} w_k \cos 4 \times 90^{\circ} + w_{a+1} \cos 4 \times 45^{\circ} + \sum_{k=a+2}^{\frac{n}{2}} w_k \cos 4 \times 0^{\circ}$$

$$= (\frac{2a}{n})^3 \times 1 + ((\frac{2(a+1)}{n})^3 - (\frac{2(a)}{n})^3) \times (-1) + (1 - (\frac{2(a+1)}{n})^3) \times 1$$

$$= 1 + \frac{2 \times 8}{n^3} (-3a^2 - 3a - 1)$$

$$= 1 + \frac{16}{n^3} (2a^3 - (\frac{n}{2})^3)$$

$$V_2^{\mathbf{D}} = \frac{32a^3}{n^3} - 1$$

By substituting the value of a obtained from the linear fit, the realizable maximum value of $V_2^{\mathbf{D}}$ can be determined. This value is a function of both the variable a and the LP $V_1^{\mathbf{D}}$. Consequently,

the realizable domain for disorientation design guideline in the $V_1^{\mathbf{D}}-V_2^{\mathbf{D}}$ space is characterized as:

$$V_2^{\mathbf{D}} \le \left(4\left(\frac{1.153}{n}\right)^3 - 1.1824\right) \left(V_1^{\mathbf{D}}\right)^2 + 2.1824 - 4\left(\frac{1.153}{n}\right)\right)^3$$
 (4.14)

$$V_1^{\mathbf{A}} - V_2^{\mathbf{A}}$$

As discussed, the in-plane LPs $V_{1,2,3,4}^{\mathbf{A}}$ are invariant of the SS. This is mathematically represented as:

$$V_{1}^{\mathbf{A}} = \sum_{k=1}^{\frac{n}{2}} w_{k} \cos 2\theta_{k}$$

$$V_{2}^{\mathbf{A}} = \sum_{k=1}^{\frac{n}{2}} w_{k} \cos 4\theta_{k}$$
(4.15)

Where,

$$w_k = \frac{2}{n}$$

Similar to the characterization of the $V_1^{\mathbf{D}}$ - $V_2^{\mathbf{D}}$ relationship, the disorientation guideline requires the inclusion of at least one $\pm 45^{\circ}$ ply to prevent abrupt fibre angle transitions. In contrast to the bending LPs, the contribution of the $\pm 45^{\circ}$ ply to the in-plane LPs is independent of its position within the laminate.

Building on this, the realizable maximum value of $V_2^{\mathbf{A}}$. Hence, the in-plane LP $V_2^{\mathbf{A}}$ is formulated as:

$$V_2^{\mathbf{A}} = \sum_{k=1}^{a} w_k \cos 4 \times 90^{\circ} + w_{a+1} \cos 4 \times 45^{\circ} + \sum_{k=a+2}^{\frac{n}{2}} w_k \cos 4 \times 0^{\circ}$$

$$= \frac{2a}{n} \times 1 + \left(\frac{2(a+1)}{n} - \frac{2(a)}{n}\right) \times (-1) + \left(\frac{n}{n} - \frac{2(a+1)}{n}\right) \times 1$$

$$= \frac{1}{n} (2a + 2a - 2a - 2 + n - 2a - 2)$$

$$V_2^{\mathbf{A}} = \frac{n-4}{n}$$

Consequently, the realizable domain for the disorientation design guideline in the $V_1^{\bf A}-V_2^{\bf A}$ space is characterized as

$$V_2^{\mathbf{A}} \le \frac{n-4}{n} \tag{4.16}$$

Using Equations 4.9, 4.14, and 4.16, the realizable domain associated with the disorientation design guideline is formally characterized.

4.2.2 Damage Tolerance

The damage tolerance design guideline constrains the fibre orientation of the outermost plies. Mathematically, the first interpretation of the damage tolerance design guideline explained in Chapter 2.1.2 is represented as:

$$|\theta_n| = 45^{\circ}$$

$$V_1^{\mathbf{D}} - V_3^{\mathbf{D}}$$

Contrary to the disorientation guideline, damage tolerance constraints both the ply position and its orientation. Hence, the vector's orientation and magnitude, representing the contribution of the outermost ply, are fixed.

This has a significant geometric implication in the LP space. Instead of tracing arcs or circles, as seen in vector rotation scenarios (see Figure 4.2b), fixing the vector's orientation and magnitude effectively shifts the origin of the vector summation. In other words, the baseline contribution of the outermost ply becomes a constant offset, altering the shape and position of the realizable domain. Therefore, when characterizing the realizable region under damage tolerance, the domain is not simply clipped or rotated; it is translated due to this fixed vector contribution.

The design guideline is analytically formulated by splitting the summation in a way that isolates the outermost ply's influence as:

$$V_{1}^{\mathbf{D}} = \sum_{k=1}^{\frac{n}{2}-1} w_{k} \cos 2\theta_{k} + w_{\frac{n}{2}} \cos 2\theta_{\frac{n}{2}} = \sum_{k=1}^{\frac{n}{2}-1} w_{k} \cos 2\theta_{k} + w_{\frac{n}{2}} \cos 2 \times 45^{\circ}$$

$$V_{1}^{\mathbf{D}} = \sum_{k=1}^{\frac{n}{2}-1} w_{k} \cos 2\theta_{k}$$

$$(4.17)$$

$$V_3^{\mathbf{D}} = \sum_{k=1}^{\frac{n}{2}-1} w_k \sin 2\theta_k + w_{\frac{n}{2}} \sin 2\theta_{\frac{n}{2}} = \sum_{k=1}^{\frac{n}{2}-1} w_k \sin 2\theta_k + w_{\frac{n}{2}} \sin 2 \times \pm 45^{\circ}$$

$$V_3^{\mathbf{D}} \mp w_{\frac{n}{2}} = \sum_{k=1}^{\frac{n}{2}-1} w_k \sin 2\theta_k$$
(4.18)

The LPs show a circular dependency as per Equations 4.17 and 4.18 because the contributions from all plies except the outermost are expressed as weighted sums of trigonometric functions $\cos 2\theta_k$ and $\sin 2\theta_k$, which naturally describe points on a unit circle. However, in the case of the damage tolerance guideline, the outermost ply's orientation is fixed, and its corresponding contribution to $V_3^{\mathbf{D}}$ is constant and non-zero, i.e., $w_{n/2}\sin(2\times \pm 45^\circ) = \pm w_{n/2}$. This shifts the origin of the circle in the $V_3^{\mathbf{D}}$ direction, while the rest of the plies still define a circular pattern centered around this shifted origin. The realizable domain for the damage tolerance design guideline in the $V_1^{\mathbf{D}} - V_3^{\mathbf{D}}$ space is characterized as:

ace is characterized as:
$$(V_1^{\mathbf{D}})^2 + (V_3^{\mathbf{D}} \mp w_{\frac{n}{2}})^2 \le (\sum_{k=1}^{\frac{n}{2}-1} w_k)^2$$

$$(V_1^{\mathbf{D}})^2 + (V_3^{\mathbf{D}} \mp w_{\frac{n}{2}})^2 \le (\frac{n-2}{n})^6$$
(4.19)

The inequality seen in Equation 4.19 arises because it describes all possible resultant vectors formed by the contributions of the inner plies alone. Given that the magnitude of their combined vector cannot exceed the total sum of their weights. This is similar to the well-known result that the magnitude of a vector composed of cos and sin terms is bounded by the Euclidean norm of their weights [Eliezer and Daykin 1967].

$$V_1^{\mathbf{D}} - V_2^{\mathbf{D}}$$

The LPs $V_1^{\mathbf{D}}$ and $V_2^{\mathbf{D}}$ are mathematically represented by separating the outer ply contribution as:

$$V_{1}^{\mathbf{D}} = \sum_{k=1}^{\frac{n}{2}-1} w_{k} \cos 2\theta_{k} + w_{\frac{n}{2}} \cos 2\theta_{\frac{n}{2}}$$

$$= \sum_{k=1}^{\frac{n}{2}-1} w_{k} \cos 2\theta_{k} + w_{\frac{n}{2}} \cos 2 \times 45^{\circ}$$

$$= \sum_{k=1}^{\frac{n}{2}-1} w_{k} \cos 2\theta_{k}$$

$$V_{2}^{\mathbf{D}} = \sum_{k=1}^{\frac{n}{2}-1} w_{k} \cos 4\theta_{k} + w_{\frac{n}{2}} \cos 4\theta_{\frac{n}{2}}$$

$$= \sum_{k=1}^{\frac{n}{2}-1} w_{k} \cos 4\theta_{k} + w_{\frac{n}{2}} \cos 4 \times 45^{\circ}$$

$$= \sum_{k=1}^{\frac{n}{2}-1} w_{k} \cos 4\theta_{k} - w_{\frac{n}{2}}$$

By representing the summation terms as a separate variable, $V_1^{\mathbf{D}}$ and $V_2^{\mathbf{D}}$ can be rewritten as:

$$V_1^{\mathbf{D}} = X \tag{4.20}$$

$$V_2^{\mathbf{D}} = Y - (1 - b) \tag{4.21}$$

Where,

$$X = \sum_{k=1}^{\frac{n}{2}-1} w_k \cos 2\theta_k$$

$$Y = \sum_{k=1}^{\frac{n}{2}-1} w_k \cos 4\theta_k$$

$$w_{\frac{n}{2}} = \frac{(n/2)^3}{(n/2)^3} - \frac{((n/2)-1)^3}{(n/2)^3}$$

$$= 1 - (\frac{n-2}{n})^3$$

Hence,

$$b = \left(\frac{n-2}{n}\right)^3$$

The outer boundary of the corresponding LP space can be traced by orienting every vector in the same direction. Since the parameters are defined with cosine terms, the variables X and Y defined earlier are written considering laminates made up of plies oriented in $+\theta$ and $-\theta$ direction.

$$Y = \sum_{k=1}^{\frac{n}{2}-1} w_k \cos 4\theta_k$$

= $((\frac{n-2}{n})^3 - (\frac{1-1}{(n/2)})^3) \cos 4\theta$
= $b \times \cos 4\theta$

Similarly,

$$X = b\cos 2\theta$$
$$b\cos 4\theta = b(2(\cos 2\theta)^2 - 1)$$
$$= 2b(\cos 2\theta)^2 - b$$

Hence, for an arbitrary SS, the equation is substituted by an inequality:

$$Y \ge \frac{2}{b}X^2 - b \tag{4.22}$$

By substituting Equations 4.20 and 4.20 in Equation 4.22, the realizable domain in the LP space is mathematically represented as:

$$V_2^{\mathbf{D}} + (1 - b) \ge \frac{2}{b} (V_1^{\mathbf{D}})^2 - b$$

$$V_2^{\mathbf{D}} \ge \frac{2}{b} (V_1^{\mathbf{D}})^2 - 1$$
(4.23)

Equation 4.23 is a parabolic equation defining the realizable domain satisfying the damage tolerance design guideline. The values of LPs $V_{1,2}^{\mathbf{D}}$ range between [-1,1]. The new range of LPs satisfying the damage tolerance design guideline is calculated as:

$$-1 \le \cos 2\theta_k \le +1$$

$$-b \le b \times \cos 2\theta_k \le +b$$
(4.24)

From Equation 4.20 the range of $V_1^{\mathbf{D}}$ is calculated as:

$$-b \le V_1^{\mathbf{D}} \le +b \tag{4.25}$$

Similarly,

$$-b \le b \times \cos 4\theta_k \le +b$$

$$-b \le Y \le +b$$

$$-b - (1-b) \le Y - (1-b) \le +b - (1-b)$$

$$-1 \le V_2^{\mathbf{D}} \le 2b - 1 \tag{4.26}$$

$$V_1^{\mathbf{A}} - V_2^{\mathbf{A}}$$

The mathematical representation of damage tolerance in $V_1^{\mathbf{A}} - V_2^{\mathbf{A}}$ space is expressed as:

$$V_1^{\mathbf{A}} = \sum_{k=1}^{\frac{n}{2}-1} w_k \cos 2\theta_k + w_{\frac{n}{2}} \cos 2\theta_{\frac{n}{2}}$$

$$V_2^{\mathbf{A}} = \sum_{k=1}^{\frac{n}{2}-1} w_k \cos 4\theta_k + w_{\frac{n}{2}} \cos 4\theta_{\frac{n}{2}}$$

Where,

$$w_k = \frac{2}{n}$$
$$\theta_{\frac{n}{2}} = \pm 45^{\circ}$$

Substituting these variables into the LPs:

$$V_1^{\mathbf{A}} = \sum_{k=1}^{\frac{n}{2}-1} \frac{2}{n} \cos 2\theta_k + \frac{2}{n} \cos (2 \times \pm 45^\circ)$$

$$= \frac{2}{n} \sum_{k=1}^{\frac{n}{2}-1} \cos 2\theta_k$$

$$V_2^{\mathbf{A}} = \frac{2}{n} \sum_{k=1}^{\frac{n}{2}-1} \cos 4\theta_k + \frac{2}{n} \cos (4 \times \pm 45^\circ)$$

$$= \frac{2}{n} \sum_{k=1}^{\frac{n}{2}-1} \cos 4\theta_k - \frac{2}{n}$$

Similar to the bending LP space, the realizable domain for the damage tolerance design guideline in $V_1^{\mathbf{A}} - V_2^{\mathbf{A}}$ space is characterized as:

$$V_{2}^{\mathbf{A}} \ge \frac{2n}{n-2} (V_{1}^{\mathbf{A}})^{2} - 1$$

$$-\frac{n-2}{n} \le V_{1}^{\mathbf{A}} \le \frac{n-2}{n}$$

$$-1 \le V_{2}^{\mathbf{A}} \le 2\frac{n-2}{n} - 1$$
(4.27)

$$V_1^{\mathbf{A}} - V_3^{\mathbf{A}}$$

As previously shown in the characterization of the $V_{1,3}^D$ LP space, the realizable domain is defined by a circular inequality, as given in Equation 4.19. A similar approach is used here, where the inequality describing the realizable domain is derived by translating the circle's origin and modifying its radius to account for the sum of vector magnitudes, excluding the contribution from the outermost ply.

$$(V_1^{\mathbf{A}})^2 + (V_3^{\mathbf{A}} \mp w_{\frac{n}{2}}) \le (\frac{n-2}{n})^2$$

$$(V_1^{\mathbf{A}})^2 + (V_3^{\mathbf{A}} \mp \frac{2}{n})^2 \le (\frac{n-2}{n})^2$$
(4.28)

4.2.3 Contiguity

The contiguity design guideline restricts the maximum number of consecutive plies sharing the same fibre orientation, which are prone to delamination and local failure. When visualized in the LP space, this constraint prevents all vector contributions from aligning in the same direction. As a result, the magnitude of the resultant vector is reduced, and the outer boundary of the realizable domain becomes unattainable.

Due to the discrete nature of the total number of plies in a laminate, a continuous approximation is used to derive an analytical formulation. The following derivation quantifies the maximum reduction in the feasible region as the total number of plies n tends to infinity.

$$\underline{V_1^{\mathbf{D}} - V_3^{\mathbf{D}}}$$

Figure 4.5 illustrates an arbitrary symmetric laminate satisfying the contiguity guideline, with the maximum allowable number of consecutive plies set to four. The parameter δ in the figure denotes the minimum allowable step size for fibre placement. For instance, if $\delta = 15^{\circ}$, fibres can only be oriented in discrete increments such as $-90^{\circ}, -75^{\circ}, \dots, 75^{\circ}$. In this study, δ is fixed at 15° , while the contiguous ply limit is treated as a variable *limit* in the derivation.

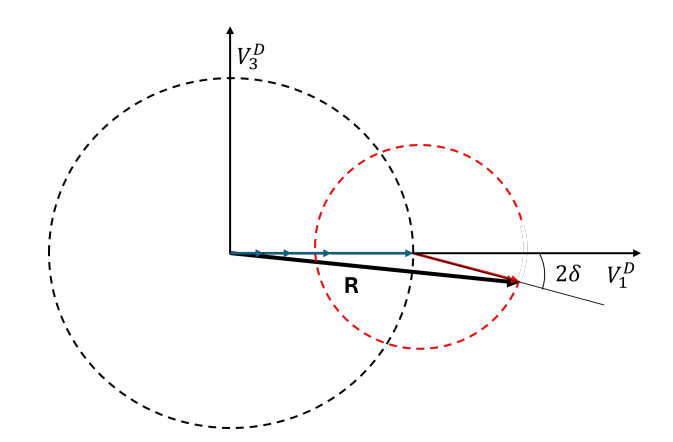


Figure 4.5: Schematic representation of vector contribution under contiguity constraint.

The derivation proceeds under the following assumptions:

- The total number of plies is approximated as a continuous variable.
- For a given contiguous ply limit L, the symmetric half-laminate is divided into equal groups of (L+1) plies, resulting in $\frac{n}{2(L+1)}$ such groups.

• The plies inserted to satisfy the contiguity rule are placed as close to the mid-plane as possible to maximize the magnitude of the resultant vector \mathbf{R}_c .

To compute the maximum magnitude of the realizable resultant vector, the contributions of the plies enforcing the contiguity constraint are isolated, assuming all other plies are oriented at 0° , while the constraint plies are oriented at δ .

The position of the inserted plies is defined as:

$$\frac{n}{2} - L \times k$$
, where $k = 1, \dots, \frac{n-2}{2 \times L}$

The corresponding vector weight is calculated using the standard weighting function for bending parameters (Equation 4.7):

$$w_k = \frac{8}{n^3} \left(3\left(\frac{n}{2} - limit \times k\right)^2 - 3\left(\frac{n}{2} - L \times k\right) + 1 \right)$$

$$= \frac{8}{n^3} \left(\frac{3n^2}{4} + 3limit^2k^2 - 3n \times L \times k - \frac{3n}{2} + 3L \times k + 1 \right)$$

$$= \frac{8}{n^3} \left(\left(\frac{3n^2}{4} - \frac{3n}{2} + 1\right) + 3L^2k^2 - (3n \times L - 3L)k \right)$$

$$w_k = \frac{8}{n^3} \left(\left(\frac{3n^2}{4} - \frac{3n}{2} + 1 \right) + 3L^2 \times k^2 - (3n \times L - 3L) \times k \right)$$
 (4.29)

Using standard summation identities:

$$\sum_{k=1}^{a} 1 = a, \quad \sum_{k=1}^{a} k = \frac{a(a+1)}{2}, \quad \sum_{k=1}^{a} k^2 = \frac{a(a+1)(2a+1)}{6}$$

The total weighted contribution is given by:

$$\sum_{k=1}^{a} w_k = \frac{8}{n^3} \left[\left(\frac{3n^2}{4} - \frac{3n}{2} + 1 \right) a + 3L^2 \times \frac{a(a+1)(2a+1)}{6} - (3n \times L - 3L) \times \frac{a(a+1)}{2} \right]$$
(4.30)

where $a = \frac{n-2}{2 \times L}$.

As $n \to \infty$, the normalized weight summation converges to:

$$\lim_{n \to \infty} \sum_{k=1}^{a} w_k = \frac{1}{L} \tag{4.31}$$

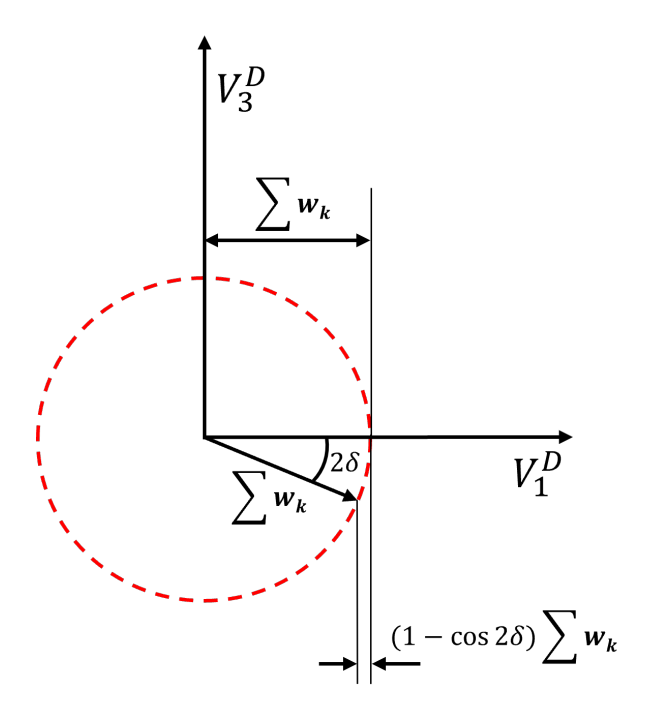


Figure 4.6: Convergence of weight summation with increasing number of plies.

The reduction in the realizable radius is computed as:

$$\begin{aligned} |\mathbf{R}_c^{\mathbf{D}}| &= \sqrt{(1 - (1 - \cos 2\delta) \times \frac{1}{L})^2 + \left(\sin 2\delta \times \frac{1}{L}\right)^2} \\ &= \frac{1}{L} \sqrt{L^2 + 4\sin^2 \delta \times (1 - L)} \end{aligned}$$

The realizable domain under the contiguity constraint for an infinite number of plies is given by:

$$(V_1^{\mathbf{D}})^2 + (V_3^{\mathbf{D}})^2 \le |\mathbf{R}_c^{\mathbf{D}}| \tag{4.32}$$

For laminates with a finite number of plies, Equation 4.30 can be substituted in place of the asymptotic value in Equation 4.31 to obtain a non-conservative characterization of the realizable domain.

$$V_1^{\mathbf{A}} - V_3^{\mathbf{A}}$$

In contrast to the bending LPs, in-plane parameters are not weighted by the ply position. Consequently, characterizing the realizable domain for the contiguity guideline in the $V_1^{\mathbf{A}} - V_3^{\mathbf{A}}$ space adopts a simplified form.

To maximize the resultant vector magnitude under the contiguity constraint, all plies not enforcing the guideline are oriented at 0° , while the plies inserted to satisfy the guideline are oriented at an angle δ . Assuming one out of every L+1 plies is assigned the angle δ , the fraction of such plies is given by:

$$a = \frac{1}{L+1}$$

The normalized radius of the realizable domain is then expressed as:

$$|\mathbf{R}_c^{\mathbf{A}}| = \sqrt{(1 - (1 - \cos \delta) \times a)^2 + (\sin \delta \times a)^2}$$
(4.33)

Substituting $a = \frac{1}{L+1}$, we obtain:

$$|\mathbf{R}_c^{\mathbf{A}}| = \sqrt{\left(1 - \frac{1 - \cos \delta}{L + 1}\right)^2 + \left(\frac{\sin \delta}{L + 1}\right)^2} \tag{4.34}$$

The realizable domain for contiguity design guideline in the $V_1^{\mathbf{A}} - V_3^{\mathbf{A}}$ space is characterized as:

$$(V_1^{\mathbf{A}})^2 + (V_3^{\mathbf{A}})^2 \le |\mathbf{R}_c^{\mathbf{A}}|^2 \tag{4.35}$$

4.2.4 Balance

The laminate must contain an equal number of plies oriented at $+\theta$ and $-\theta$ to satisfy the balance condition. This equates the A_{16} and A_{26} terms in the extensional stiffness matrix to 0, and ensures the decoupling of laminates' in-plane normal and shear properties.

$$V_1^{\mathbf{D}} - V_3^{\mathbf{D}}$$

For analytical convenience, the laminate is constructed by grouping all $+\theta$ plies and all $-\theta$ plies separately. It enables a simplified mathematical treatment without violating the balanced condition. This grouping allows separation of the contributions from the two angular families to the bending LPs.

Due to the even symmetry of cosine and the odd symmetry of sine, the trigonometric identities,

$$cos(2\theta) = cos(-2\theta), \quad sin(2\theta) = -sin(-2\theta)$$

allow simplification of the LP expressions. Specifically, the cosine contributions reinforce, while the sine contributions cancel out.

Assuming the laminate is symmetric and consists of n plies, with half above the mid-plane, and with $\frac{n}{4}$ plies at $+\theta$ and $\frac{n}{4}$ plies at $-\theta$, the bending LPs are given by:

$$V_1^{\mathbf{D}} = \sum_{k=1}^{\frac{n}{4}} w_k \cos 2\theta + \sum_{k=\frac{n}{4}+1}^{\frac{n}{2}} w_k \cos -2\theta$$

$$= \sum_{k=1}^{\frac{n}{2}} w_k \cos 2\theta = \cos 2\theta$$

$$V_3^{\mathbf{D}} = \sum_{k=1}^{\frac{n}{4}} w_k \sin 2\theta + \sum_{k=\frac{n}{4}+1}^{\frac{n}{2}} w_k \sin -2\theta$$

$$= \left(\frac{2n}{4n}\right)^3 \sin 2\theta - \left(1 - \frac{2n}{4n}\right)^3 \sin 2\theta$$

$$= \left(\frac{1}{4} - 1\right) \sin 2\theta = -\frac{3}{4} \sin 2\theta$$

This construction shows that $V_1^{\mathbf{D}}$ reaches its maximum magnitude, while $V_3^{\mathbf{D}}$ is scaled by a factor of $-\frac{3}{4}$ due to the asymmetry in the distribution of $\sin 2\theta$ terms around the mid-plane.

Accordingly, the realizable domain in the $V_1^{\mathbf{D}} - V_3^{\mathbf{D}}$ space is bounded by an ellipse defined by:

$$(V_1^{\mathbf{D}})^2 + \left(\frac{V_3^{\mathbf{D}}}{0.75}\right)^2 \le 1$$
 (4.36)

Equation 4.36 describes the elliptic constraint surface induced by the balance design guideline in the bending LP space.

Table 4.1: Definitions of variables used in characterized equations.

Variable	Definition	
a	Intermediate ply count for maximizing $V_2^{\mathbf{D}}$	
	solution of $2a^3 + 3a^2 + 3a + 1 = \left(\frac{n}{2}\right)^3 \Rightarrow a = 0.3978V_1^{\mathbf{D}} - 0.5765$	
b	Fractional weight of inner plies for damage tolerance: $b = \left(\frac{n-2}{n}\right)^3$	
$W_{\frac{n}{2}}$	Weight of the outermost ply for bending LPs	
$egin{array}{c} w_{rac{n}{2}} \ \mathbf{R}_d \end{array}$	Minimum magnitude of the resultant vector under disorientation guide-	
	line	
$ \mathbf{R}_c^{\mathbf{D}} $	Maximum magnitude of the resultant vector obeying contiguity guideline	
	in $V_1^{\mathbf{D}} - V_3^{\mathbf{D}}$ space	
$ \mathbf{R}_c^{\mathbf{A}} $	Maximum magnitude of the resultant vector obeying contiguity guideline	
	in $V_1^{\mathbf{A}} - V_3^{\mathbf{A}}$ space	

Table 4.2: Summary of analytically characterized realizable domains for each design guideline.

Design Guideline	LP Pair	Characterized Equation	Eq. Ref.
Disorientation	$V_1^{\mathbf{D}} - V_3^{\mathbf{D}}$	$(V_1^{\mathbf{D}})^2 + (V_3^{\mathbf{D}})^2 \ge \mathbf{R}_d ^2$	4.9
	$V_1^{\mathbf{D}} - V_2^{\mathbf{D}}$	$V_2^{\mathbf{D}} \le (4(\frac{1.153}{n})^3 - 1.1824) (V_1^{\mathbf{D}})^2 + 2.1824 - 4(\frac{1.153}{n})^3$	4.14
	$V_1^{\mathbf{A}} - V_2^{\mathbf{A}}$	$V_2^{\mathbf{A}} \leq rac{n-4}{n}$	4.16
Damage Tolerance	$V_1^{\mathbf{D}} - V_3^{\mathbf{D}}$	$(V_1^{\mathbf{D}})^2 + \left(V_3^{\mathbf{D}} \mp w_{\frac{n}{2}}\right)^2 \le \left(\frac{n-2}{n}\right)^6$	4.19
	$V_1^{\mathbf{D}} - V_2^{\mathbf{D}}$	$V_2^{\mathbf{D}} \geq rac{2}{b}(V_1^{\mathbf{D}})^2 - 1$	4.23
	$V_1^{\mathbf{A}} - V_2^{\mathbf{A}}$	$V_2^{\mathbf{A}} \ge \frac{2n}{n-2} (V_1^{\mathbf{A}})^2 - 1$	4.27
	$V_1^{\mathbf{A}} - V_3^{\mathbf{A}}$	$(V_1^{\mathbf{A}})^2 + \left(V_3^{\mathbf{A}} \mp \frac{2}{n}\right)^2 \le \left(\frac{n-2}{n}\right)^2$	4.28
Contiguity	$V_1^{\mathbf{D}} - V_3^{\mathbf{D}}$	$(V_1^{\mathbf{D}})^2 + (V_3^{\mathbf{D}})^2 \le \mathbf{R}_c^{\mathbf{D}} ^2$	4.32
	$V_1^{\mathbf{A}} - V_3^{\mathbf{A}}$	$(V_1^{\mathbf{A}})^2 + (V_3^{\mathbf{A}})^2 \le \mathbf{R}_c^{\mathbf{A}} ^2$	4.35
Balance	$V_1^{\mathbf{D}} - V_3^{\mathbf{D}}$	$(V_1^{\mathbf{D}})^2 + \left(\frac{V_3^{\mathbf{D}}}{0.75}\right)^2 \le 1$	4.36

4.2.5 Disorientation - Damage Tolerance - Balance

This section investigates the implications of simultaneously enforcing multiple design guidelines on the realizable domain. In such cases, the SS must be designed to satisfy all conditions simultaneously, thereby introducing stricter limitations on allowable ply orientations. The resulting space is inherently more restricted than any of the individually characterized domains and provides insight into the overlap and interaction between the design constraints.

$$\underline{V_1^{\mathbf{D}} - V_3^{\mathbf{D}}}$$

In earlier analyses, the inner boundary of the realizable domain under the disorientation constraint was characterized as a circle centered at the origin in the $V_1^{\mathbf{D}} - V_3^{\mathbf{D}}$ space. For the balance design guideline, the outer boundary followed an elliptical form with its major axis aligned along the $V_1^{\mathbf{D}}$ axis. The damage tolerance requirement introduced an offset along the $V_3^{\mathbf{D}}$ axis due to the enforced outermost ply orientation.

When all three guidelines are enforced simultaneously, the realizable domain is bounded from the inside by the disorientation limit and from the outside by the intersection of balance and damage tolerance constraints. The following assumptions are made in the derivation of this composite domain:

Assumptions:

- The **outer boundary** of the realizable domain is modeled as an ellipse:
 - Its width corresponds to the full range of $V_1^{\mathbf{D}}$ values realizable under the damage tolerance constraint.
 - Its height is twice the vertical offset from the origin to the maximum value of $V_3^{\mathbf{D}}$ derived from the balance constraint.

These are computed as:

width
$$W=2 \times (\text{maximum value of } V_1^{\mathbf{D}}) = 2\left(\frac{n-2}{n}\right)^3$$
 height $H=2 \times \left(0.75-w_{\frac{n}{2}}\right)$

Hence, the outer elliptical boundary is characterized by:

$$\left(\frac{2V_1^{\mathbf{D}}}{W}\right)^2 + \left(\frac{2(V_3^{\mathbf{D}} \pm w_{\frac{n}{2}})}{H}\right)^2 \le 1 \tag{4.37}$$

• The **inner boundary** is modeled as a circle centered at the same offset as the ellipse, with its radius computed using the reduced SS of $\frac{n}{2} - 1$ plies. This reflects the removal of the outermost ply used to enforce damage tolerance.

Using the same approach as in Equation 4.8, the radius is calculated as:

$$|\mathbf{R}_{com}| = |\mathbf{w}_{\frac{n}{2}-1} + \mathbf{w}_{\frac{n}{2}-2} + \mathbf{w}_{\frac{n}{2}-3}| - \sum_{k=1}^{\frac{n}{2}-4} |\mathbf{w}_{k}|$$

$$= \sqrt{(6n-30)^{2} + (0.75n^{2} - 7.5n + 19)^{2}} - \left(\frac{n-8}{2n}\right)^{3}$$

The corresponding inequality for the inner circular boundary is:

$$(V_1^{\mathbf{D}})^2 + (V_3^{\mathbf{D}} \pm w_{\frac{n}{2}})^2 \ge |\mathbf{R}_{com}|^2 \tag{4.38}$$

Under these assumptions, the realizable domain in the $V_1^{\mathbf{D}} - V_3^{\mathbf{D}}$ space is bounded between a shifted ellipse and a concentric inner circle, forming an annular region offset along the $V_3^{\mathbf{D}}$ axis. All SSs that generate this region adhere to the disorientation, damage tolerance, and balance guidelines. The resulting geometry reflects the compounded limitations introduced by the interaction of these three constraints.

$$V_1^{\mathbf{D}} - V_2^{\mathbf{D}}$$

Although $V_1^{\mathbf{D}}$ and $V_2^{\mathbf{D}}$ are related through cosine-based trigonometric formulations, the entire region within the theoretical parabola cannot be fully realized due to the restrictions imposed by the disorientation guideline. To characterize the lower bound of $V_2^{\mathbf{D}}$, plies oriented at $\pm 15^{\circ}$ or $\pm 75^{\circ}$ are introduced between $\pm 45^{\circ}$ plies, creating a disallowed configuration that violates disorientation.

The minimum value of $V_2^{\mathbf{D}}$ under these conditions is calculated using:

$$\begin{split} V_2^{\mathbf{D}} &= \sum_{k=1}^{\frac{n}{4}-1} w_k \times \cos 4\theta_k + \sum_{k=\frac{n}{4}}^{\frac{n}{4}+1} w_k \times \cos 4\theta_k + \sum_{k=\frac{n}{4}+2}^{\frac{n}{2}} w_k \times \cos 4\theta_k \\ &= \sum_{k=1}^{\frac{n}{4}-1} w_k \times \cos (4 \times -45^\circ) + \sum_{k=\frac{n}{4}}^{\frac{n}{4}+1} w_k \times \cos (4 \times \pm 15^\circ) + \sum_{k=\frac{n}{4}+2}^{\frac{n}{2}} w_k \times \cos (4 \times 45^\circ) \\ &= \sum_{k=1}^{\frac{n}{4}-1} w_k \times (-1) + \sum_{k=\frac{n}{4}}^{\frac{n}{4}+1} w_k \times \left(\frac{1}{2}\right) + \sum_{k=\frac{n}{4}+2}^{\frac{n}{2}} w_k \times (-1) \end{split}$$

Upon simplification, the lower bound is characterized as:

$$V_2^{\mathbf{D}} \ge \frac{3}{2n^3} (16 + 3n^2) - 1 \tag{4.39}$$

The upper bound of $V_2^{\mathbf{D}}$ is obtained by extending the method used in the isolated disorientation case. Here, a $\pm 45^{\circ}$ ply is inserted between 0° and 90° plies, and the topmost ply is fixed at $\pm 45^{\circ}$ to satisfy the damage tolerance constraint. The remaining $\frac{n}{2}-1$ plies are arranged such that disorientation and balance are satisfied, and the maximum $V_2^{\mathbf{D}}$ is computed accordingly.

To enforce $V_1^{\mathbf{D}} = 0$, the value of a — representing the number of 90° plies — is obtained by solving the following equation:

$$V_{1}^{\mathbf{D}} = \sum_{k=1}^{a} w_{k} \cos(2 \times 90^{\circ}) + w_{a+1} \cos(2 \times -45^{\circ}) + \sum_{k=a+2}^{\frac{n}{2}-1} w_{k} \cos(0^{\circ}) + w_{\frac{n}{2}} \cos(2 \times 45^{\circ})$$

$$= \left(\frac{2a}{n}\right)^{3} \times (-1) + 0 + \left[\left(\frac{n-2}{n}\right)^{3} - \left(\frac{2(a+1)}{n}\right)^{3}\right] \times 1 + 0$$

$$2a^{3} + 3a^{2} + 3a + 1 - \left(\frac{n-2}{2}\right)^{3} = 0$$

$$(4.40)$$

To simplify the analytical model, the evaluation of the root is approximated with a linear fit (see Figure 4.7). The fit shows a high R^2 value of 1.0, indicating an excellent linear correlation.

Then, the corresponding $V_2^{\mathbf{D}}$ is computed as:

$$\begin{split} V_{2}^{\mathbf{D}} &= \sum_{k=1}^{a} w_{k} \cos(4 \times 90^{\circ}) + w_{a+1} \cos(4 \times -45^{\circ}) + \sum_{k=a+2}^{\frac{n}{2}-1} w_{k} \cos(0^{\circ}) + w_{\frac{n}{2}} \cos(4 \times 45^{\circ}) \\ &= \left(\frac{2a}{n}\right)^{3} \times 1 + \left[\left(\frac{2(a+1)}{n}\right)^{3} - \left(\frac{2a}{n}\right)^{3}\right] \times (-1) + \left[\left(\frac{n-2}{n}\right)^{3} - \left(\frac{2(a+1)}{n}\right)^{3}\right] \times 1 \\ &+ \left(1 - \left(\frac{n-2}{n}\right)^{3}\right) \times (-1) \end{split}$$

Simplifying:

$$V_2^{\mathbf{D}} = \frac{16}{n^3} \left(2a^3 - \left(\frac{n}{2} \right)^3 \right) + 1$$
$$= \frac{32a^3}{n^3} - 1$$

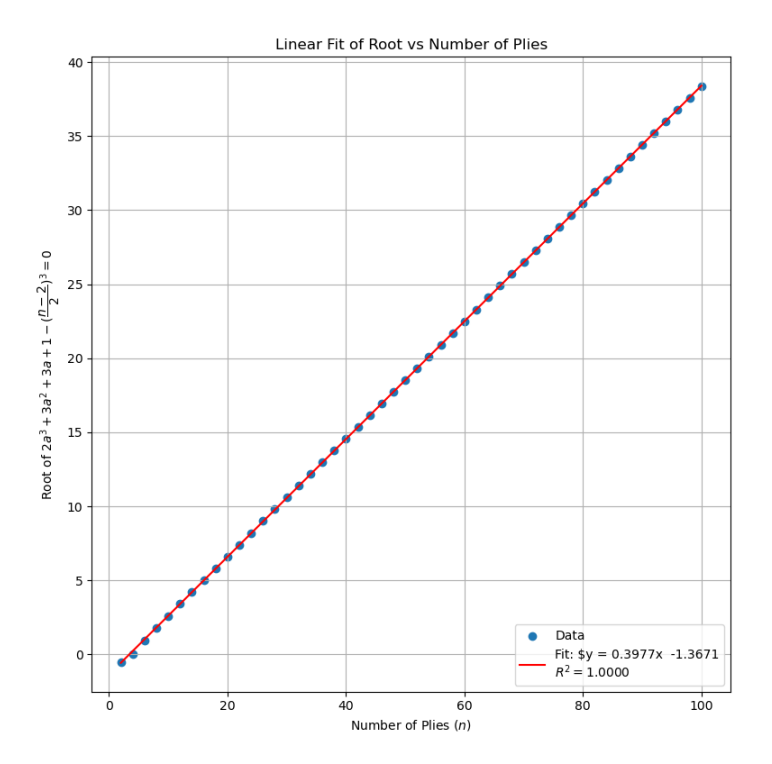


Figure 4.7: Linear regression of the root of the cubic equation $2a^3 + 3a^2 + 3a + 1 = \left(\frac{n-2}{2}\right)^3$ with respect to total number of plies n.

The calculated $V_2^{\mathbf{D}}$ value defines the vertex of the parabolic boundary. The upper bound of the realizable domain in the $V_1^{\mathbf{D}} - V_2^{\mathbf{D}}$ space is then given by:

$$V_2^{\mathbf{D}} \le \frac{2b - 1 - c}{b^2} (V_1^{\mathbf{D}})^2 + c \tag{4.41}$$

where:

$$b = \left(\frac{n-2}{n}\right)^3$$
$$c = \frac{32a^3}{n^3} - 1$$

$$\underline{V_1^{\mathbf{A}} - V_2^{\mathbf{A}}}$$

Since the in-plane LPs are independent of ply position, the contributions to $V_1^{\mathbf{A}}$ and $V_2^{\mathbf{A}}$ depend solely on the number and orientation of the plies. Under the simultaneous enforcement of

disorientation, damage tolerance, and balance guidelines, at least two plies must be oriented at $\pm 45^{\circ}$ - one to satisfy damage tolerance, and one to maintain a valid transition between fiber angles under the disorientation constraint. Together, these plies also satisfy the balance guideline by forming a conjugate pair.

The contribution of these two $\pm 45^{\circ}$ plies to $V_2^{\mathbf{A}}$ is:

$$V_2^{\mathbf{A}} = \frac{2}{n} \times \cos(4 \times 45^\circ) + \frac{2}{n} \times \cos(4 \times (-45^\circ))$$
$$= \frac{2}{n} \times (-1) + \frac{2}{n} \times (-1) = \frac{-4}{n}$$

Thus, even in an ideal configuration where all other plies are oriented at either 0° or 90° , the maximum realizable value of $V_2^{\mathbf{A}}$ is reduced by the contribution of these two required plies:

$$V_2^{\mathbf{A}} \le \frac{n-8}{n} \tag{4.42}$$

To characterize the lower bound of $V_2^{\mathbf{A}}$, a symmetric laminate is constructed where all plies are oriented at angles $\pm 45^{\circ}$), and $\pm 15^{\circ}$ plies are inserted in between to satisfy the disorientation constraint. Mathematically, it can be represented as:

$$V_2^{\mathbf{A}} \ge \left(\frac{n/2 - 2}{n/2}\right) \times (-1) + \frac{4}{n} \times 0.5$$
$$= \frac{6 - n}{n}$$

Therefore, the minimum value of $V_2^{\mathbf{A}}$ under these constraints is:

$$V_2^{\mathbf{A}} \ge \frac{6-n}{n} \tag{4.43}$$

Table 4.3: Realizable domain equations for simultaneously enforced Disorientation, Damage Tolerance, and Balance guidelines.

LP Pair	Characterized Equation	Equation Ref.
$V_1^{\mathbf{D}} - V_3^{\mathbf{D}}$	$\left(\frac{2V_1^{\mathbf{D}}}{W}\right)^2 + \left(\frac{2(V_3^{\mathbf{D}} \pm w_{\frac{n}{2}})}{H}\right)^2 \le 1 \text{ (outer bound)}$	
	$(V_1^{\mathbf{D}})^2 + (V_3^{\mathbf{D}} \pm w_{\frac{n}{2}})^2 \ge \mathbf{R}_{com} ^2$ (inner bound)	4.37, 4.38
$V_1^{\mathbf{D}} - V_2^{\mathbf{D}}$	$\frac{3}{2n^3}(16+3n^2)-1 \le V_2^{\mathbf{D}} \le \frac{2b-1-c}{b^2}(V_1^{\mathbf{D}})^2+c$	4.39, 4.41
$V_1^{\mathbf{A}} - V_2^{\mathbf{A}}$	$\frac{6-n}{n} \le V_2^{\mathbf{A}} \le \frac{n-8}{n}$	4.43, 4.42

Table 4.4: Definition of variables used in the realizable domain equations for Disorientation—Damage Tolerance—Balance case.

Variable	Description	
а	Solved using a cubic polynomial $2a^3 + 3a^2 + 3a + 1 - \left(\frac{n-2}{2}\right)^3 = 0 \Rightarrow a = 0.3977V_1^{\mathbf{D}} - 1.3671$	
$W^{\frac{n}{2}}$	Contribution of the outermost ply used to satisfy the damage tolerance guideline	
b	Maximum value of $V_1^{\mathbf{D}}$ under damage tolerance, defined as $b = \left(\frac{n-2}{n}\right)^3$	
C	Maximum realizable value of $V_2^{\mathbf{D}}$ when $V_1^{\mathbf{D}} = 0$, defined as $c = \frac{32a^3}{n^3} - 1$	
$ \mathbf{R}_{com} $	Radius of the inner circle in $V_1^{\mathbf{D}} - V_3^{\mathbf{D}}$ space, computed using $\frac{n}{2} - 1$ plies after removing the outermost ply	
width	Horizontal span of the outer elliptical domain in $V_1^{\mathbf{D}} - V_3^{\mathbf{D}}$ space: $2b = 2\left(\frac{n-2}{n}\right)^3$	
height	Vertical span of the ellipse: $2 \times (0.75 - w_{\frac{n}{2}})$, accounting for offset from the balance and damage tolerance constraints	

4.3 Laminate optimization using lamination parameters

The bi-level optimization framework is implemented to assess the practical implications of the realizable domains characterized in this thesis. The optimization framework models a realistic composite panel. It performs stiffness optimization at the first level using LPs, followed by SS retrieval at the second level. This section outlines the model setup and the tools employed at both optimization levels.

4.3.1 Benchmark case setup

Constraints on LPs, derived based on the realizable domains characterized (see Table 4.2 and 4.3), were imposed at the first level to ensure manufacturability and mitigate epistemic uncertainty associated with infeasible SSs. A single composite panel model with an aspect ratio of 4 [Bloomfield et al. 2008] was used to evaluate the optimization procedure. The panel is simply supported along all edges and subjected to a combination of in-plane normal and shear loads (see Figure 4.8). The five standard load cases considered in Bloomfield et al. 2008 were adopted as shown in Table 4.5:

Table 4.5: Load Cases.

Sl. no	N _x	N _{xy}
1	0	-800
2	0	400
3	-100	500
4	-300	-300
5	-500	200
6	500000	100

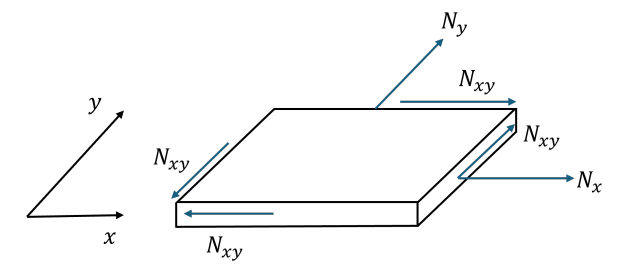


Figure 4.8: Illustration of an arbitrary panel under the defined loads.

In addition, a sixth case is introduced in this work to evaluate performance under tension-dominated loading, which is relevant to stiffened panels under service loading.

4.3.2 First-Level stiffness optimization

The first level of the bi-level optimization problem involves minimizing weight, while satisfying compliance to strain and buckling with respect to LPs. The in-house tool developed at the German Aerospace Center (DLR), named lightworks [Dähne et al. 2024], was used to perform this task. In lightworks tool, the design space is handled by using hyperplanes derived from the mathematically feasible region.

IPOPT algorithm is utilized in lightworks, which employs an interior-point filter line-search algorithm suitable for large-scale nonlinear programming. The algorithm ensures convergence from poor starting points and accommodates inequality constraints through its filter-based merit approach. Further details on the algorithm and its implementation can be found in Wächter and Biegler 2006.

4.3.3 Second-level stacking sequence design

Once the optimal set of LPs was obtained, the second level of the bi-level optimization involved retrieving a SS that closely matches the optimized parameters. This was achieved using LAYLA, an open-source beam-search-based SS generator [Fedon et al. 2020].

LAYLA enforces design guideline enforcement (e.g., disorientation, balance, contiguity) during SS design, ensuring that retrieved sequences are mechanically optimal and manufacturable. The search is guided by heuristic cost functions designed to promote convergence toward a sequence that yields LPs close to the optimized targets. If the retrieved sequence does not sufficiently match the targets, a refinement loop is executed to iteratively improve alignment with the optimized stiffness matrix.

The complete implementation can be summarized as follows:

- Input: Define panel geometry, boundary conditions, and loading scenarios
- First Level: Use lightworks to solve for optimal LPs within realizable domains
- **Second Level:** Use LAYLA to retrieve a SS satisfying the optimized LPs and design guidelines
- Output: Find the predicted performance (critical SF) under defined load cases

Results obtained using this setup are discussed in Chapter 5, where the impact of realizable domain enforcement on structural performance and manufacturability is evaluated.

5 Results

This chapter presents the outcomes of the study in two parts. The first section evaluates the realizable domains characterized analytically in Chapter 4.2, and the second demonstrates their integration within the bi-level optimization procedure as explained in Chapter 4.3. Finally, this serves as a foundation for the validation of the theoretical framework and assessments of the designed laminates.

5.1 Validation of Realizable Domains

The objective is to evaluate how well the characterized boundaries align with the practically realizable regions in the LP space and to quantify the coverage efficiency. As discussed in Chapter 4:

- The symmetric laminates are generated using fibre orientations in $[-90^{\circ}, 90^{\circ}]$ with a step of $\delta 15^{\circ}$ (see Appendix A).
- The design guidelines characterized are disorientation, damage tolerance, contiguity, balance, and the coupled disorientation, damage tolerance, and balance.
- Their corresponding realizable domain equations are summarized in Tables 4.2 and 4.3.

5.1.1 Disorientation

The disorientation design guideline limits the allowable angular difference between consecutive plies, translating to nonlinear geometric constraints in the LP space. The equations for these bounds, derived in Chapter 4.2, required solving a cubic polynomial (Equation 4.13). To visually validate the derived realizable domain, Figures 5.1 to 5.3 present scatter plots of LP pairs obtained from symmetric laminates with 8, 10, and 12 total plies. The blue points represent laminates within the analytically defined disorientation boundaries, while red points indicate misclassifications, i.e., laminates that obey disorientation beyond allowable limits.

Figure 5.1 shows the result for an 8-ply laminate. Subfigure 5.1a shows the in-plane LP space $(V_1^{\mathbf{A}}, V_2^{\mathbf{A}})$, where the upper bound $V_2^{\mathbf{A}} \leq \frac{n-4}{n}$, derived directly from the maximum permitted disorientation is shown. Subfigure 5.1b presents the bending lamination parameter space $(V_1^{\mathbf{D}}, V_2^{\mathbf{D}})$ with the parabolic upper bound derived from the cubic polynomial fit. Subfigure 5.1c shows $(V_1^{\mathbf{D}}, V_3^{\mathbf{D}})$, where a circular inner bound characterizes the realizable domain.

The same three projections are shown for 10-ply (Figure 5.2) and 12-ply (Figure 5.3) laminates. It is evident that increasing ply count leads to a more dense and quasi-continuous space. The proportion of misclassified points consistently decreases. This trend validates the analytical model's improved coverage accuracy with increasing ply count. The reason behind this is that as the number of plies increases, the discrete nature of stacking possibilities starts to resemble a continuous distribution. This allows the discrete laminate configurations to better approximate the analytically derived realizable domain, which is based on treating the number of plies as a continuous variable in the theoretical formulation.

The summation definitions of LPs indicate that certain pairs, such as $(V_2^{\mathbf{D}}, V_4^{\mathbf{D}})$ and $(V_2^{\mathbf{A}}, V_4^{\mathbf{A}})$, also rely on sine and cosine functions. However, their interaction with the disorientation constraint differs due to the argument inside the trigonometric functions. The key difference between these groups is the frequency of oscillation in trigonometric terms. $V_{2,4}^{\mathbf{A},\mathbf{D}}$ follow a $4\theta_k$ dependency, meaning that the same 45° constraint the vectors rotate in the range of $[-180^{\circ}, 180^{\circ}]$ instead of $[-90^{\circ}, 90^{\circ}]$ (see Figure 4.2b). As a result, vectors are no longer confined to a semicircle but instead to a full circular region. Since the resultant vector can explore the entire circular domain, the disorientation constraint does not impose any additional limitations in this space.

Table 5.1 summarizes the percentage of laminates that violate the analytically defined disorientation bounds to quantify these visual insights. The table includes the proportion of misclassified points across three LP pairs for each ply count. This shows, the percentage of misclassified laminates decreases as the number of plies increases, consequently confirming that the analytical bounds become tighter and more accurate with finer discretization of ply count. However, for the $V_1^{\bf A}-V_2^{\bf A}$ projection, a small portion of misclassified laminates (0.26%) persists even at higher ply counts. This residual misclassification is due to the linear approximation used to characterize the realizable domain in this space. Specifically, the straight-line boundary does not enclose certain unidirectional laminates, particularly those fully oriented at 0° or 90° , which lie outside the realizable domain despite satisfying the disorientation guideline. This limitation highlights a trade-off between model simplicity and exact coverage.

Table 5.1: Percentage of laminates misclassified by the characterized disorientation constraints for varying ply counts.

Total Plies	$V_1^{\mathbf{D}} - V_3^{\mathbf{D}}$	$V_1^{\mathbf{D}} - V_2^{\mathbf{D}}$	$V_1^{\mathbf{A}} - V_2^{\mathbf{A}}$
8	0.00%	4.96%	5.20%
10	0.00%	1.46%	1.33%
12	0.00%	0.58%	0.26%

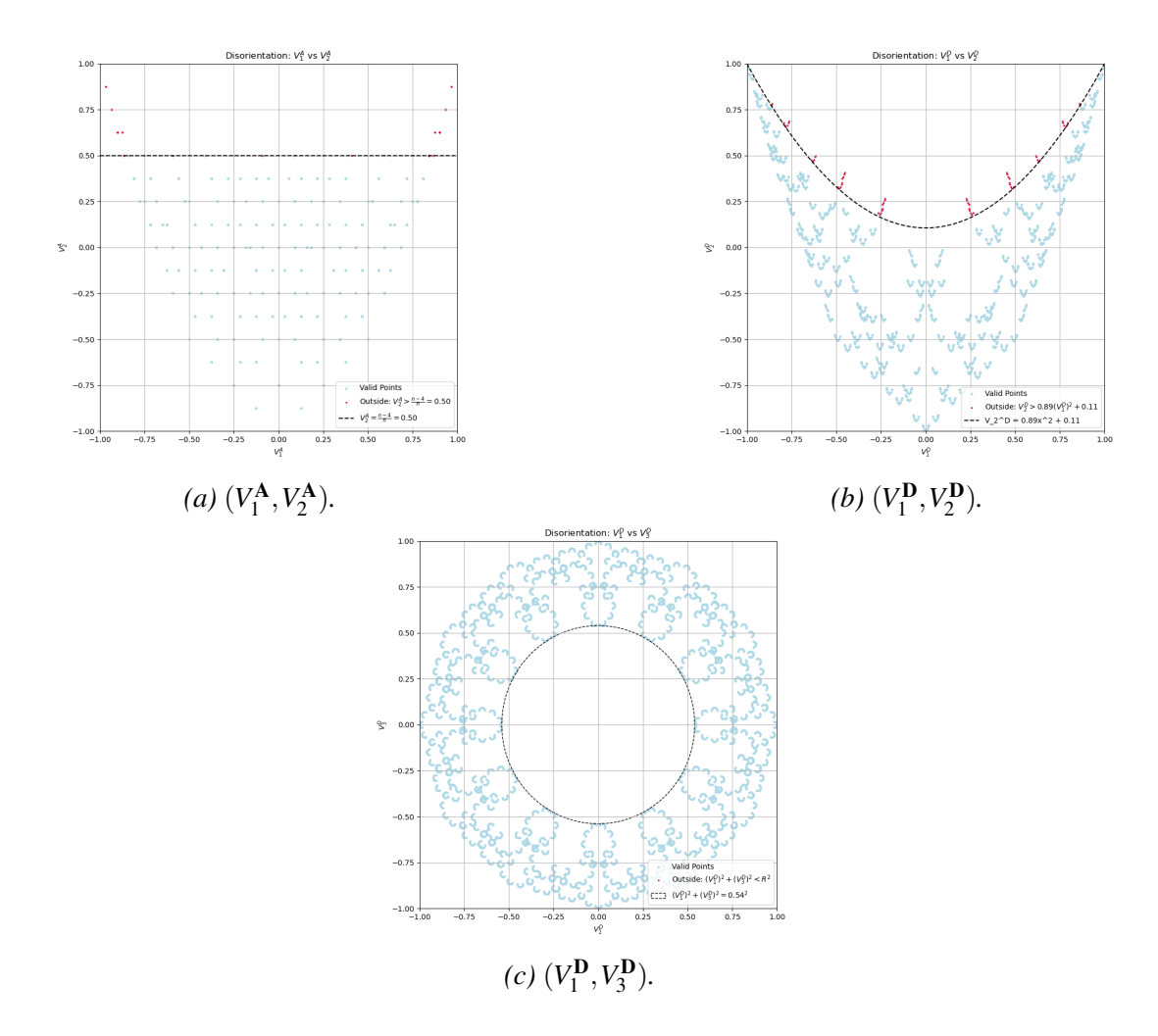


Figure 5.1: Characterized realizable domains under the disorientation design guideline for a symmetric 8-ply laminate.

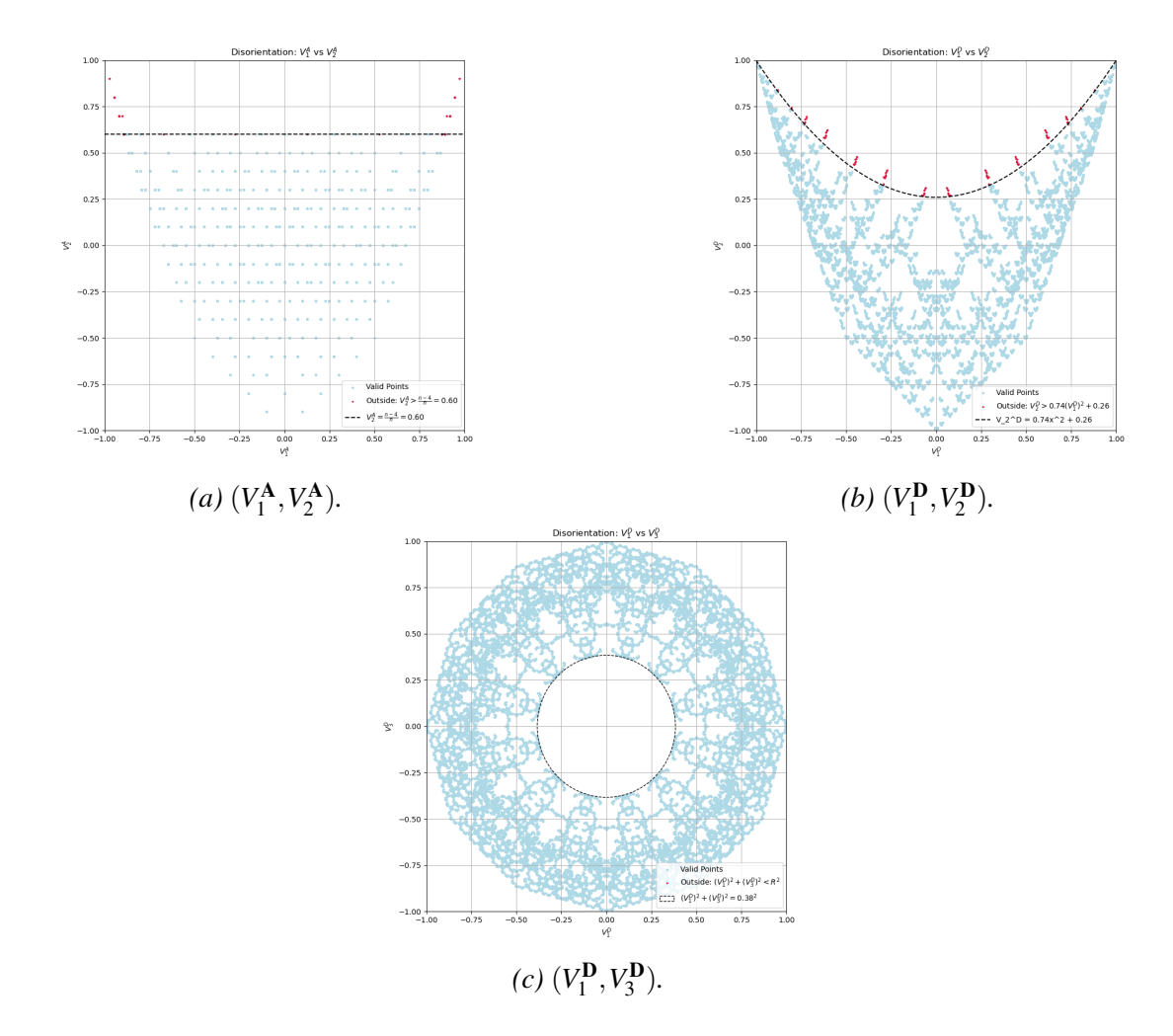


Figure 5.2: Characterized realizable domains under the disorientation design guideline for a symmetric 10-ply laminate.

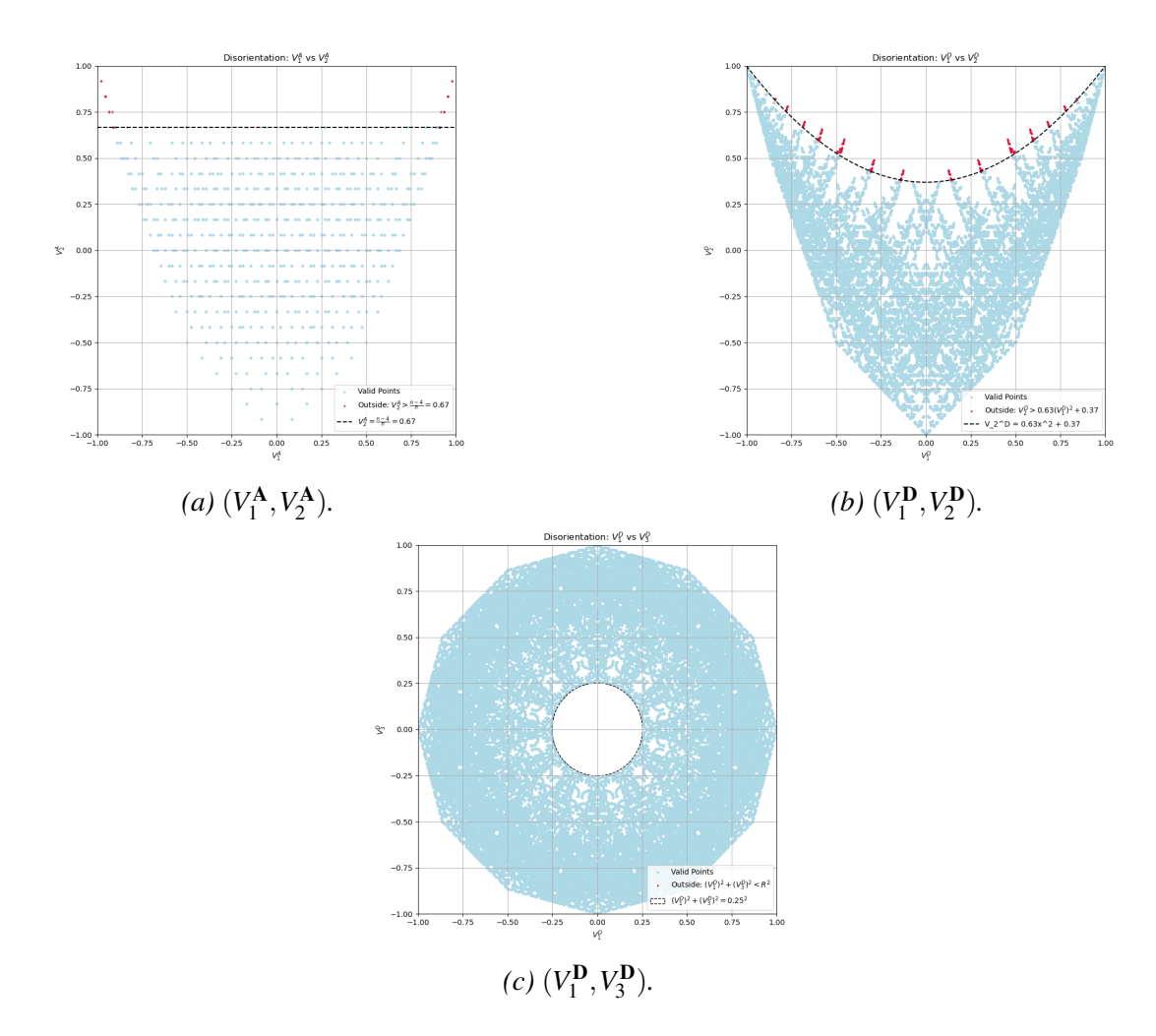


Figure 5.3: Characterized realizable domains under the disorientation design guideline for a symmetric 12-ply laminate.

5.1.2 Damage Tolerance

The damage tolerance guideline constrains the fibre orientation of the outermost plies. To analytically characterize the realizable domain for this guideline, three equations were derived (see Chapter 4.2):

- A parabolic constraint in the (V_1^A, V_2^A) space: $V_2^A \ge \frac{2n}{n-2}(V_1^A)^2 1$
- An upper bound in $(V_1^{\mathbf{A}}, V_2^{\mathbf{A}})$: $V_2^{\mathbf{A}} \leq \frac{2n-2}{n-1}$
- A circular bound in (V_1^A, V_3^A) : $(V_1^A)^2 + (V_3^A \frac{2}{n})^2 \le (\frac{n-2}{n})^2$

Similarly, the bending parameters are constrained by:

- $V_2^{\mathbf{D}} \ge \frac{2}{b} (V_1^{\mathbf{D}})^2 1$, with $b = \left(\frac{n-2}{n}\right)^3$
- $V_2^{\mathbf{D}} \le 2b 1$
- $(V_1^{\mathbf{D}})^2 + (V_3^{\mathbf{D}} w_{n/2})^2 \le R^2$, with $w_{n/2} = 1 b$

Figures 5.4 to 5.6 visualize these constraints for n = 8, 10, 12, highlighting the region that satisfies all analytical bounds. Any misclassified laminates outside the region are highlighted. As shown in Table 5.2, the percentage of laminates lying outside the realizable domain for damage tolerance is extremely low (< 1%), especially for higher ply counts. For 10- and 12-ply laminates, most combinations show no misclassification at all, while for 8-ply laminates, the deviation is marginal. These small percentages are likely due to computational errors, such as numerical rounding or interpolation errors during domain boundary checks. This reinforces the robustness of the characterized constraints in accurately capturing the realizable region, especially as the ply count increases. Results for the alternate interpretation of the damage tolerance design guideline can be referred to in Appendix C.

Table 5.2: Percentage of laminates misclassified by the characterized damage tolerance constraints for varying ply counts.

Total Plies	$V_1^{\mathbf{D}} - V_3^{\mathbf{D}}$	$V_1^{\mathbf{D}} - V_2^{\mathbf{D}}$	$V_1^{\mathbf{A}} - V_2^{\mathbf{A}}$	$V_1^{\mathbf{A}} - V_3^{\mathbf{A}}$
8	0.29%	0.98%	0.00%	0.12%
10	0.00%	0.00%	0.01%	0.00%
12	0.00%	0.00%	0.03%	0.00%

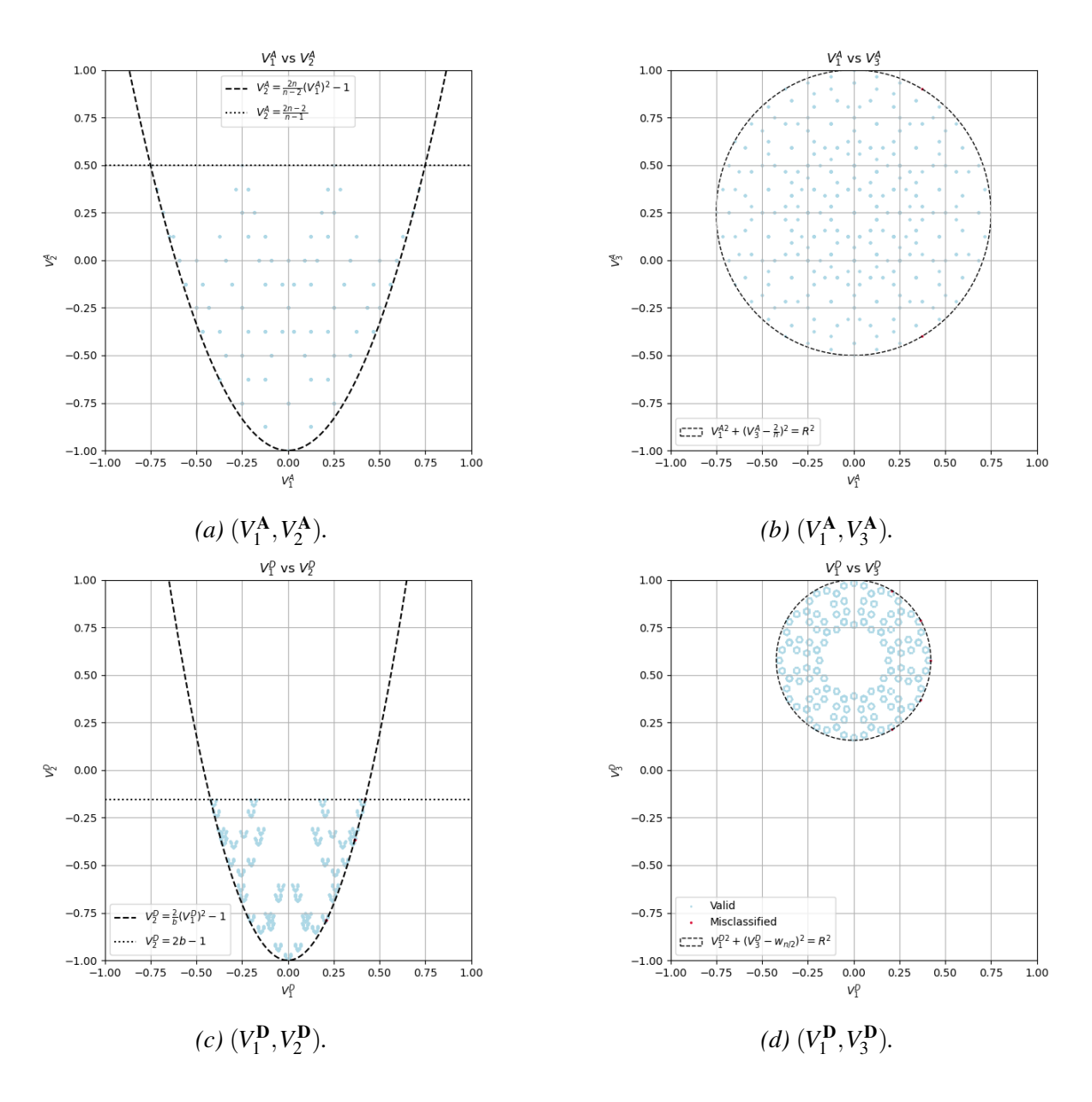


Figure 5.4: Characterized realizable domains under the damage tolerance guideline for an 8-ply symmetric laminate.

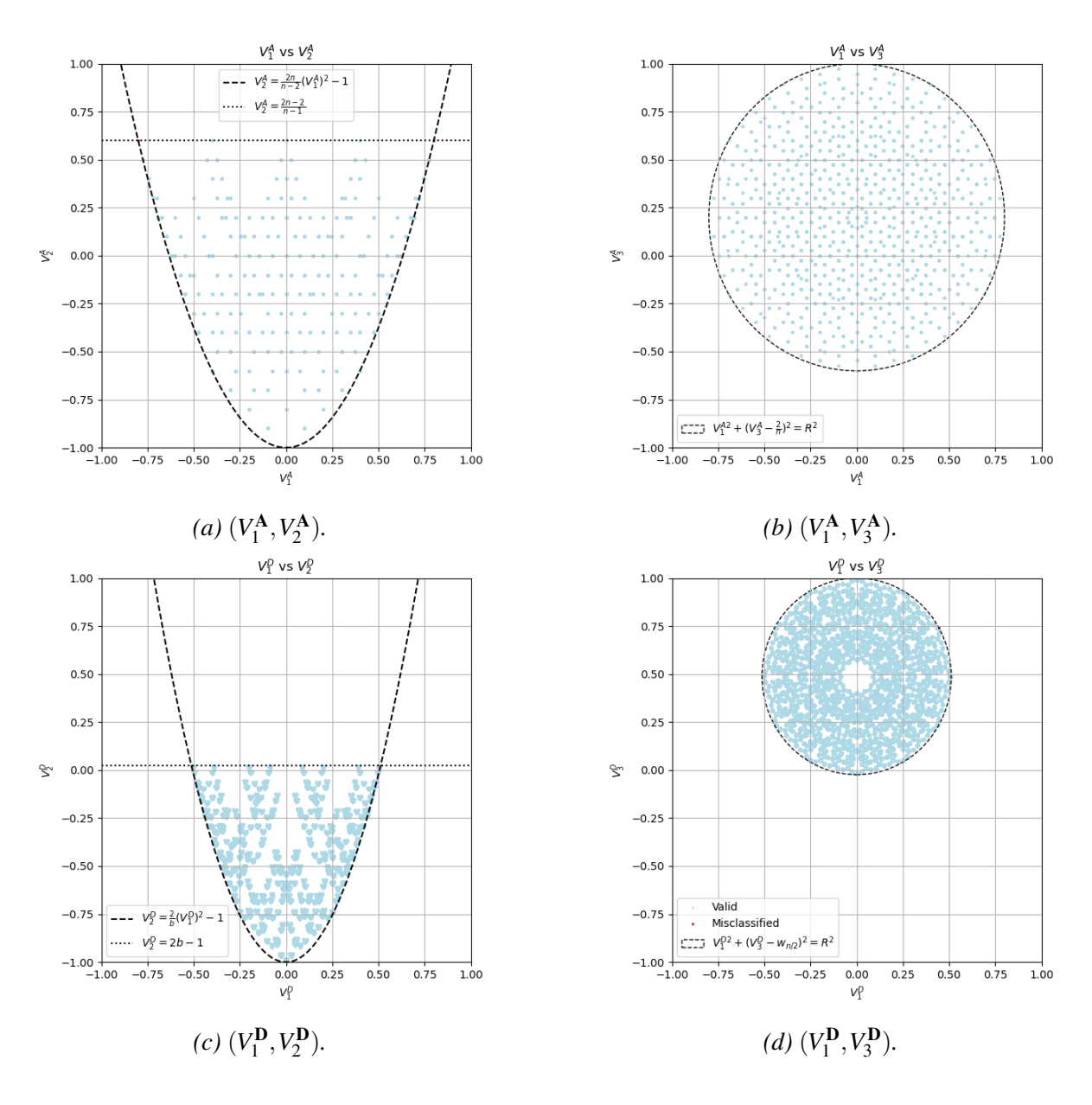


Figure 5.5: Characterized realizable domains under the damage tolerance guideline for a 10-ply symmetric laminate.

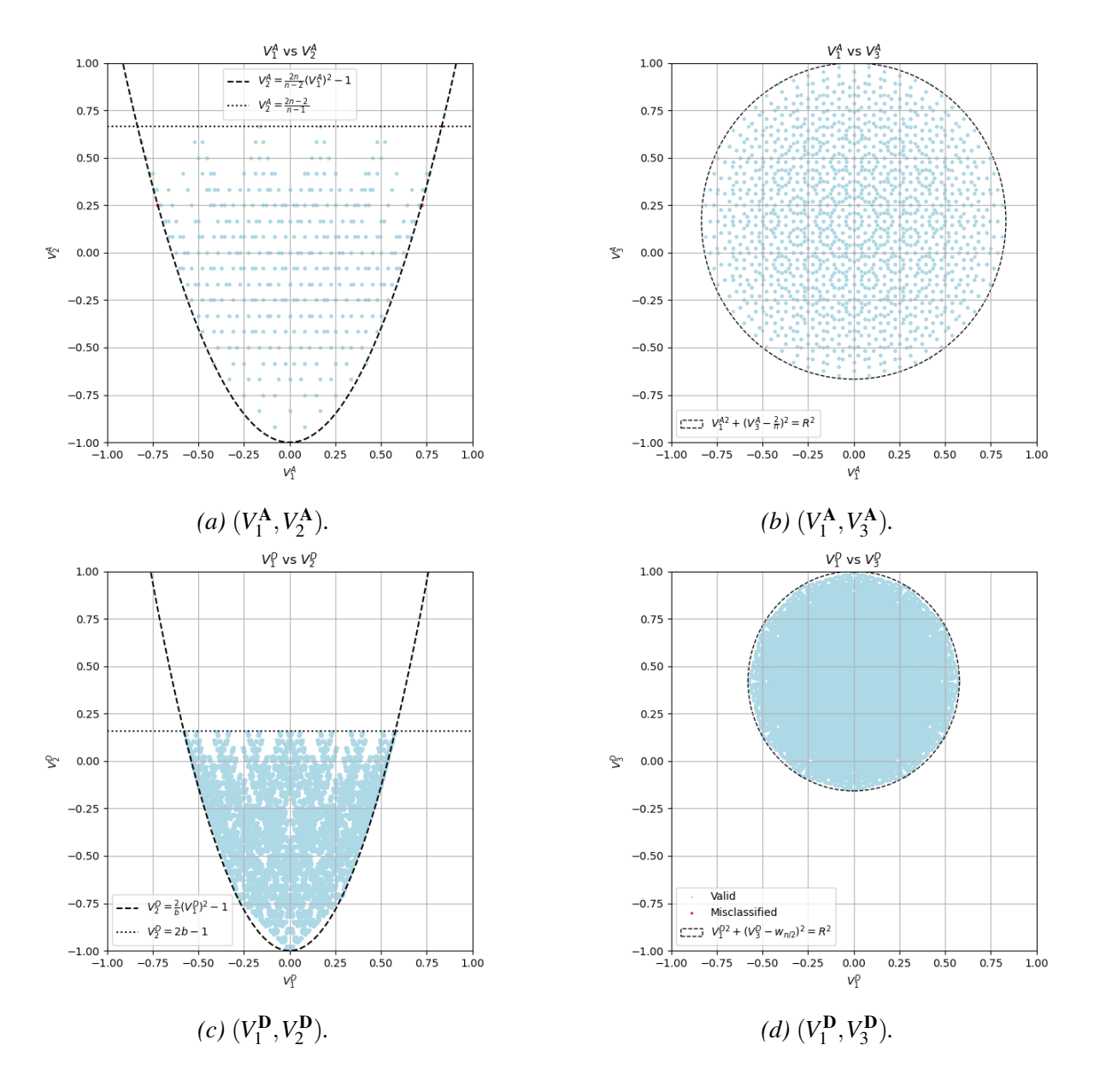


Figure 5.6: Characterized realizable domains under the damage tolerance guideline for a 12-ply symmetric laminate.

5.1.3 Contiguity

As described in Chapter 4.2, the realizable domain under this constraint is characterized by a circular outer bound in the lamination parameter space, defined in terms of $(V_1^{\mathbf{D}}, V_3^{\mathbf{D}})$. The maximum realizable radius was derived analytically and varies slightly (< 1% for thin laminates) depending on the ply count.

Figures 5.7 present the distribution of laminates in the $(V_1^{\mathbf{D}}, V_3^{\mathbf{D}})$ space for 8, 10, and 12-ply symmetric laminates, respectively.

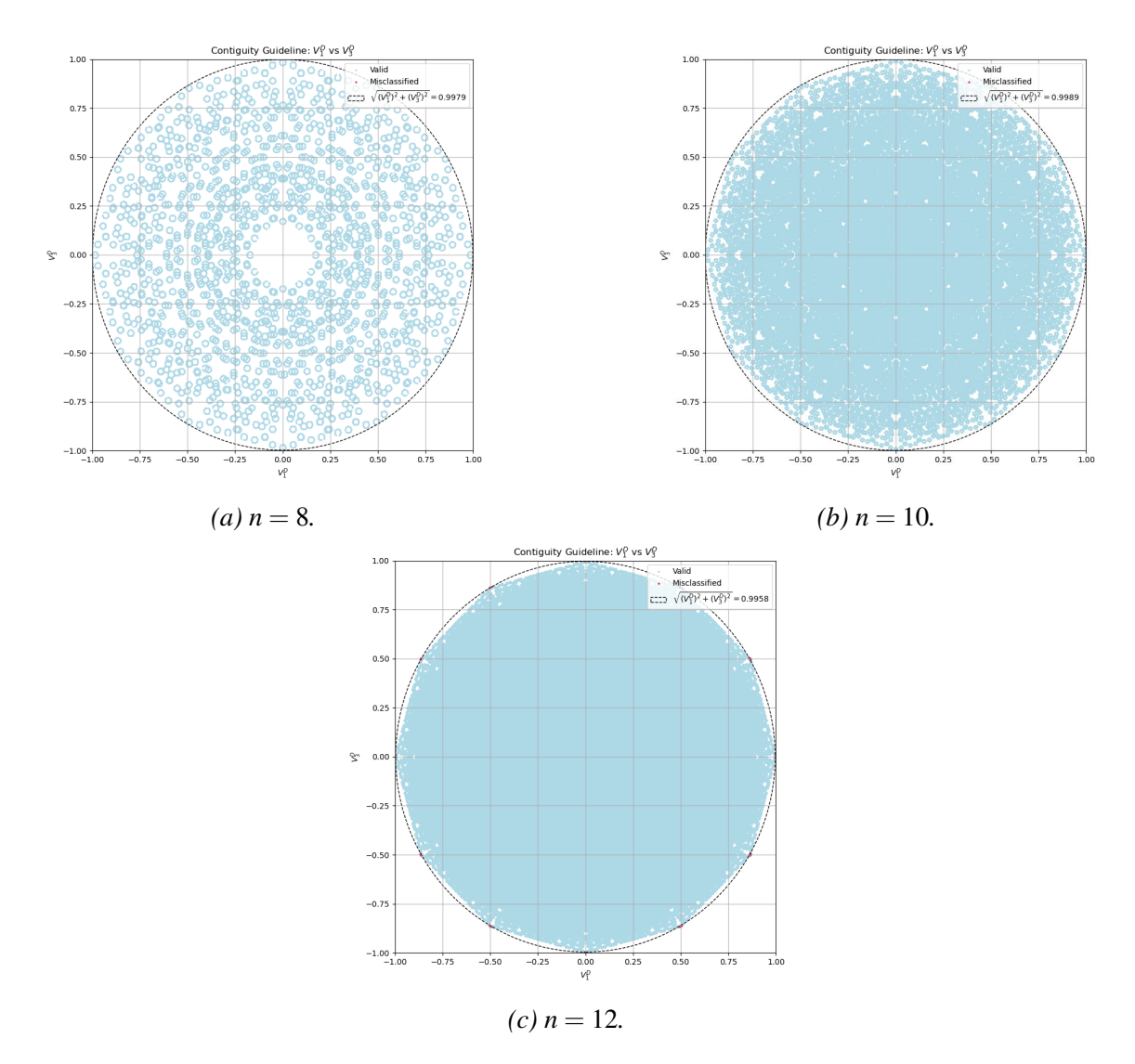


Figure 5.7: Characterized realizable domains under the contiguity guideline in $(V_1^{\mathbf{D}}, V_3^{\mathbf{D}})$ space.

The figures show that the analytical bound exactly matches the realizable region. The percentage of misclassified points (i.e., those lying outside the characterized domain) is summarized in Table 5.3. Although the realizable domain was described entirely, the mathematically feasible LP space reduction is negligible (maximum 2.5%) as observed in Figure 5.8. In the Figure 5.8 the difference in the analytically derived solution for $|\mathbf{R}|_c^{\mathbf{D}}$ is seen. This difference occurs due to the discreteness of the ply count. Also, the kink observed in the Figure 5.8 occurs when the number of plies just crosses the contiguity limit L. Since the observed reduction of $|\mathbf{R}|_c^{\mathbf{D}}$ is negligible for non-conventional laminates, it is concluded that characterizing this guideline with respect to LPs offers no significant advantage. However, contiguity has a significant effect in conventional laminates (i.e., laminates with fibre orientations in $[0^{\circ}, 45^{\circ}, -45^{\circ}, 90^{\circ}]$). The results for the same are presented in Appendix B.

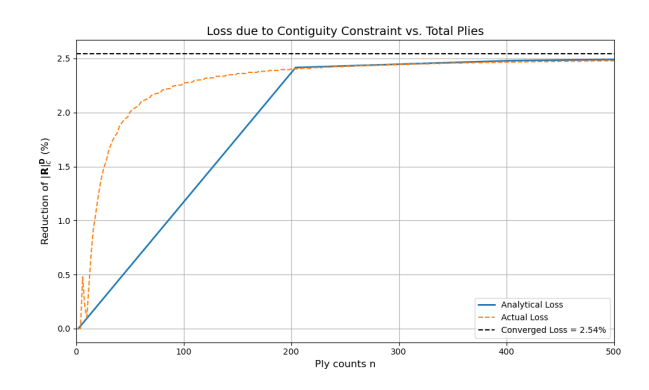


Figure 5.8: Reduction of $|\mathbf{R}|_c^{\mathbf{D}}$ with increasing ply counts.

Table 5.3: Percentage of laminates violating the characterized contiguity constraint in $(V_1^{\mathbf{D}}, V_3^{\mathbf{D}})$ space.

Total Plies	Misclassified (%)
8	0.00%
10	0.00%
12	0.00%

5.1.4 Balance

Analytically, the realizable domain under this guideline is characterized as an elliptical region in the $(V_1^{\mathbf{D}}, V_3^{\mathbf{D}})$ space (Equation 4.36). The equation of the outer boundary is defined as:

$$\left(\frac{V_1^{\mathbf{D}}}{1}\right)^2 + \left(\frac{V_3^{\mathbf{D}}}{0.75}\right)^2 \le 1$$

Figure 5.9 shows the projection of SSs onto the $V_1^{\mathbf{D}} - V_3^{\mathbf{D}}$ space for different ply counts. The analytically characterized elliptical bound is overlaid, and misclassified points outside the domain are highlighted.

Most SSs across all ply count respect the elliptical nature of the domain. A few outliers appear at the edges, especially for lower ply counts, as quantified in Table 5.4. Similar to the damage tolerance case, the few misclassified laminates are likely the result of numerical or interpolation errors rather than inaccuracies in the realizable domain formulation itself. Moreover, as the total number of laminates increases with ply count, the sampling density of the LP space improves. In effect, a denser dataset reduces the relative impact of numerical inaccuracies and validates the robustness of the analytical domain formulation.

Table 5.4: Percentage of laminates violating the characterized balance constraints for varying ply counts.

Total Plies	$V_1^{\mathbf{D}} - V_3^{\mathbf{D}}$ Misclassification (%)	
8	1.52%	
10	0.34%	
12	0.03%	

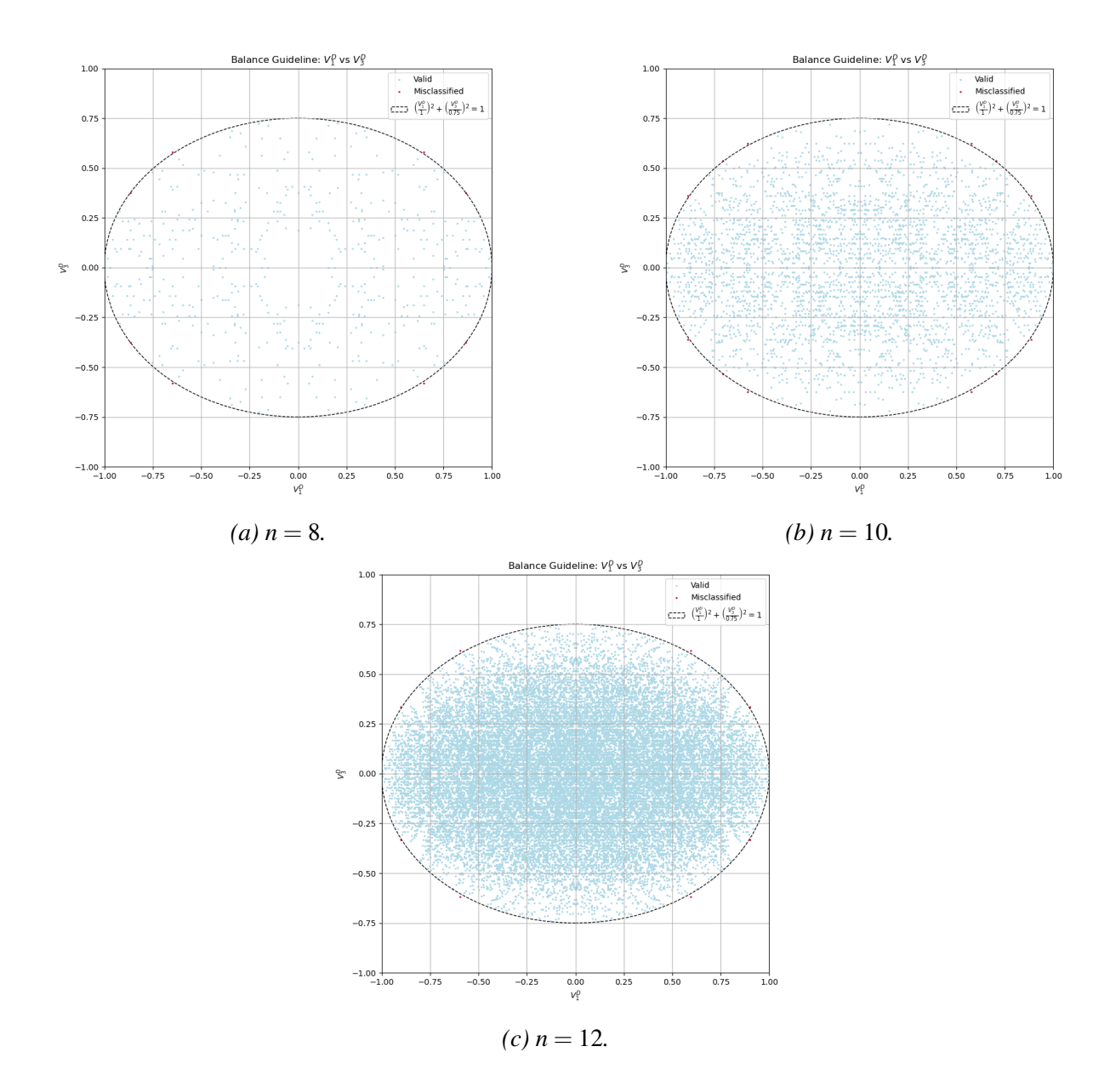


Figure 5.9: Characterized realizable domains subjected to the balance guideline in $V_1^{\mathbf{D}}-V_3^{\mathbf{D}}$ space.

5.1.5 Disorientation – Damage Tolerance – Balance

The realizable domain of combined design guidelines was characterized in Chapter 4.2.5. A conservative boundary was derived, since the equations were sensitive to the discrete nature of ply counts n. This is reflected by an increase in misclassified points as shown in Table 5.5. The derived conservative boundaries converge to the actual boundary with increasing n. Visualization of the characterized realizable domain along with the misclassifications is shown in Figures 5.10 to 5.12.

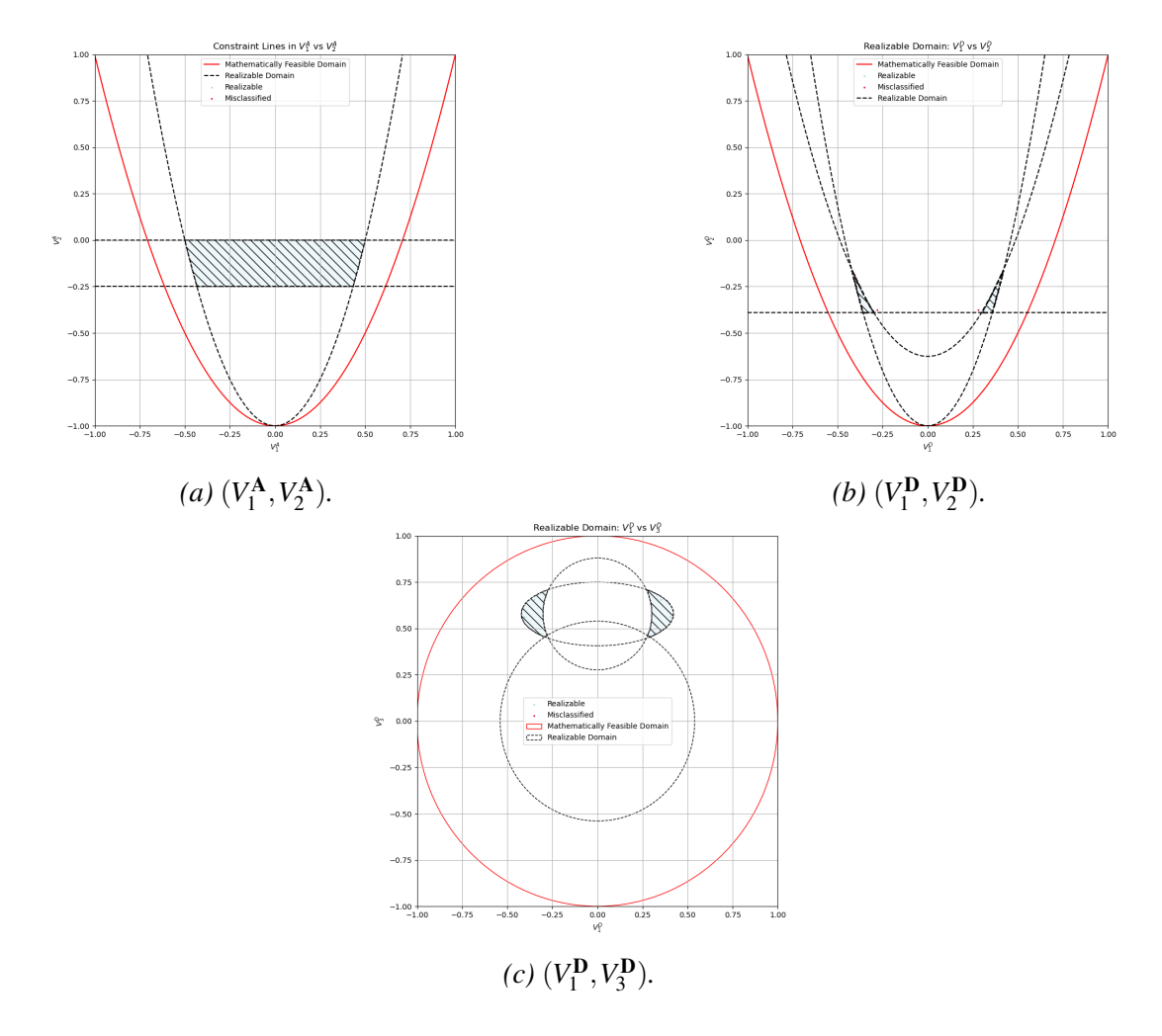


Figure 5.10: Characterized realizable domains under the combined design guideline for a symmetric 8-ply laminate.

Table 5.5: Percentage of laminates misclassified by the characterized combined guidelines for different ply counts.

Total Plies	$V_1^{\mathbf{D}} - V_3^{\mathbf{D}}$	$V_1^{\mathbf{D}} - V_2^{\mathbf{D}}$	$V_1^{\mathbf{A}} - V_2^{\mathbf{A}}$
8	12.5%	50.0%	12.5%
10	0.00%	31.25%	12.5%
12	1.33%	9.33%	5.33%

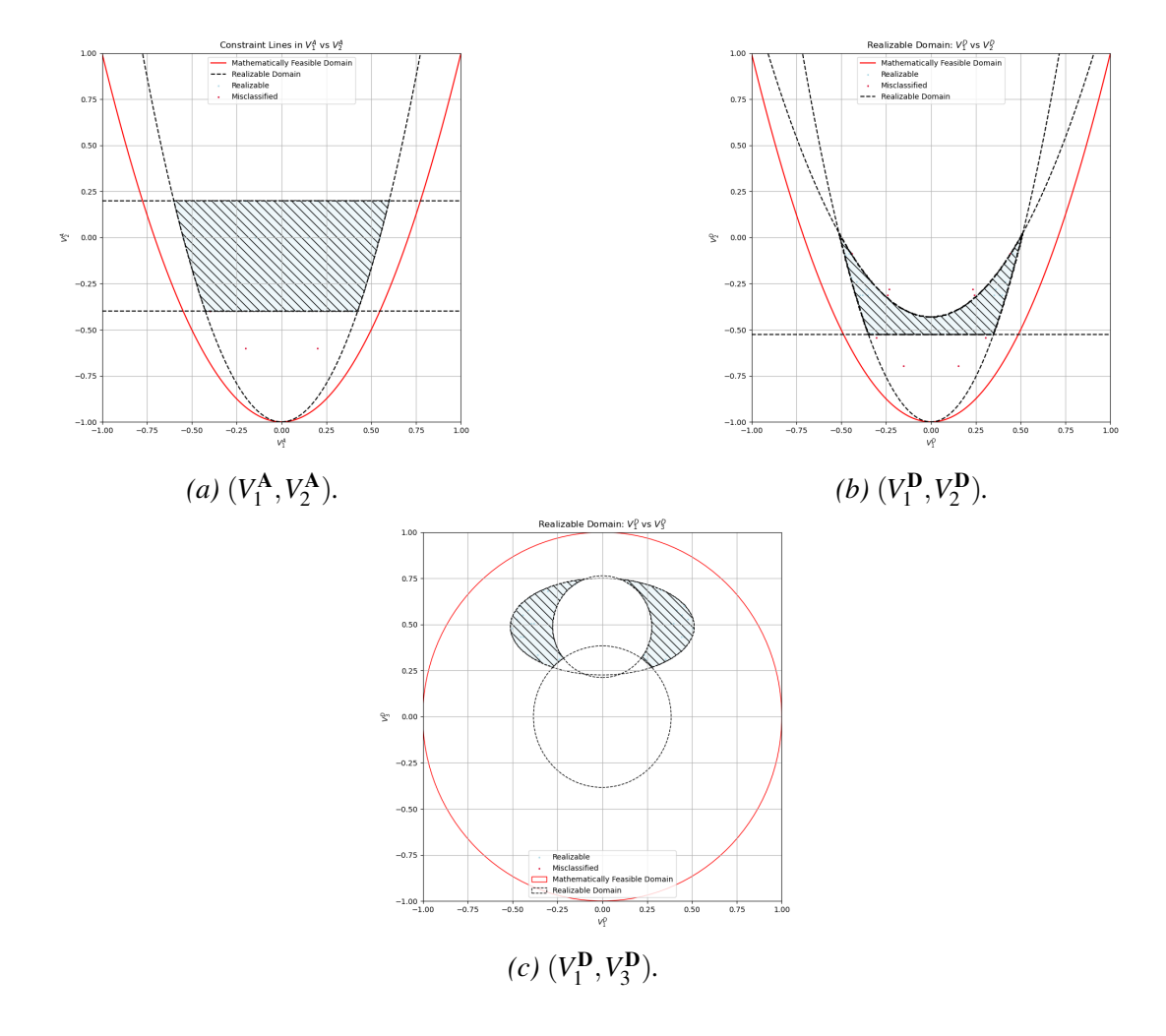


Figure 5.11: Characterized realizable domains under the combined design guideline for a symmetric 10-ply laminate

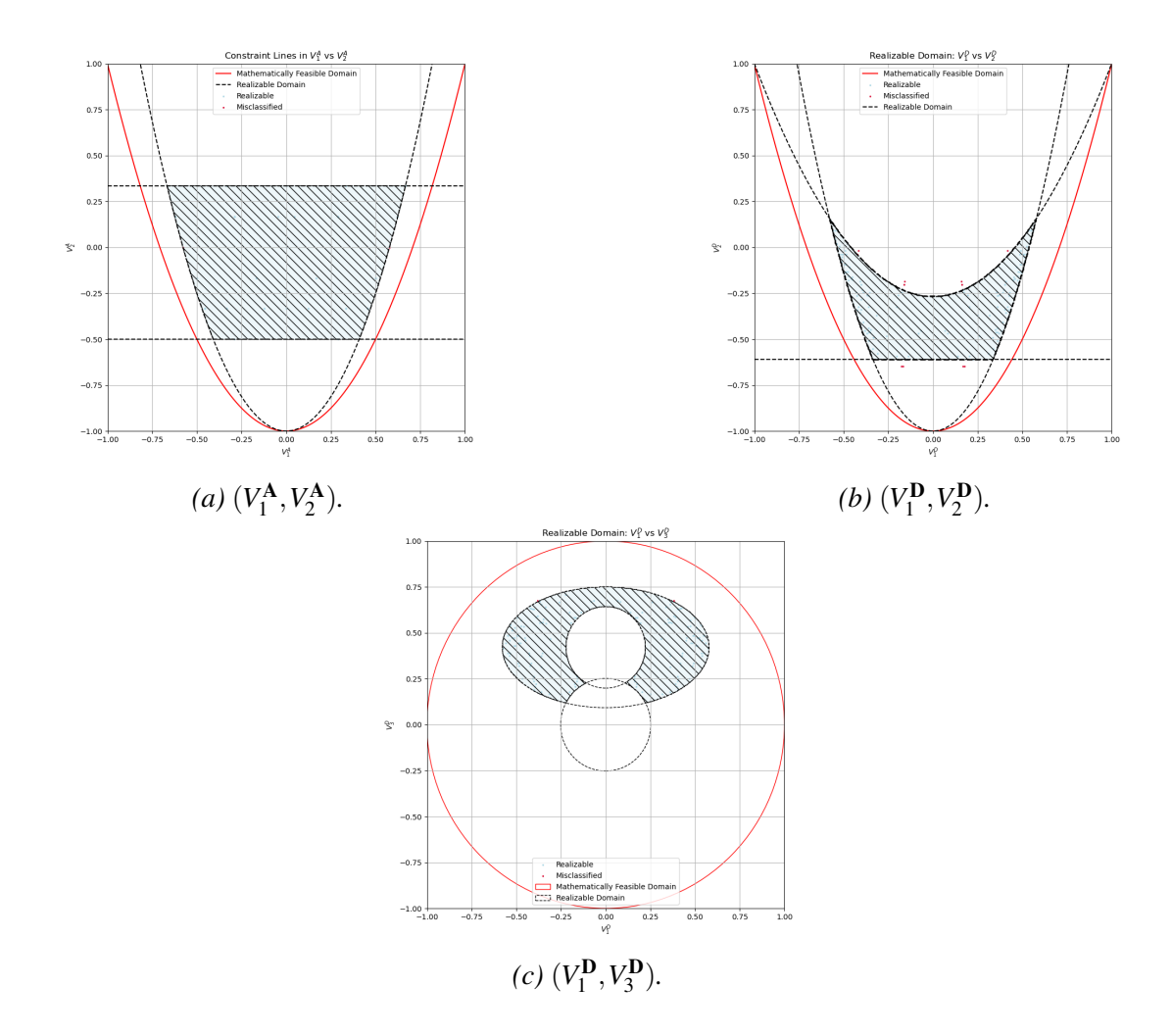


Figure 5.12: Characterized realizable domains under the combined design guideline for a symmetric 12-ply laminate.

5.2 Benchmark optimization problem

To evaluate the effectiveness of the characterized realizable domains, a structured test plan is followed. A single-panel problem is studied under various load cases using a bi-level optimization approach. In the first part of the study, the optimization with respect to the LPs (Level 1) is performed without enforcing any of the derived realizable domains. The optimal LPs and their corresponding critical SFs are recorded. Subsequently, in Level 2, SSs are designed to closely match the optimized LPs. These SSs are explicitly designed to satisfy all design guidelines. FEA is then performed on the designed SSs to compute the critical SFs. By comparing the SFs between Level 1 and Level 2, the difference is quantified, where any reduction in SF indicates a potential structural or stability failure due to mismatch.

In the second part of the study, the same optimization procedure is repeated, this time incorporating the analytically derived realizable domain constraints into Level 1. Again, the optimal LPs, designing the SSs, and their respective SFs are recorded and compared. The objective is to analyze whether the mismatch between the two levels reduces when the realizable domain is enforced at the first level. A reduction in this mismatch would indicate that defining realizable domains improves consistency across optimization levels and contributes to structurally safer laminate designs.

Tables 5.6 and 5.8 present the results from the first test scenario, where the optimization is performed without enforcing the characterized realizable domains. This introduced a mismatch between the optimized LPs and those retrieved from valid SSs, reflected in the changes in the critical SFs.

While some cases (e.g., Sl. no 1–4) showed a positive difference, indicating that the retrieved SS unexpectedly improved the structural performance, cases like 5 and 6 demonstrated a decrease in SF, implying potential structural or buckling failure. These outcomes highlight the risk of ignoring practical design constraints in Level 1: the optimization may select theoretically optimal, but practically unrealizable, designs.

To address this, the second scenario incorporated the characterized realizable domains as inequality constraints during Level 1 optimization. The results are shown in Tables 5.9 and 5.11. Notably, the optimized LPs from Level 1 now already satisfies the design guidelines, ensuring better alignment with the designed SSs in Level 2. Consequently, the mismatch in SFs reduced significantly across most load cases.

This effect is systematically quantified in Table 5.12, which compares the difference in SFs between the two scenarios. The reduction column shows how much mismatch was eliminated by enforcing the characterized realizable domain. For instance, in Sl. Nos. 5 and 6, where the original mismatch led to a SF drop of more than 20%, the mismatch was notably corrected, resulting in safer, more reliable designs.

Table 5.6: Optimal lp obtained and the retrieved SS without realizable domains enforced as constraints during optimization.

Loads (N) Vector		Vector	Design Variables		
N_{x}	N_{xy}		$\operatorname{LP}\left[V_1^{\mathbf{A}}, V_2^{\mathbf{A}}, V_1^{\mathbf{D}}, V_2^{\mathbf{D}}, V_3^{\mathbf{D}}, V_4^{\mathbf{D}}\right]$	h (mm)	
0	-800	Optimal	[-0.2023, -0.2473,-0.4096, -0.1907, 0.1366, 0]	1.39	
	-000	Retrieved	[-0.3333, -0.3333, -0.3148, -0.3703, 0.1666, 0]	1.5	
0	400	Optimal	[-0.2226, -0.3793, -0.4096, -0.1907, 0.1596, 0]	1.11	
	400	Retrieved	[-0.2738, -0.1111, -0.3740, -0.3470, 0.5761, -0.1425]	1.125	
-100	500	Optimal	[-0.1976, -0.2465, -0.3060, -0.3978, 0.1375, 0]	1.26	
-100 300		Retrieved	[-0.2727, -0.2727, -0.3448, -0.4891, 0.6201, -0.1873]	1.375	
-300	-300	Optimal	[-0.2200, -0.3807, -0.0415, -0.9269, 0, 0]	1.26	
-300 -300		Retrieved	[-0.2727, -0.4545, -0.1645, -0.6709, 0.6491, 0]	1.375	
-500	200	Optimal	[0.5623, -0.7302, -0.0050, -1.00, 0, 0]	1.36	
-300 200		Retrieved	[0.0909, -0.4545, 0.1630, -0.6709, 0.6491, 0]	1.375	
500000	100	Optimal	[1.00, 0.9528, 0.9704, 0.8973, 0.0003, 0]	1.48	
300000 100		Retrieved	[0.6667, 0.3333, 0.5740, 0.1481, 0.4167, 0]	1.5	

It is important to note that the characterized realizable domain does not exclusively contain LP sets that always yield SSs obeying all design guidelines. Rather, a point within the realizable domain merely guarantees the existence of at least one real SS that satisfies the design guidelines and maps to that LP vector. A huge overlap of laminates violating the design guidelines over the realizable domain is shown in Figure 5.13. This explains why, in several cases, the SF did not decrease even when the characterized realizable domain was not defined in the first optimization level. Since the realizable domain is a subset of the broader mathematically feasible space, it is possible for the optimizer to naturally converge to a solution that lies within this subset, even without constraining the search. In such cases, the retrieved SS aligns well with the original LPs, and the observed SF mismatch remains the same for both constrained and unconstrained scenarios, resulting in a 0% reduction in mismatch. The position of the optimal LP vector depends on the applied load case. As seen in Table 5.6 initial 3 load cases (shear dominant) lie within the realizable domain. Whereas, tension dominant load case (6^th case) and combined load cases with high compression and shear (5^th case) push the optimum outside the realizable

Sl.no	Retrieved SS
1	$\ \ [\ 45^{\circ}, 90^{\circ}, -45^{\circ}, -45^{\circ}, 90^{\circ}, 45^{\circ}, 45^{\circ}, 90^{\circ}, -45^{\circ}, -45^{\circ}, 90^{\circ}, 45^{\circ}]$
2	$[45^{\circ}, 75^{\circ}, -75^{\circ}, -45^{\circ}, 0^{\circ}, -45^{\circ}, -75^{\circ}, 75^{\circ}, 45^{\circ}]$
3	$[45^{\circ}, 60^{\circ}, 90^{\circ}, -60^{\circ}, -45^{\circ}, 0^{\circ}, -45^{\circ}, -60^{\circ}, 90^{\circ}, 60^{\circ}, 45^{\circ}]$
4	$[-45^{\circ}, -45^{\circ}, 90^{\circ}, 45^{\circ}, 45^{\circ}, 90^{\circ}, 45^{\circ}, 45^{\circ}, 90^{\circ}, -45^{\circ}, -45^{\circ}]$
5	$[45^{\circ}, 45^{\circ}, 0^{\circ}, -45^{\circ}, -45^{\circ}, 90^{\circ}, -45^{\circ}, -45^{\circ}, 0^{\circ}, 45^{\circ}, 45^{\circ}]$
6	$[45^{\circ},0^{\circ},0^{\circ},0^{\circ},0^{\circ},-45^{\circ},-45^{\circ},0^{\circ},0^{\circ},0^{\circ},0^{\circ},45^{\circ}]$

Table 5.7: Retrieved ss for optimal lp obtained without enforcing the design guidelines.

domain. The characterized realizable domain plays a major role in such cases (as seen in Table 5.12).

Moreover, due to the discrete nature of ply counts, laminate thickness is rounded up to the nearest manufacturable value. This slight increase in thickness can contribute to an increased SF in the second level, offering a structural buffer that compensates for any residual mismatches.

Table 5.8: sf calculated for the defined load cases at each level of the bi-level optimization procedure, where realizable domains were not defined as constraints at Level-1.

Sl.no	Safety	Difference in Safety Factor (%)	
51.110	Optimum	Optimum Retrieved	
1	0.999999990211397	1.22453157807513	22.45315901
2	0.99999990206508	1.0503357815691	5.033588443
3	0.999999981285433	1.27112204641014	27.11220702
4	0.999999990239191	1.10688193846731	10.68819493
5	0.999999988755915	0.780581122327177	-21.94188689
6	0.999999985349831	0.751509210705762	-24.84907783

Table 5.9: Optimal lp obtained and the retrieved SS with realizable domains enforced as constraints during optimization.

Loads (N) Vector		Vector	Design Variables		
N_{x}	N_{xy}		$LP\left[V_1^{\mathbf{A}}, V_2^{\mathbf{A}}, V_1^{\mathbf{D}}, V_2^{\mathbf{D}}, V_3^{\mathbf{D}}, V_4^{\mathbf{D}}\right]$	h (mm)	
0	-800	Optimal	[-0.2076, -0.2105, -0.4076, -0.1847, 0.1623, 0]	1.39	
	-000	Retrieved	[-0.3333, -0.3333, -0.3148, -0.3703, 0.1667, 0]	1.5	
0	400	Optimal	[-0.2608, -0.2195, -0.4076, -0.1847, 0.2349, 0]	1.11	
	400	Retrieved	[-0.2737, -0.1111, -0.3740, -0.3470, 0.5761, -0.1425]	1.125	
-100	500	Optimal	[-0.2079, -0.2074, -0.3474, -0.3052, 0.1419, 0]	1.26	
-100	300	Retrieved	[-0.2727, -0.2727, -0.3448, -0.4891, 0.6201, -0.1874]	1.375	
-300	-300	Optimal	[-0.2601, -0.2170, -0.2293, -0.5412, 0.2806, 0]	1.26	
-300 -300		Retrieved	[-0.2727, -0.2727, -0.3448, -0.4891, 0.6201, -0.1874]	1.375	
-500	200	Optimal	[-0.2059, -0.2100, -0.2078, -0.5843, 0.2121, 0]	1.36	
-300 200		Retrieved	[-0.3333, -0.3333, -0.3148, -0.3703, 0.1667, 0]	1.375	
500000	100	Optimal	[0.8626, 0.6905, 0.6112, 0.2225, -0.0074, 0]	1.48	
300000		Retrieved	[0.6667, 0.3333, 0.5463, 0.0926, -0.3889, 0]	1.5	

Table 5.10: Retrieved ss for optimal lp obtained with enforcing the design guidelines.

Sl.no	Retrieved SS
1	$\ \ [\ 45^{\circ}, 90^{\circ}, -45^{\circ}, -45^{\circ}, 90^{\circ}, 45^{\circ}, 45^{\circ}, 90^{\circ}, -45^{\circ}, -45^{\circ}, 90^{\circ}, 45^{\circ}]$
2	$[45^{\circ}, 75^{\circ}, -75^{\circ}, -45^{\circ}, 0^{\circ}, -45^{\circ}, -75^{\circ}, 75^{\circ}, 45^{\circ}]$
3	$[45^{\circ}, 60^{\circ}, 90^{\circ}, -60^{\circ}, -45^{\circ}, 0^{\circ}, -45^{\circ}, -60^{\circ}, 90^{\circ}, 60^{\circ}, 45^{\circ}]$
4	$[45^{\circ}, 60^{\circ}, 90^{\circ}, -60^{\circ}, -45^{\circ}, 0^{\circ}, -45^{\circ}, -60^{\circ}, 90^{\circ}, 60^{\circ}, 45^{\circ}]$
5	$[45^{\circ}, 90^{\circ}, -45^{\circ}, -45^{\circ}, 90^{\circ}, 45^{\circ}, 45^{\circ}, 90^{\circ}, -45^{\circ}, -45^{\circ}, 90^{\circ}, 45^{\circ}]$
6	$[-45^{\circ}, 0^{\circ}, 0^{\circ}, 0^{\circ}, 45^{\circ}, 0^{\circ}, 0^{\circ}, 0^{\circ}, 0^{\circ}, 45^{\circ}, 0^{\circ}, 0^{\circ}, 0^{\circ}, -45^{\circ}]$

Table 5.11: sf calculated for the defined load cases at each level of the bi-level optimization procedure, where realizable domains were defined as constraints at Level-1.

Sl.no	S	Difference in	
	Optimum	Retrieved	SF (%)
1	0.999999990208326	1.22453157807513	22.45315901
2	0.999999990268234	1.0503357815691	5.033579179
3	0.999999990172361	1.27112204641014	27.11220589
4	1.00000001368227	1.07949457899591	7.949456423
5	1.00000001073767	1.14714404793283	14.71440356
6	0.999999985349831	0.923659810741142	-7.634017573

Table 5.12: Reduction of SF mismatch occurring due to the derived equations for realizable domain.

Sl.no	Difference i	Reduction of	
	Without Guidelines	With Guidelines	Difference (%)
1	22.45315901	22.45315901	0.0000
2	5.033588443	5.033579179	0.0000
3	27.11220702	27.11220589	0.0000
4	10.68819493	7.949456423	-25.6240
5	-21.94188689	14.71440356	167.0608
6	-24.84907783	-7.634017573	69.2785

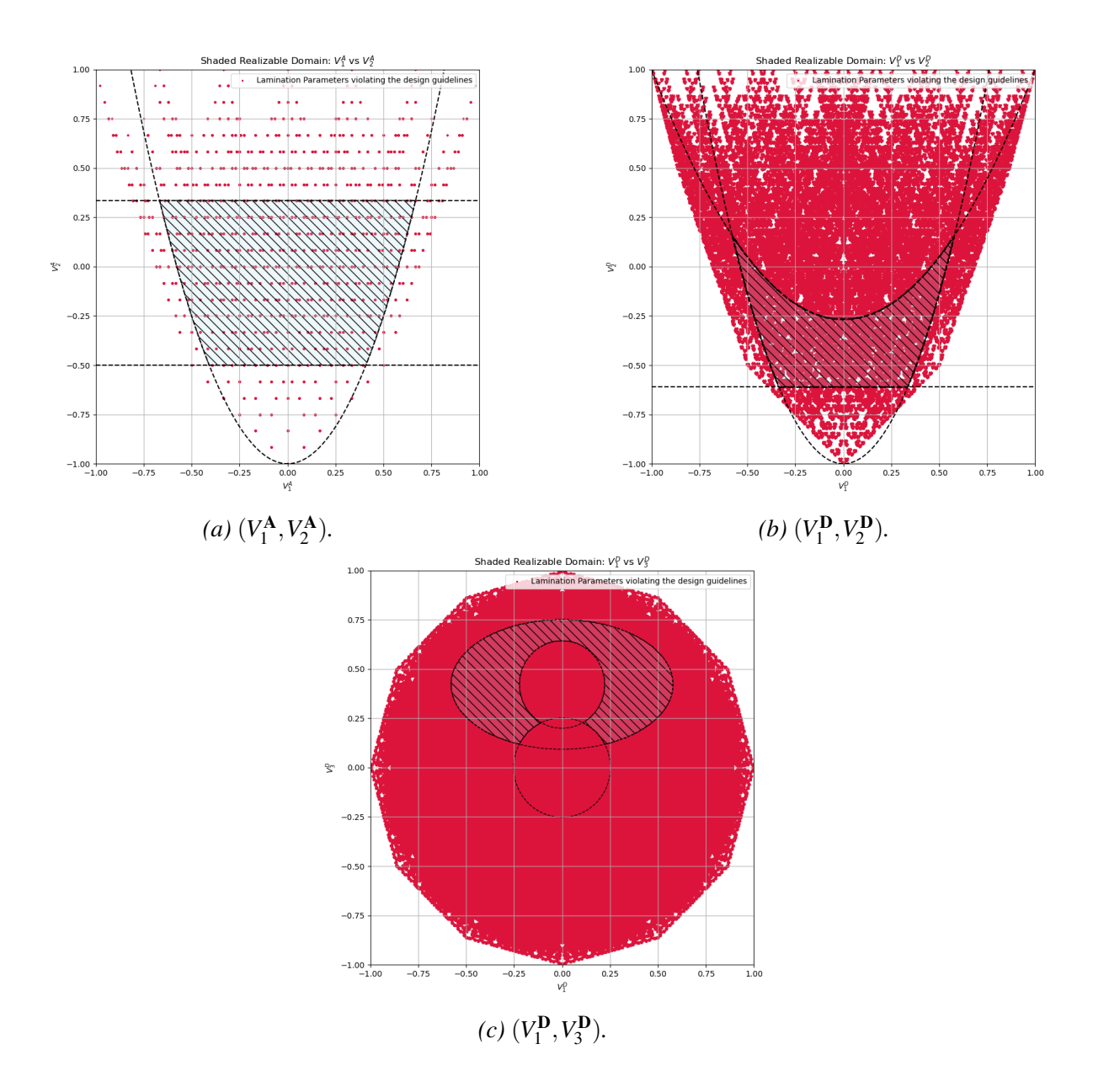


Figure 5.13: Overlap of lp violating the design guidelines for 12-ply symmetric laminates in the characterized realizable domain.

6 Conclusions

6.1 Summary of the Thesis

This thesis aimed to bridge the gap between mathematically feasible LPs and those that correspond to physically realizable SSs adhering to practical design guidelines. The *realizable domain* was introduced to characterize the subset of LP space (pertaining to design guidelines). LP space maps SS, which is feasible with respect to the design guidelines such as disorientation, damage tolerance, contiguity, and balance.

Analytical expressions for the realizable domain were derived for each guideline and visualized in various LP projection spaces for different ply counts (n = 8, 10, 12). These domains were validated against brute-force enumeration of symmetric laminates with fiber angles ranging from -90° to 90° in $\delta15^{\circ}$ steps. The results confirmed that the derived constraints accurately enclosed the practically realizable regions with minimal misclassification (1% - 10% for 12-ply laminates subjected to the combined design guidelines).

The realizable domains were then incorporated into a bi-level optimization framework. Two test scenarios were compared: (1) with the domains enforced, and (2) without the domains enforced during the 1st level of optimization. Across multiple load cases, the SF mismatches between Level 1 and Level 2 were computed to assess the impact of the realizable domain constraints. For the load cases where there was a high reduction in SF (> 20% for tension dominant case), defining the realizable domain at earlier stages proved beneficial, and a minimum mismatch reduction of 69.3% was observed.

6.2 Inferences from the Results

Several important insights emerged from the numerical evaluation:

- Improved accuracy with higher ply counts: Across all design guidelines, the proportion of misclassified laminates decreased as the number of plies increased. This is attributed to the discrete nature of SSs better approximating the continuous assumption used in the analytical derivations.
- **High fidelity of characterized domains:** The analytically defined realizable domains showed excellent agreement with actual realizable regions, particularly for disorientation, damage tolerance, and balance guidelines. Misclassification rates were mostly below 1%, with outliers often yielding from numerical rounding and/or boundary approximation.

- Limited utility of contiguity domain: For contiguity, the realizable domain closely matched the mathematically feasible space. Since the constraint offered a negligible reduction in design space (for $\delta\theta = 15^{\circ}$), enforcing it in LP space yielded limited benefit.
- Mismatch reduction in bi-level optimization: Incorporating the realizable domain at the
 first level of bi-level optimization led to a clear reduction in SF mismatch between the
 two levels, especially in cases where the unconstrained optimum lay outside the realizable
 region.
- **Robustness of the approach:** Even in cases where the mismatch was initially negligible, the use of realizable domains did not deteriorate performance. This confirms that realizable domains only restrict infeasible regions and never exclude good solutions.
- **Insight into zero reduction cases:** When the unconstrained optimum already lies within the realizable domain, the retrieved SS aligns well with the target LP, and the SF difference remains unchanged. Thus, the mismatch reduction is zero, not because the domain is ineffective, but because the optimizer naturally chose a realizable point.
- Benefits observed in non-zero reduction cases: For tension dominant, and coupled (shear and compression) load cases, the optimum was observed to be outside the characterized realizable domain. The critical SF of the retrieved SS was reduced by 20 25%. Defining the realizable domain for obtaining the conceptual stiffness reduced the mismatch completely for the coupled (shear and compression) load case. Whereas, a mismatch reduction of 69.3% was observed for the tension dominant case.

6.3 Future work

While this study provides a strong foundation for integrating design guidelines into early-stage laminate optimization, several directions remain open for further research:

- Extension to variable stiffness laminates: The current work is limited to symmetric laminates with constant stiffness. Extending realizable domain characterization to more complex configurations (multi-panel problems) is needed for generalization. Guidelines such as the 10%-rule and blending constraints may be studied and potentially coupled with the derived realizable domains.
- Improved boundary approximation: The few misclassifications observed may be addressed by refining the current linear or polynomial fits with machine learning models or spline-based interpolations.
- Probabilistic Realizable Domains: Rather than binary classification (inside or outside
 the domain), a probabilistic confidence metric may be introduced, enabling risk-aware
 optimization and robust laminate design.

• Characterization of higher dimensional LP space: For the visualization purposes, pairs of LPs were considered to characterize the realizable domain. Characterizing the realizable domain in a higher-dimensional vector space could be beneficial to uncouple the realizable and non-realizable laminates.

In conclusion, this thesis demonstrates that realizable domains offer a computationally and structurally effective means of ensuring guideline-compliant laminate designs. Their integration into optimization workflow reduces epistemic uncertainty, enhances design safety, and supports a more streamlined transition from conceptual to manufacturable composite structures.

Bibliography

- Abdalla, M., C. Kassapoglou, and Z. Gürdal (Jan. 2009). "Formulation of composite laminate robustness constraint in lamination parameters space". In: *Collection of Technical Papers AIAA/ASME/ASCE/AHS/ASC Structures, Structural Dynamics and Materials Conference*.
- Aboudi, J. (1991). *Mechanics of composite materials: a unified micromechanical approach*. Studies in applied mechanics. Includes bibliographical references and index. Elsevier.
- Achenbach, J. (1975). A Theory of Elasticity with Microstructure for Directionally Reinforced Composites. English. Springer Verlag.
- Bailie, J. A., R. P. Ley, and A. Pasricha (1997). "A SUMMARY AND REVIEW OF COMPOSITE LAMINATE DESIGN GUIDELINES". In: URL: https://api.semanticscholar.org/CorpusID:138632302.
- Barbero, E. J. (2010). *Introduction to Composite Materials Design*. 2nd. CRC Press.
- Belegundu, A. D. (1985). "A Study of Mathematical Programming Methods for Structural Optimization". In: URL: https://api.semanticscholar.org/CorpusID: 59878906.
- Bletzinger, K.-U. (2021). "Structural Optimization [Lecture Notes]". Available: https://www.moodle.tum.de/pluginfile.php/4138872/mod_resource/content/1.
- Bloomfield, M., J. Herencia, and P. Weaver (Apr. 2008). "Optimisation of Anisotropic Composite Plates Incorporating Non-Conventional Ply Orientations". In: DOI: 10.2514/6.2008-1918.
- Bordogna, M., T. Macquart, D. Bettebghor, and R. De Breuker (June 2016). "Aeroelastic Optimization of Variable Stiffness Composite Wing with Blending Constraints". In: DOI: 10.2514/6.2016-4122.
- Boyd, S. and L. Vandenberghe (2004). *Convex Optimization*. Cambridge, UK: Cambridge University Press.
- Bruyneel, M. (2008). "Optimization of laminated composite structures: problems, solution procedures and applications". In: URL: https://api.semanticscholar.org/CorpusID:112386609.
- Chawla, K. K. (1988). "Composite materials: science and engineering". In.

- Dähne, S., E. Werthen, D. Zerbst, L. Tönjes, H. Traub, and C. Hühne (May 2024). "Lightworks, a scientific research framework for the design of stiffened composite-panel structures using gradient-based optimization". In: *Structural and Multidisciplinary Optimization* 67, pp. 1–15. DOI: 10.1007/s00158-024-03783-1.
- Daniel, I. M. and O. Ishai (1994). *Engineering Mechanics of Composite Materials*. 2nd. New York: Oxford University Press.
- Diaconu, C., M. Sato, and H. Sekine (Mar. 2002). "Feasible Region in General Design Space of Lamination Parameters for Laminated Composites". In: *Aiaa Journal AIAA J* 40, pp. 559–565. DOI: 10.2514/2.1683.
- Diaconu, C. and H. Sekine (Oct. 2004). "Layup Optimization for Buckling of Laminated Composite Shells with Restricted Layer Angles". In: *Aiaa Journal AIAA J* 42, pp. 2153–2163. DOI: 10.2514/1.931.
- Diaconu, C. G., M. Sato, and H. Sekine (2002). "Buckling characteristics and layup optimization of long laminated composite cylindrical shells subjected to combined loads using lamination parameters". In: *Composite Structures* 58.4, pp. 423–433. DOI: https://doi.org/10.1016/S0263-8223(02)00130-7. URL: https://www.sciencedirect.com/science/article/pii/S0263822302001307.
- Ekeland, I. and T. Turnbull (1983). "Infinite-Dimensional Optimization And Convexity". In: URL: https://api.semanticscholar.org/CorpusID:117953609.
- Eliezer, C. J. and D. E. Daykin (Jan. 1967). "GENERALIZATIONS AND APPLICATIONS OF CAUCHY-SCHWARZ INEQUALITIES". In: *The Quarterly Journal of Mathematics* 18.1, pp. 357–360. DOI: 10.1093/qmath/18.1.357. eprint: https://academic.oup.com/qjmath/article-pdf/18/1/357/4498774/18-1-357.pdf. URL: https://doi.org/10.1093/qmath/18.1.357.
- Fedon, N., P. Weaver, A. Pirrera, and T. Macquart (Nov. 2020). "A method using beam search to design the lay-ups of composite laminates with many plies". In: *Composites Part C: Open Access* 4, p. 100072. DOI: 10.1016/j.jcomc.2020.100072.
- Franz, M., B. Schleich, and S. Wartzack (July 2019). "Variation Analysis of Design Parameters of Fibre-Reinforced Plastic Parts". In: *Proceedings of the Design Society: International Conference on Engineering Design* 1, pp. 2725–2734. DOI: 10.1017/dsi.2019.279.
- Fukunaga, H. and H. Sekine (1992). "Stiffness design method of symmetric laminates using lamination parameters". In: *AIAA Journal* 30.11, pp. 2791–2793. DOI: 10.2514/3.11304. eprint: https://doi.org/10.2514/3.11304. URL: https://doi.org/10.2514/3.11304.

- Ghiasi, H., K. Fayazbakhsh, D. Pasini, and L. Lessard (2010). "Optimum stacking sequence design of composite materials Part II: Variable stiffness design". In: *Composite Structures* 93.1, pp. 1–13. DOI: https://doi.org/10.1016/j.compstruct.2010.06.001. URL: https://www.sciencedirect.com/science/article/pii/S0263822310001947.
- Ghiasi, H., D. Pasini, and L. Lessard (2009). "Optimum stacking sequence design of composite materials Part I: Constant stiffness design". In: *Composite Structures* 90.1, pp. 1–11. DOI: https://doi.org/10.1016/j.compstruct.2009.01.006. URL: https://www.sciencedirect.com/science/article/pii/S026382230900018X.
- Grenestedt, J. and P. Gudmundson (Dec. 1993). "Layup Optimization of Composite Material Structures". In: *Optimal Design with Advanced Materials*. DOI: 10.1016/B978-0-444-89869-2.50027-5.
- Gürdal, Z., R. T. Haftka, and P. Hajela (1999). *Design and Optimization of Laminated Composite Materials*. Wiley.
- Haftka, R. T. and Z. Gürdal (1992). *Elements of Structural Optimization*. 3rd ed. Vol. 11. Solid Mechanics and Its Applications. Springer Science+Business Media Dordrecht. Springer Dordrecht, pp. XIV + 481. DOI: 10.1007/978-94-011-2550-5. URL: https://doi.org/10.1007/978-94-011-2550-5.
- Herakovich, C. T. (1998). Mechanics of Fibrous Composites. Wiley.
- IJsselmuiden, S. (2011). "Optimal Design of Variable Stiffness Composite Structures Using lamination Parameters". English. Dissertation (TU Delft). Delft University of Technology.
- Irisarri, F.-X., A. Lasseigne, F.-H. Leroy, and R. Le Riche (2014). "Optimal design of laminated composite structures with ply drops using stacking sequence tables". In: *Composite Structures* 107, pp. 559–569. DOI: https://doi.org/10.1016/j.compstruct.2013.08.030. URL: https://www.sciencedirect.com/science/article/pii/S0263822313004376.
- Jones, R. M. (1999). *Mechanics of Composite Materials*. Taylor & Francis.
- Kaw, A. K. (2005). *Mechanics of Composite Materials*. 2nd. CRC Press.
- Love, A. E. H. (1888). "The Small Free Vibrations and Deformation of a Thin Elastic Shell". In: *Philosophical Transactions of the Royal Society of London. A* 179, pp. 491–546. DOI: 10.1098/rsta.1888.0016. URL: https://royalsocietypublishing.org/doi/10.1098/rsta.1888.0016.
- Mallick, P. (2007). Fiber-Reinforced Composites: Materials, Manufacturing, and Design. 3rd. CRC Press.

- Matsuzaki, R. and A. Todoroki (2007). "Stacking-sequence optimization using fractal branch-and-bound method for unsymmetrical laminates". In: *Composite Structures* 78.4, pp. 537—550. DOI: https://doi.org/10.1016/j.compstruct.2005.11.015. URL: https://www.sciencedirect.com/science/article/pii/S0263822305003454.
- Miki, M. (1983). "A Graphical Method for Designing Fibrous Laminated Composites with Required In-Plane Stiffness". In: *Transactions of the Japan Society for Composite Materials* (*JSCM*) 9, pp. 51–55.
- Miki, M. and Y. Sugiyama (1993). "Optimum Design of Laminated Composite Plates Using Lamination Parameters". In: AIAA Journal 31.5, pp. 921–922. DOI: 10.2514/3.49033. eprint: https://doi.org/10.2514/3.49033. URL: https://doi.org/10.2514/3.49033.
- Nettles, A. (Oct. 1994). "Basic Mechanics of Laminated composite plates". In.
- Niu, M. C.-Y. (1992). Composite airframe structures: practical design information and data. Conmilit Press.
- Papalambros, P. Y. and D. J. Wilde (2017). *Principles of Optimal Design: Modeling and Computation*. 3rd ed. Cambridge University Press.
- Pipes, R. B. and N. Pagano (1970). "Interlaminar Stresses in Composite Laminates Under Uniform Axial Extension". In: *Journal of Composite Materials* 4.4, pp. 538–548. DOI: 10.1177/002199837000400409. URL: https://doi.org/10.1177/002% 20199837000400409.
- Soutis, C. (2005). "Fibre reinforced composites in aircraft construction". In: *Progress in Aerospace Sciences* 41.2, pp. 143–151. DOI: 10.1016/j.paerosci.2005.02.004.
- Tsai, S. W. and N. J. Pagano (1968). "INVARIANT PROPERTIES OF COMPOSITE MATERIALS." In: URL: https://api.semanticscholar.org/CorpusID:136436586.
- Design, and Analysis. Routledge: Materials Usage. Verchery, G. (Mar. 2011). "Design rules for the laminate stiffness". In: *Mechanics of Composite*

US Dept of Defense (1999). Composite Materials Handbook-MIL 17. 1st. Vol. III: doi:10.1201/9781315139890

- Materials 47, pp. 47–58. DOI: 10.1007/s11029-011-9186-x.
- Wächter, A. and L. Biegler (Mar. 2006). "On the Implementation of an Interior-Point Filter Line-Search Algorithm for Large-Scale Nonlinear Programming". In: *Mathematical programming* 106, pp. 25–57. DOI: 10.1007/s10107-004-0559-y.
- Zimmermann, M. (Apr. 2022a). Lecture notes in Multidisciplinary Design Optimization, Lecture 1: Introduction. Laboratory for Product Development and Lightweight Design (LPL), Technical University of Munich.

- Zimmermann, M. (Apr. 2022b). Lecture notes in Multidisciplinary Design Optimization, Lecture 5: Optimization Algorithms 1. Laboratory for Product Development and Lightweight Design (LPL), Technical University of Munich.
- Zimmermann, M. (Apr. 2022c). Lecture notes in Multidisciplinary Design Optimization, Lecture 6: Optimization Algorithms 2. Laboratory for Product Development and Lightweight Design (LPL), Technical University of Munich.
- Zimmermann, M. (Oct. 2024). Lecture notes in Methods of Product Development, Lecture 5: Models. Laboratory for Product Development and Lightweight Design (LPL), Technical University of Munich.

Appendix

A Computational approach for laminate dataset generation and filtering

This section presents the computational framework developed to validate the analytically characterized realizable domains discussed in Section 4.2. A brute-force laminate generation approach is employed to evaluate all possible symmetric laminates constructed from discrete fibre orientation sets. These laminates are tested against several design guidelines, and their corresponding LPs are computed. The validated laminates are then visualized in various parameter spaces to examine their alignment with the analytically derived bounds.

Analytical characterization presented in Chapter 4.2 offers closed-form expressions for LP realizable domain under the given constraints. However, these derivations involve idealized assumptions, continuous approximations, or asymptotic behaviors. In contrast, SSs are inherently discrete, especially in manufacturing contexts where fiber angles can only assume a discrete set of values. Hence, a brute-force computational search helps bridge the gap between analytical idealization and practical realizability.

The objective is to:

- Generate all possible symmetric laminates given an angle step size and ply count.
- Apply design guideline filters to exclude non-feasible laminates.
- Compute all eight LPs $(V_{1-4}^{\mathbf{A}} \text{ and } V_{1-4}^{\mathbf{D}})$.
- Store and plot feasible laminates to compare against theoretical realizable domains.

Table A.1: Breakdown of the use of Python scripts for the verification of the derived realizable domains.

Requirement	Solution
Memory management (see Figure A.1)	With an increasing number of pies, the number of feasible laminates increases exponentially. For example, a 12-ply symmetric laminate has 2,985,984 different possible combinations of fibre orientations for $\delta15^{\circ}$. To account for this huge set of data, batch processing is used to split the generated laminates into smaller batches for further processing and save them as .pkl files before clearing the memory. This prevents RAM exhaustion.
Design guideline filtering (see Figures A.2 to A.5)	While studying the laminates that obey the design guidelines, LPs are calculated only once they pass the guideline check. Also, just the unique set of parameters is stored to reduce the computational load.
Post processing and visualization	The stored .pkl files are loaded to visualize the 2-D projections of LPs. This way, the characterized realizable domains are verified for their accuracy.

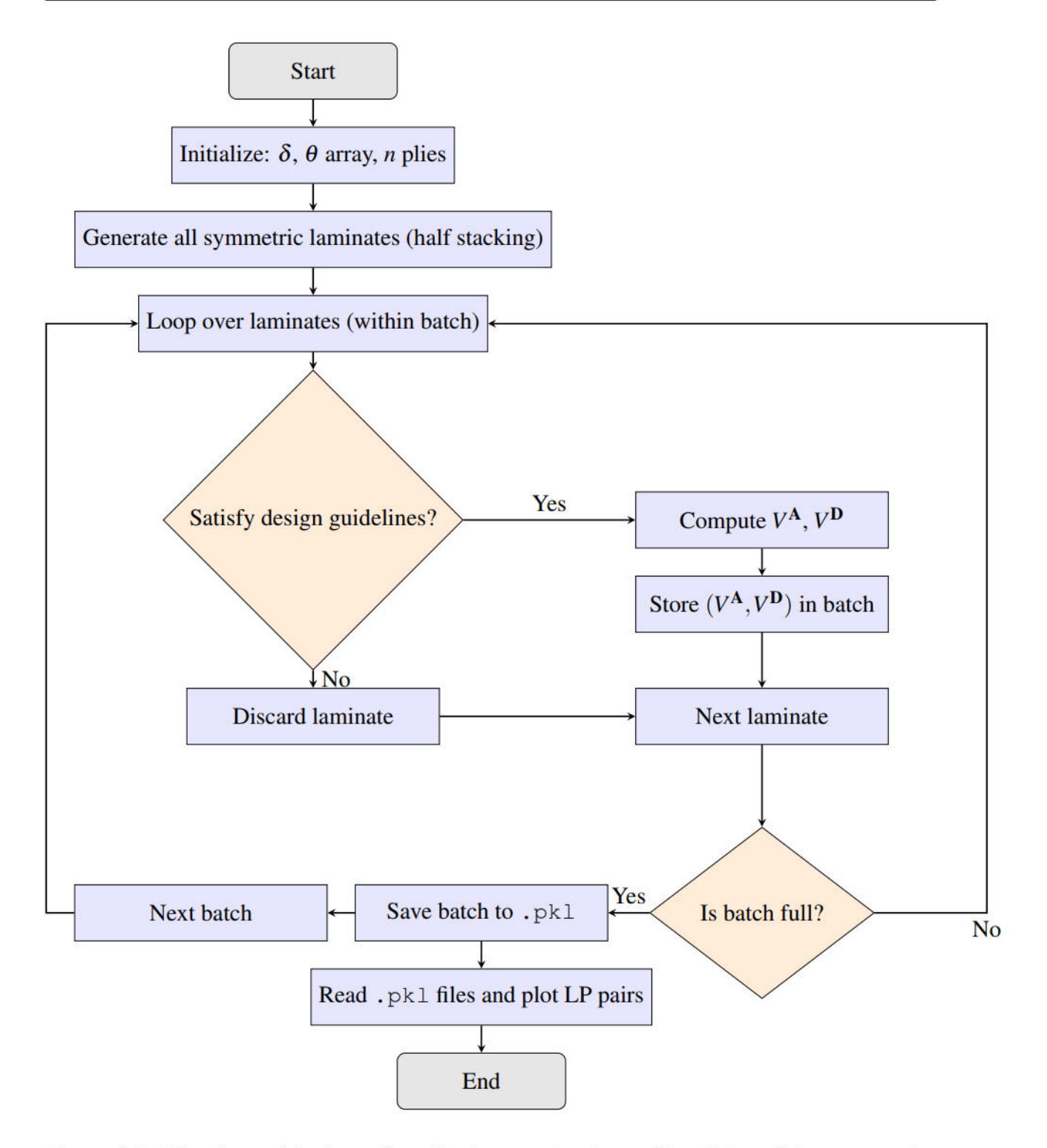


Figure A.1: Flowchart of the brute-force laminate evaluation and batch-based data generation and plotting process.

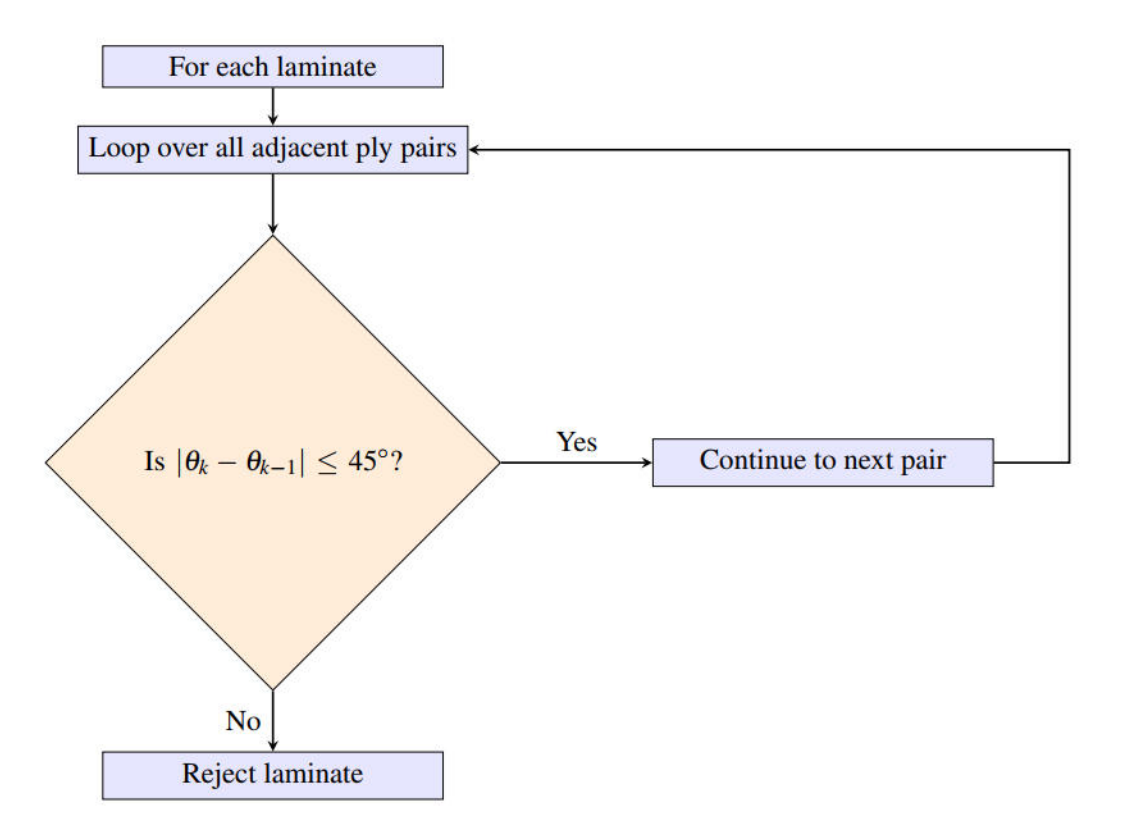


Figure A.2: Flowchart for enforcing the disorientation design guideline.

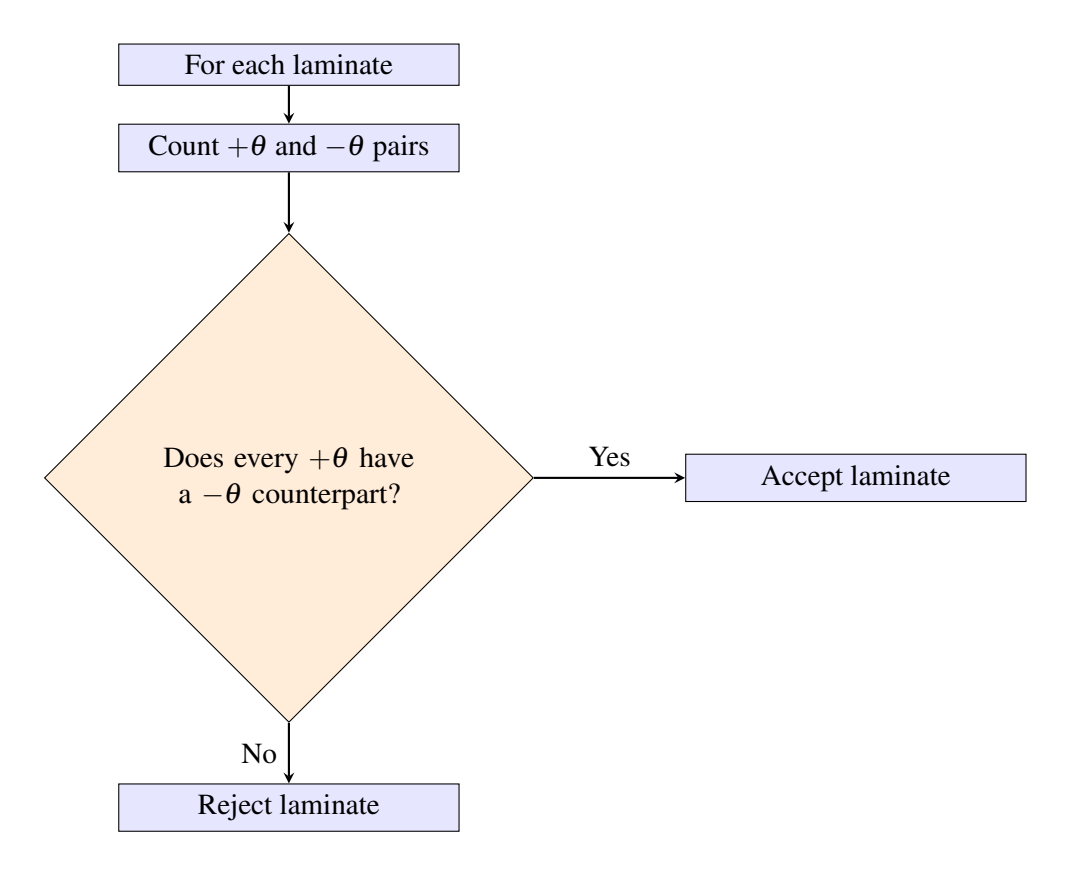


Figure A.3: Flowchart for enforcing the balanced design guideline.

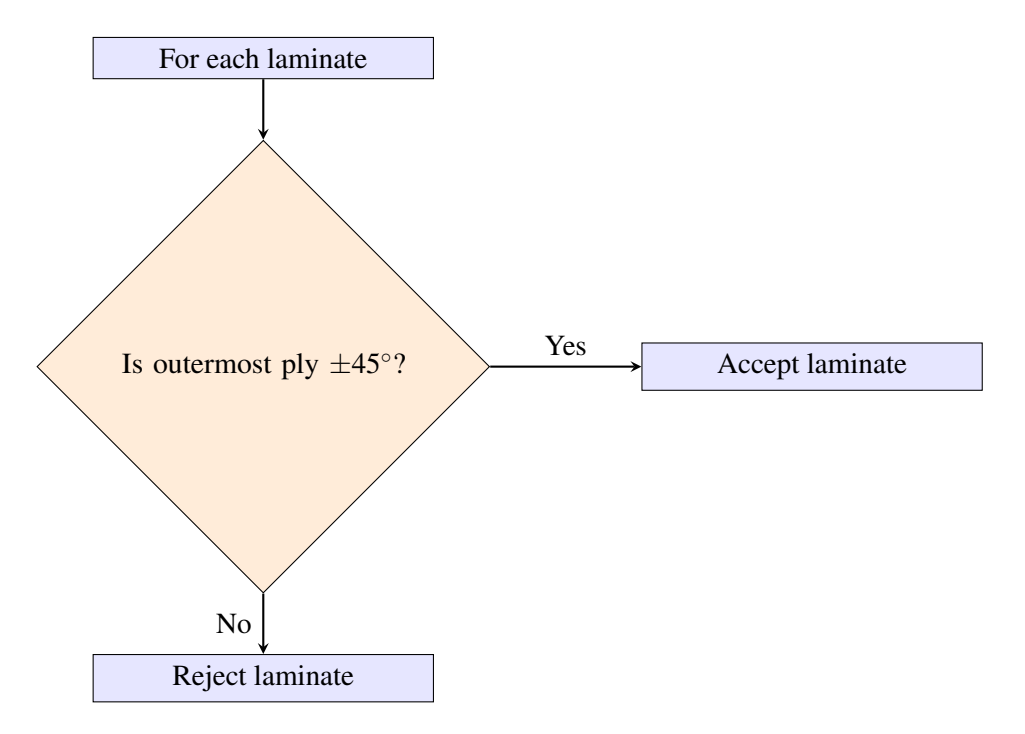


Figure A.4: Flowchart for enforcing the damage tolerance design guideline.

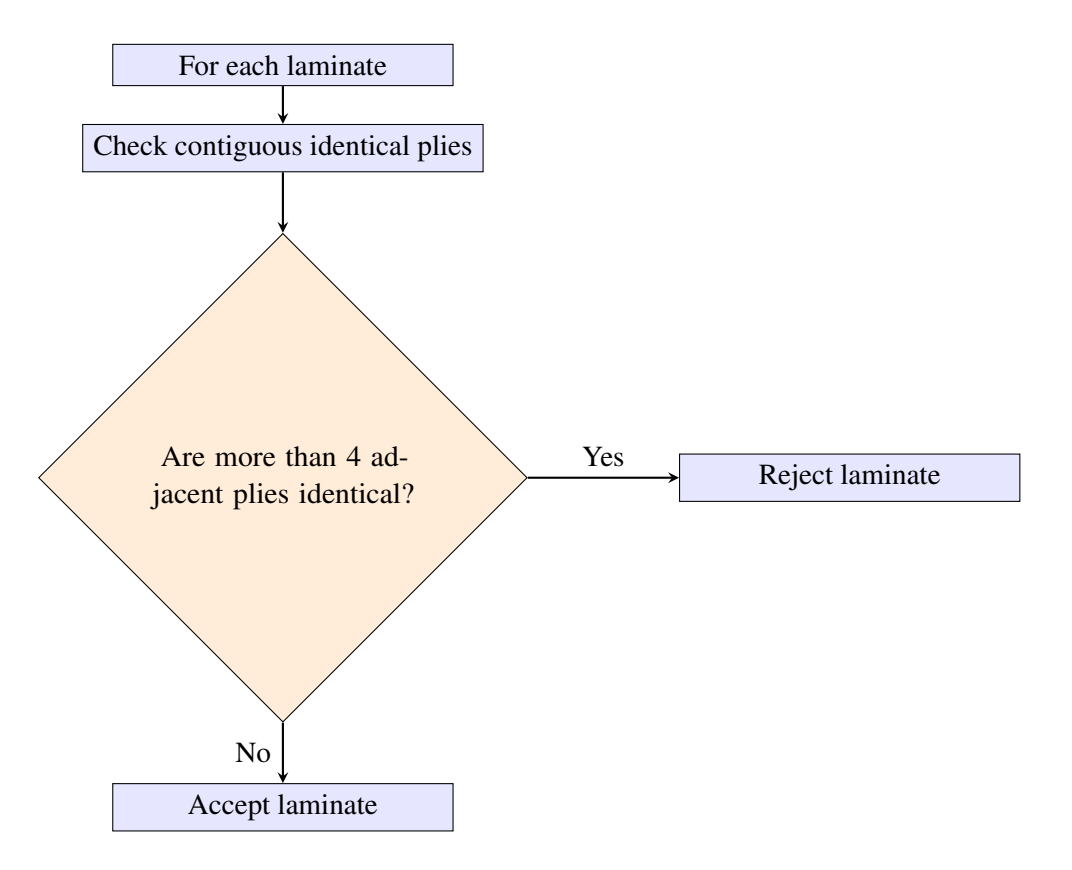


Figure A.5: Flowchart for enforcing the contiguity design guideline.

B Contiguity design guideline enforced on conventional laminates

Conventional laminates are made of fibre orientations in $[0^{\circ}, \pm 45^{\circ}, 90^{\circ}]$. The equation defining the contiguity design guideline in LP space was derived in Chapter 4.2.3 (see Equation 4.32). By substituting the value of δ with 45°, the equation for the realizable domain for conventional laminates is obtained. In Figure B.1, the realizable domain for varying ply counts is visualized, and the percentage of misclassified points is summarized in Table B.1.

Table B.1: Percentage of conventional laminates violating the characterized contiguity constraint for varying ply counts.

Total Plies	$V_1^{\mathbf{D}} - V_3^{\mathbf{D}}$ Misclassification (%)
14	0.0%
16	0.0%
18	0.0%
20	0.0%

From the percentage of misclassification, it is concluded that the derived realizable domain defines the contiguity guideline in the LP space perfectly. Also, from Figure B.1 it is observed that the rate of reduction of the $|\mathbf{R}|_c^{\mathbf{D}}$ is higher when compared to non-conventional laminates. To validate this hypothesis, the reduction of $|\mathbf{R}|_c^{\mathbf{D}}$ is plotted across varying ply counts (see Figure B.2).

Although $|\mathbf{R}|_c^{\mathbf{D}}$ is reduced by over 20% for conventional laminates with n > 200, the reduction is not negligible for smaller ply counts. Hence, when optimizing the conventional laminates, the contiguity guideline should also be defined and enforced during the optimization process with LPs as design variables.

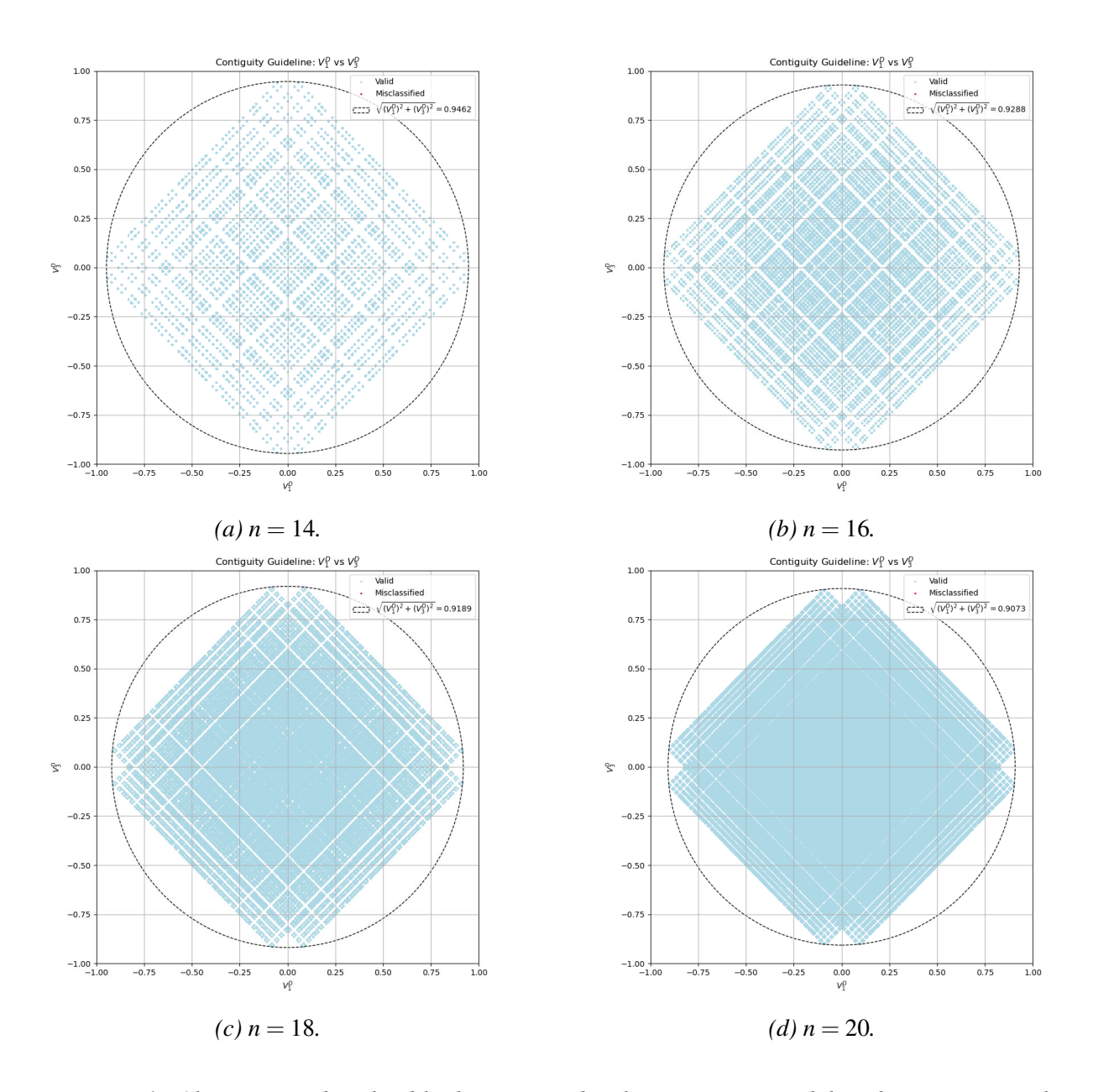


Figure B.1: Characterized realizable domains under the contiguity guideline for conventional laminates $\delta\theta=45^{\circ}$.

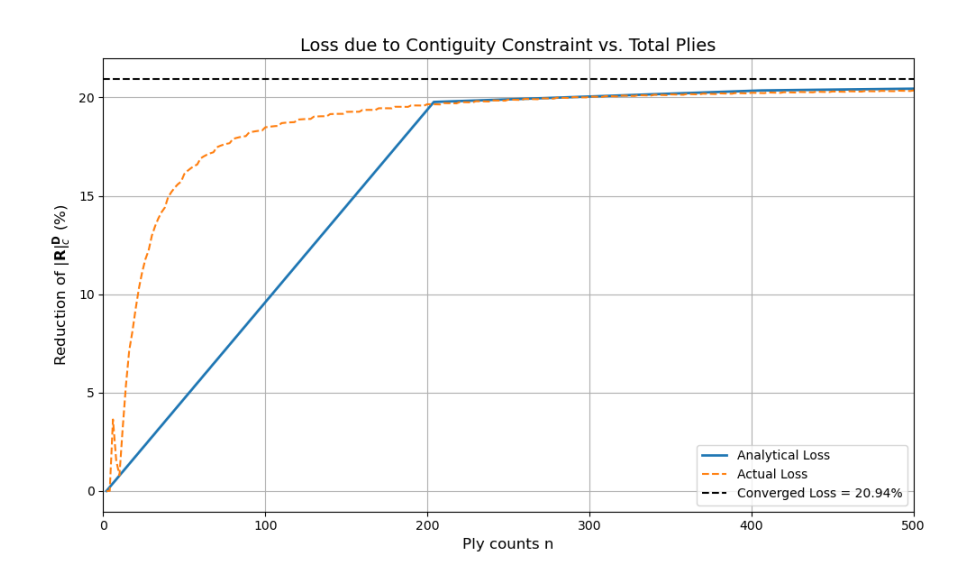


Figure B.2: Reduction of $|\mathbf{R}|_c^{\mathbf{D}}$ with increasing ply counts for conventional laminates.

C Different interpretation of damage tolerance design guideline

Multiple interpretations of the damage tolerance design guideline were presented in Chapter 2.1.2. The theoretical formulation and visualization of results for the outermost ply orientation fixed at 45° were also presented. Similarly, by expanding the summation, the results for the second interpretation of damage tolerance (outermost two plies are fixed at 45° and -45° angles) can be easily derived. The derivation follows similar steps to those in Chapter 4.2.2. To show the reliability of the derivation procedure, the results, along with the expansion of summation terms, are hereby shown:

$$\begin{split} V_{1}^{\mathbf{D}} &= \sum_{k=1}^{\frac{n}{2}-2} w_{k} \cos 2\theta_{k} + w_{\frac{n}{2}} \cos 2\theta_{\frac{n}{2}} + w_{\frac{n}{2}-1} \cos 2\theta_{\frac{n}{2}-1} \\ &= \sum_{k=1}^{\frac{n}{2}-1} w_{k} \cos 2\theta_{k} + w_{\frac{n}{2}} \cos 2 \times 45^{\circ} + w_{\frac{n}{2}-1} \cos 2 \times -45^{\circ} \\ V_{3}^{\mathbf{D}} &= \sum_{k=1}^{\frac{n}{2}-2} w_{k} \sin 2\theta_{k} + w_{\frac{n}{2}} \sin 2\theta_{\frac{n}{2}} + w_{\frac{n}{2}-1} \cos 2\theta_{\frac{n}{2}-1} \\ &= \sum_{k=1}^{\frac{n}{2}-1} w_{k} \sin 2\theta_{k} + w_{\frac{n}{2}} \sin 2 \times 45^{\circ} + w_{\frac{n}{2}-1} \sin 2 \times -45^{\circ} \\ V_{1}^{\mathbf{D}} &= \sum_{k=1}^{\frac{n}{2}-2} w_{k} \cos 4\theta_{k} + w_{\frac{n}{2}} \cos 4\theta_{\frac{n}{2}} + w_{\frac{n}{2}-1} \cos 4\theta_{\frac{n}{2}-1} \\ &= \sum_{k=1}^{\frac{n}{2}-1} w_{k} \cos 4\theta_{k} + w_{\frac{n}{2}} \cos 4 \times 45^{\circ} + w_{\frac{n}{2}-1} \cos 4 \times -45^{\circ} \\ V_{1}^{\mathbf{A}} &= \sum_{k=1}^{\frac{n}{2}-2} w_{k} \cos 2\theta_{k} + w_{\frac{n}{2}} \cos 2\theta_{\frac{n}{2}} + w_{\frac{n}{2}-1} \cos 2\theta_{\frac{n}{2}-1} \\ V_{3}^{\mathbf{A}} &= \sum_{k=1}^{\frac{n}{2}-2} w_{k} \sin 2\theta_{k} + w_{\frac{n}{2}} \sin 2\theta_{\frac{n}{2}} + w_{\frac{n}{2}-1} \sin 2\theta_{\frac{n}{2}-1} \end{split}$$

Similar to the results obtained in Chapter 5.1.2, the derived realizable domain shows a good fit as seen in Figures C.1 to C.3. Hence, it can be stated with confidence that the procedure followed for the derivation of the realizable domain in the respective LP spaces can be extended for different interpretations with minimal changes.

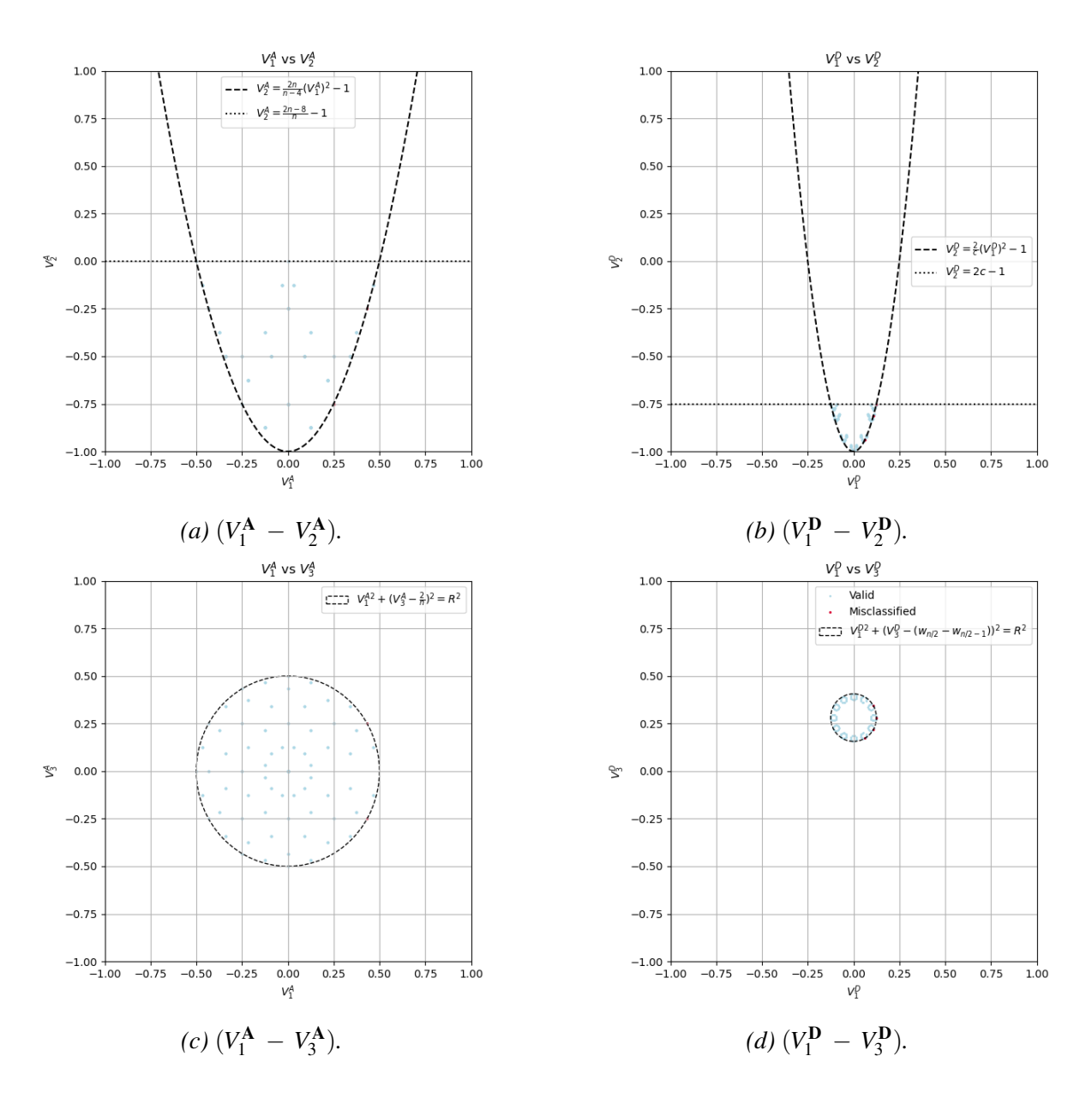


Figure C.1: Characterized realizable domains under the second interpretation of the damage tolerance guideline for n = 8 ply laminates.

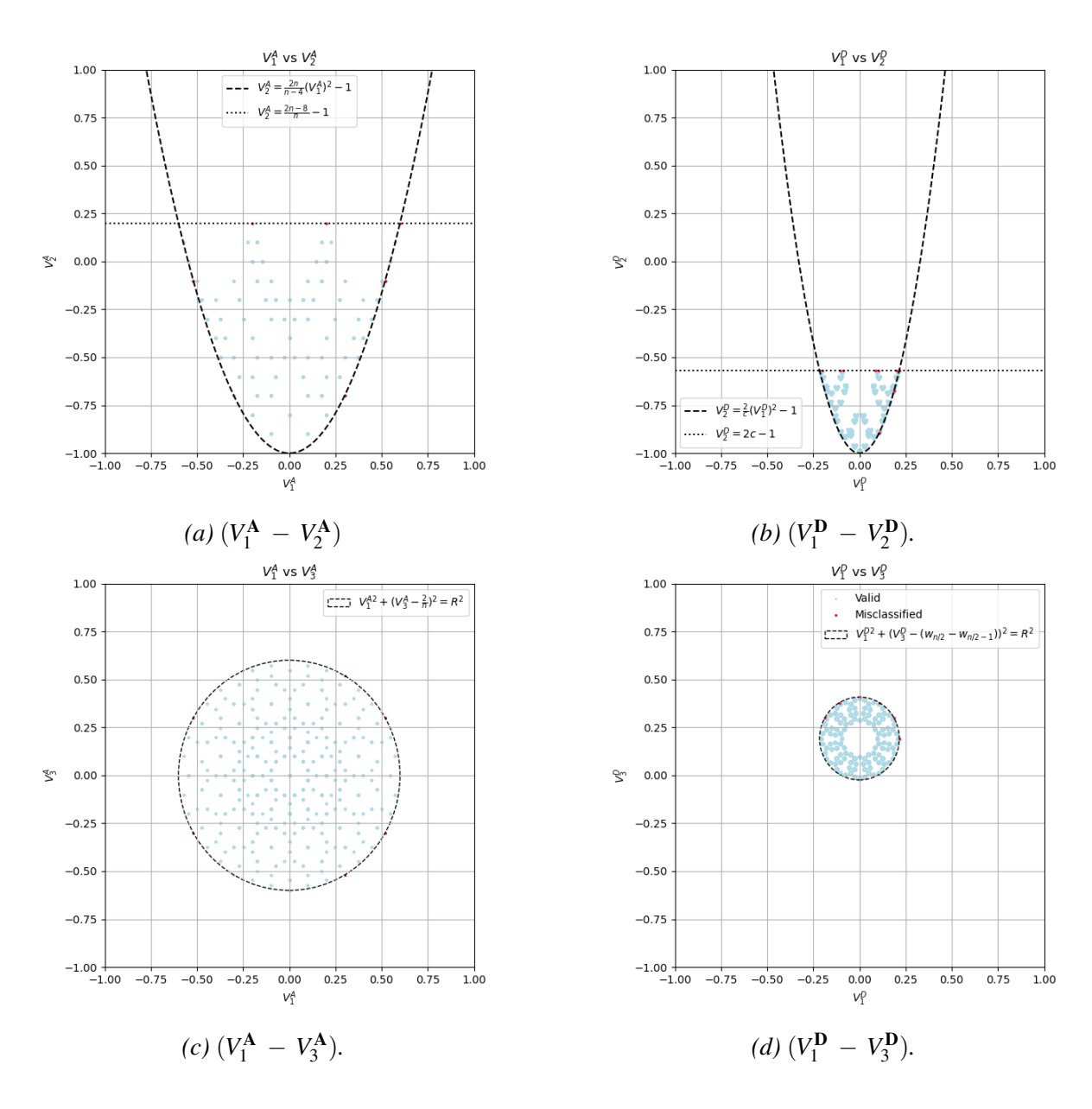


Figure C.2: Characterized realizable domains under the second interpretation of the damage tolerance guideline for n = 10 ply laminates.

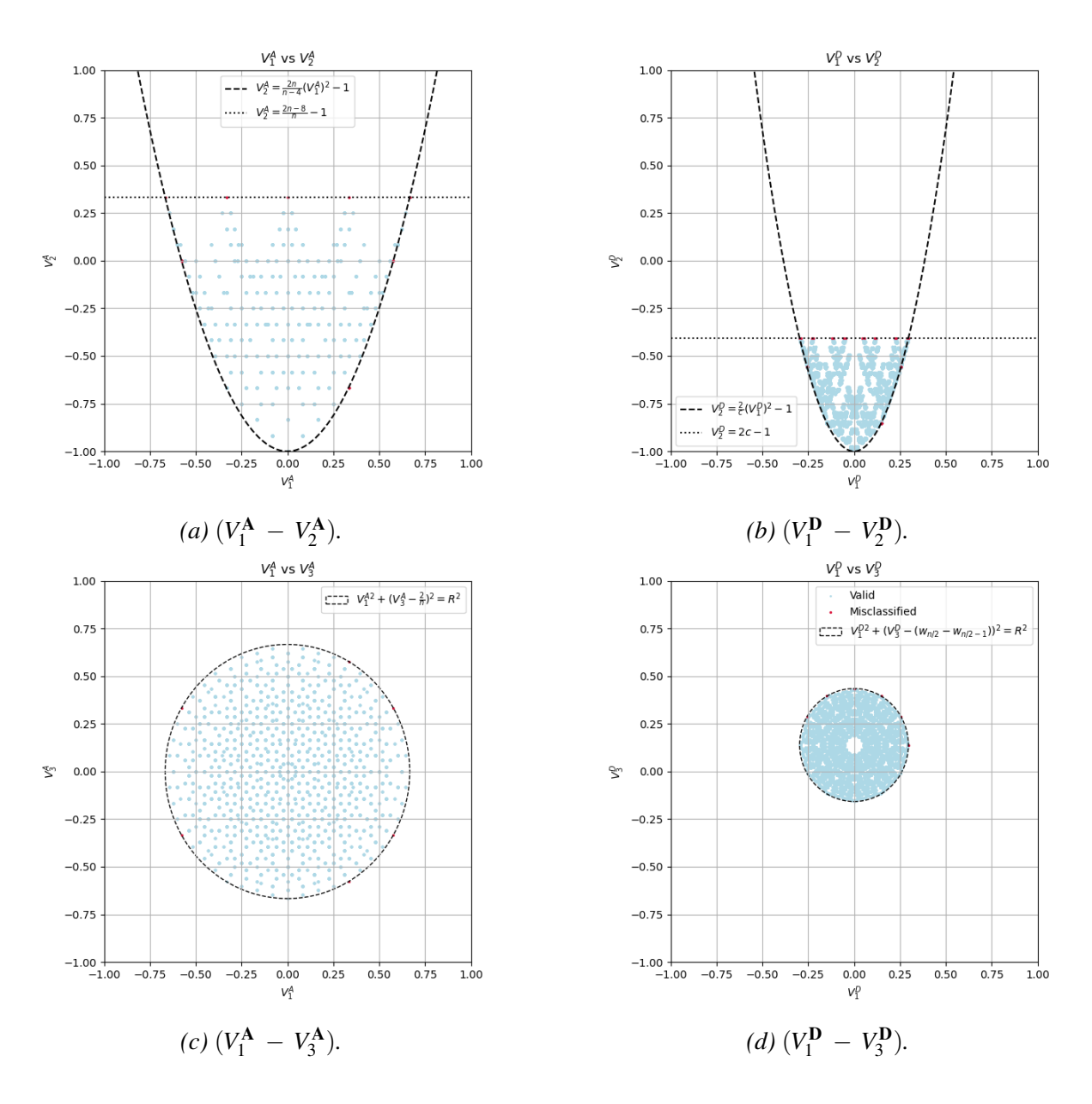


Figure C.3: Characterized realizable domains under the second interpretation of the damage tolerance guideline for n = 12 ply laminates.